ISSN 2683-9288

Science Reviews from the end of the world

Volume 1
Number 4
September 2020

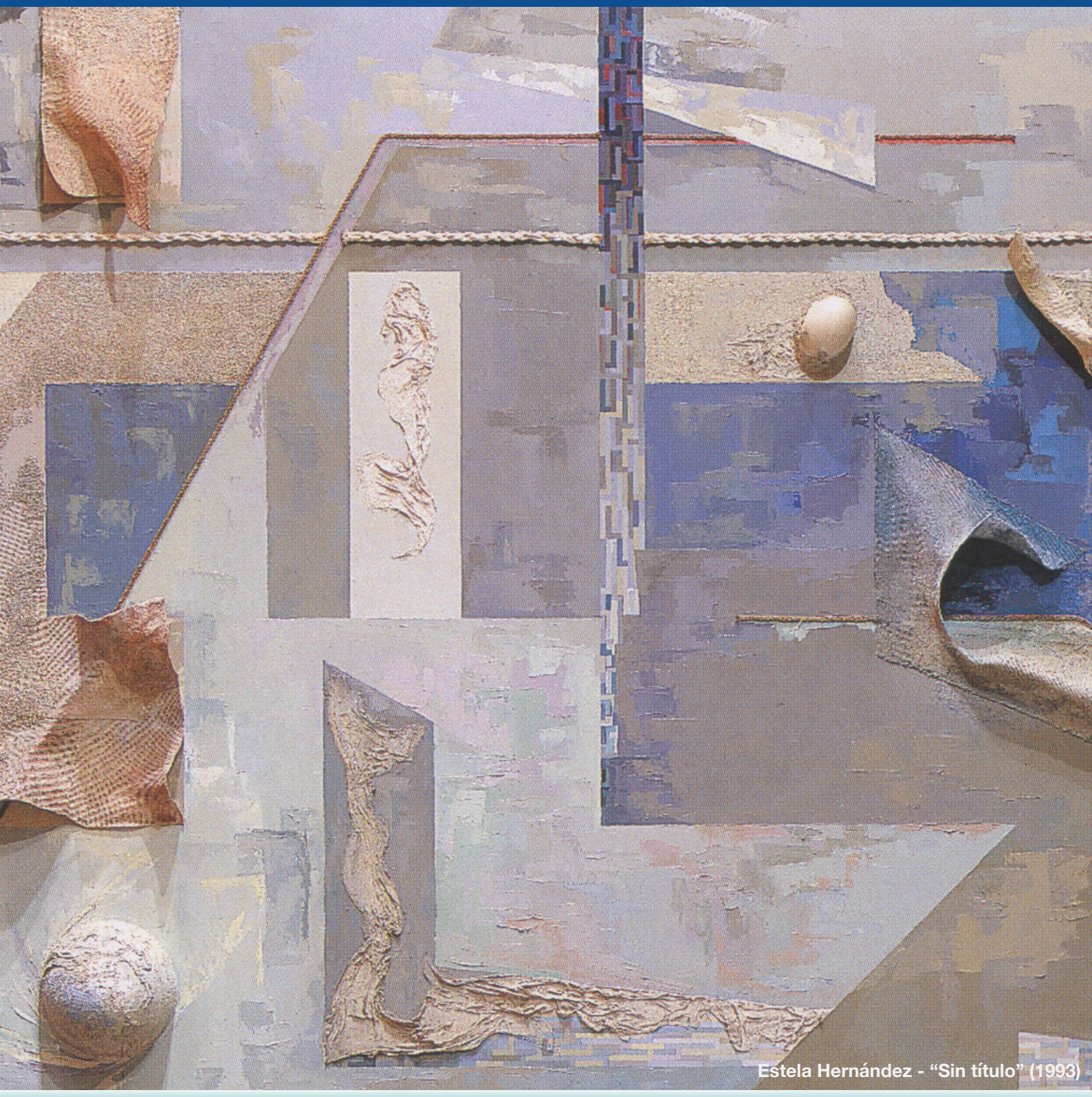

Estela Hernández - “Sin título” (1993)

Science Reviews
from the end of the world

Science Reviews - from the end of the world **is a quarterly publication that aims at providing authoritative reviews on hot research topics developed mainly by scientists that carry out their work far away from the main centers of science. Its research reviews are short, concise, critical and easy-reading articles describing the state of the art on a chosen hot topic, with focus on the research carried out by the authors of the article. These articles are commissioned by invitation and are accessible not only to hardcore specialists, but also to a wider readership of researchers interested in learning about the state-of-the-art in the reviewed subject. The reviews cover all fields of science and are written exclusively in English. They are refereed by peers of international prestige and the evaluation process follows standard international procedures.**

Centro de Estudios sobre Ciencia, Desarrollo y Educación Superior
538 Pueyrredón Av. - 2° C – Second building
Buenos Aires, Argentina - C1032ABS
(54 11) 4963-7878/8811
sciencereviews@centroredes.org.ar
www.scirevfew.net

Vol. 1, No. 4
September 2020

ISSN 2683-9288

Our cover: *Sin título* (1993), by Estela Hernández. From the "Artistas Plásticos con la ciencia" collection. Reproduced by permission from the Comisión Administradora Permanente de la Exposición de Arte Centro Atómico Constituyentes, Comisión Nacional de Energía Atómica.

Science Reviews
from the end of the world

Table of Contents

INTRODUCTION

Exploring the Universe from Argentina

In this publication the four major international projects in astrophysics and cosmology being developed in Argentina are described: QUBIC and LLAMA in the Puna of the province of Salta, the Pierre Auger Observatory and ANDES in the region of Cuyo.

The Pierre Auger Observatory is the largest observatory of cosmic rays in the world developed by a collaboration of about 400 scientists, engineers and technicians from 17 countries. The construction of the Observatory in the Departments of Malargüe and San Rafael of the Province of Mendoza, on a flat area at 1340−1610m above sea level spanning a surface of thousands square kilometers was concluded in 2008. Its purpose is the study of cosmic rays that are massive, charged particles coming from beyond the solar system. Of topical interest in Particle Physics and High Energy Astrophysics are the cosmic rays of the highest known energies, up to few times 10^{20} electron-volts, nearly one hundred million times the highest energies produced so far by the most powerful accelerator on Earth. The ultimate origin and the full detailed properties of those ultra-high energy particles remain open questions. Cosmic rays with energies greater than few times 10^{20} electron volts have not been observed, and it is not known whether this is due to suppression in the propagation of cosmic rays in the intergalactic medium, or if it is due to an exhaustion of the injection power of astrophysical sources in nature. It is expected that an answer of this fundamental question will be found by the observatory's current upgrade called AugerPrime. It began in 2015, with a planned complete installation in 2022, and will operate for over a decade. The protagonist role of Argentine institutions, scientists, engineers and technicians in the successful realization of this project, provides our country with an excellent international reputation and is an example to follow to host future international projects.

ANDES (Agua Negra Deep Experiment Site) is a Deep Underground Laboratory (DUL) project, foreseen as an international laboratory to be constructed in the planned Agua Negra tunnel that will connect the San Juan Argentine province to the Coquimbo province in Chile. The main scientific motivation is to find the properties of dark matter and neutrinos. Dark matter is thought to account for approximately 85% of the matter in the Universe, and it is believed to be composed of particles that do not absorb, reflect, or emit light, so dark matter cannot be detected by electromagnetic radiation. Neutrinos are elusive subatomic particles that zip through the cosmos at nearly the speed of light and that only interact via the weak subatomic force and gravity. To avoid the intense background of penetrating cosmic rays that makes difficult the detection of the weakly interacting dark matter and neutrino particles, DULs that use a great overload of rock as natural protection have been constructed in the Northern Hemisphere. ANDES would be the first DUL to be constructed in the Southern Hemisphere with more than 1000m of overburden. ANDES will be important to study the transformation of one neutrino species (flavor) into another one in media with varying mass density, which may lead to the explanation of the cosmological dominance of matter over antimatter in the present Universe. Furthermore, a DUL in the Southern Hemisphere will be necessary to know whether a tentative detection of dark matter signal modulation is due to the movement of the Earth around the Sun or to possible seasonal atmospheric effects. Besides contributions to fundamental physics, astrophysics and cosmology, ANDES will allow unique experimental possibilities for a diversity of other disciplines.

LLAMA (Large Latin American Millimeter Array). In the 1980's, new horizons for ground-based astrophysics and cosmology by the observation of the Universe at millimeter wavelengths were open thanks to the development of new technological capabilities. To take advantage of those new capabilities, in the 1990's a preliminarily search began in the provinces of Salta and Jujuy for the dry and high-altitude sites that are needed for sub-millimeter/millimeter observations. To install an antenna for sub-millimeter/millimeter observations (LLAMA), such early searches were followed systematically during several years by meteorological and topographical campaigns in different locations of the Puna by the Argentine Institute for Radio Astronomy (IAR), with instrumentation lent by the National Autonomous University of México (UNAM). Two potential sites were identified. To comply with the required atmospheric and logistic conditions for the installation of the LLAMA antenna, it was finally chosen a site called Alto Chorrillos at 4832m altitude, about 18 km in straight line from the small town of San Antonio de los Cobres, in the Puna of the province of Salta.

LLAMA is a binational collaboration to install a millimeter antenna of 12m diameter in Alto Chorrillos. After site selection, members of IAR and the University of Sao Paulo (USP) worked on different aspects of project planning and management. The Brazilian Foundation FAPESP bought the antenna with a grant of USD9 million in 2012, and in 2014 an agreement was signed between the Argentine ministry of science and technology MinCyT, FAPESP and USP. At 180 km from the Atacama Large Millimeter Array (ALMA), the interferometric connection of LLAMA with that array will allow to increase by an order of magnitude the angular resolution of the sources, enhancing the scientific return of the observations. As an additional antenna in the Event Horizon Telescope (EHT), LLAMA will be able to participate in global astrophysical projects, as the one that recently produced the first image of the shadow of a supermassive black hole. Therefore, at a relative low cost compared with the fees to become member country of ALMA (which had an initial construction cost of USD1.4 billon), LLAMA will allow the participation of Argentine and Brazilian scientists in international projects of front-line research. The LLAMA antenna is a multipurpose instrument that will also operate as a stand-alone telescope making contributions in solar and planetary sciences, astrophysics, and cosmology. Presently, all components of the antenna are on site, but it should be assembled with the participation of the staff that will be in charge of the future operations.

QUBIC (Q&U Bolometric Interferometer for Cosmology) is being built by an international collaboration between laboratories in France, Italy, UK, Ireland, USA and Argentina. It will be deployed in Alto Chorrillos at about 400m from LLAMA. The scientific motivation of QUBIC is to find in the polarization of the cosmic microwave background (CMB) the signature of primordial gravitational waves generated by a very early accelerated expansion of the Universe. That cosmic inflationary phase is the current paradigm that accounts for the main large-scale properties of the Universe. So far polarizations of the CMB in the first order E modes due to density fluctuations, and in the secondary B modes at small angular scales (due to weak gravitational lensing) have been observed. However, primordial B-modes due to gravitational waves produced during the inflation epoch that stretched quantum fluctuations by a factor larger than 10^{30} to expected angular scales of about one degree, have not been observed. The observation of primordial B-modes is a great experimental challenge, due to their likely tiny amplitude, and because their signature can be contaminated with polarized foregrounds of galactic origin, as has been the case in a reported tentative detection of B-mode polarization. Currently, there are several experimental efforts pursuing the search for primordial B-modes. QUBIC will join them with a novel control of systematic instrumental effects, and improved subtraction methods of astrophysical foregrounds, by interferometry with bolometers of high sensitivity. The successful performance of QUBIC will open a new road to search for the elusive primordial B-modes of CMB polarization, footprints of gravitational waves from an inflationary period during the earliest moments in the history of the Universe.

Félix Mirabel

Bio

Félix Mirabel

Félix Mirabel proposed in December 2007 to the Ministry of Science and Technology of Argentina the idea of the project LLAMA described in this publication, initiating the steps for the financial participation of Brazil in this project. As scientific researcher, Mirabel has been principal driver in the discoveries of three new classes of cosmic objects: Microquasars, which are objects of topical interest in High Energy Astrophysics, and Ultraluminous Infrared Galaxies, and Tidal Dwarf Galaxies. In the last decade, Mirabel has concentrated his research in Cosmology, working on the role of astrophysical high energy sources at cosmic dawn. Because of his scientific contributions he received several distinctions in Europe, USA and Argentina: The Doctorate Honoris Causa from the University of Barcelona, the Prize on Scientific Excellence of the French Atomic Energy Commission, the "Grand Prize Deslandes" of the French Academy of Sciences, the Rossi Prize of the High Energy Division of the American Astronomical Society, the EPSCOR Prize for

Science Productivity of the National Science Foundation of USA, and the Guggenheim fellowship to finance his research at Caltech. In Argentina he received the Houssay Prize of MinCyT for the Trajectory, the Konex foundation Prize for research in Physics and Astronomy in the 2000-2010 decade, and the Dr. Sahade Prize of the Argentine Astronomical Association in 2018. Félix Mirabel was born in Uruguay and is a naturalized citizen of Argentina. After finishing high school in Montevideo, obtained a Ph.D. in Astronomy at the University of La Plata, and the title of Professor of Philosophy from the University of Buenos Aires. In March 1976, he leaves to England as a post-doc fellow at the Jodrell Bank Radio Observatory, financed by fellowships of the British Council and the University of Manchester. Two years later he moved to the USA carrying out research at several institutions: as post-doc at the University of Maryland, as associate researcher at Caltech, and as Professor of Physics at the University of Puerto Rico with research at the Arecibo Radio Observatory. Before his return to Argentina, he moved back to Europe becoming Director of Research at the French Atomic Commission, from where he was later commissioned as Representative and Director of the Office of Science in Chile of the European Southern Observatories (ESO). At present, Mirabel is *emeritus* Researcher of the National Research Council of Argentina at the Institute of Astronomy and Space Physics in Buenos Aires, and member of the National Academy of Exact, Physical and Natural Sciences of Argentina.

Guest Editor of this Issue

Karen Hallberg

After finishing high school in the province of Jujuy, Argentina, Karen Hallberg studied two years of electronic engineering at the National University of Rosario and later obtained a full scholarship to study physics at the Instituto Balseiro in Bariloche (National Atomic Energy Commission CNEA, and National University of Cuyo), where she also did her PhD in Physics. She had postdoctoral positions at the Max-Planck Institutes in Stuttgart and in Dresden, Germany. Currently, she is Principal Researcher of the Argentine Council for Science and Technology (CONICET) working at the Bariloche Atomic Center (CAB) and is Professor at the Balseiro Institute. She was recently elected as International Councilor of the American Physical Society (APS) and invited as a member of the World Economic Forum's Global Future Council on Quantum Applications. She is also a Council member of the Pugwash Conferences for Science and World Affairs (1995 Peace Nobel Prize), member of the Argentine Committee for Ethics in Science and Technology, corresponding member of the Argentine Academy for Exact, Physical and Natural Sciences, member of the Latin American Academy of Sciences, Senior Associate of the ICTP (International Center for Theoretical Physics, Trieste), Associate Member ICTP-SAIFR, member of the International Advisory Council of the International Institute of Physics, Natal (Brazil) and member of the Editorial Board of Physical Review Research (APS). She served as the Head of the Condensed Matter Department at CAB, as the Argentine representative to the Latin American Center of Physics (CLAF), as member of the Board of Directors of the Aspen Science Center, and on several other national and international committees. She was awarded the 2019 L'Oreal-UNESCO International Award For Women in Science (for Latin America), honorary doctorates at the National University of Jujuy and at the University Siglo XXI, an honorary IAEA Marie Sklodowska Curie Fellowship, the 2005 Guggenheim Fellowship and was an Aspen Ideas Festival Scholar. Her research topics include the development of state-of-the-art computational approaches to understand the physics of quantum matter and nanoscopic systems. She is actively committed to reducing the gender gap and increasing awareness of ethical considerations in science.

IN THIS ISSUE

Science Reviews
from the end of the world

Vol. 1, No. 4, September 2020 // pp. 8-33 /

The Pierre Auger Observatory and its Upgrade

The Pierre Auger Collaboration*:

A. Aab[76], P. Abreu[68], M. Aglietta[51,50], J.M. Albury[12], I. Allekotte[1], A. Almela[8,11], J. Alvarez-Muñiz[75], R. Alves Batista[76], G.A. Anastasi[59,50], L. Anchordoqui[83], B. Andrada[8], S. Andringa[68], C. Aramo[48], P.R. Araújo Ferreira[40], H. Asorey[8], P. Assis[68], G. Avila[10], A.M. Badescu[71], A. Bakalova[30], A. Balaceanu[69], F. Barbato[57,48], R.J. Barreira Luz[68], K.H. Becker[36], J.A. Bellido[12], C. Berat[34], M.E. Bertaina[59,50], X. Bertou[1], P.L. Biermann[c], T. Bister[40], J. Biteau[35], J. Blazek[30], C. Bleve[34], M. Boháčová[30], D. Boncioli[54,44], C. Bonifazi[24], L. Bonneau Arbeletche[19], N. Borodai[65], A.M. Botti[8], J. Brack[h], T. Bretz[40], F.L. Briechle[40], P. Buchholz[42], A. Bueno[74], S. Buitink[14], M. Buscemi[55,45], K.S. Caballero-Mora[63], L. Caccianiga[56,47], A. Cancio[11,8], F. Canfora[76,78], I. Caracas[36], J.M. Carceller[74], R. Caruso[55,45], A. Castellina[51,50], F. Catalani[17], G. Cataldi[46], L. Cazon[68], M. Cerda[9], J.A. Chinellato[20], K. Choi[13], J. Chudoba[30], L. Chytka[31], R.W. Clay[12], A.C. Cobos Cerutti[7], R. Colalillo[57,48], A. Coleman[89], M.R. Coluccia[53,46], R. Conceição[68], A. Condorelli[43,44], G. Consolati[47,52], F. Contreras[10], F. Convenga[53,46], C.E. Covault[81,e], S. Dasso[5,3], K. Daumiller[38], B.R. Dawson[12], J.A. Day[12], R.M. de Almeida[26], J. de Jesús[8,38], S.J. de Jong[76,78], G. De Mauro[76,78], J.R.T. de Mello Neto[24,25], I. De Mitri[43,44], J. de Oliveira[26], D. de Oliveira Franco[20], V. de Souza[18], E. De Vito[53,46], J. Debatin[37], M. del Río[10], O. Deligny[32], N. Dhital[65], A. Di Matteo[50], C. Dobrigkeit[20], J.C. D'Olivo[64], R.C. dos Anjos[23], M.T. Dova[4], J. Ebr[30], R. Engel[37,38], I. Epicoco[53,46], M. Erdmann[40], C.O. Escobar[a], A. Etchegoyen[8,11], H. Falcke[76,79,78], J. Farmer[88], G. Farrar[86], A.C. Fauth[20], N. Fazzini[f], F. Feldbusch[39], F. Fenu[59,50], B. Fick[85], J.M. Figueira[8], A. Filipčič[73,72], T. Fodran[76], M.M. Freire[6], T. Fujii[88,i], A. Fuster[8,11], C. Galea[76], C. Galelli[56,47], B. García[7], A.L. Garcia Vegas[40], H. Gemmeke[39], F. Gesualdi[8,38], A. Gherghel-Lascu[69], P.L. Ghia[32], U. Giaccari[76], M. Giammarchi[47], M. Giller[66], J. Glombitza[40], F. Gobbi[9], F. Gollan[8], G. Golup[1], M. Gómez Berisso[1], P.F. Gómez Vitale[10], J.P. Gongora[10], N. González[8], I. Goos[1,38], D. Góra[65], A. Gorgi[51,50], M. Gottowik[36], T.D. Grubb[12], F. Guarino[57,48], G.P. Guedes[21], E. Guido[50,59], S. Hahn[38,8], R. Halliday[81], M.R. Hampel[8], P. Hansen[4], D. Harari[1], V.M. Harvey[12], A. Haungs[38], T. Hebbeker[40], D. Heck[38], G.C. Hill[12], C. Hojvat[f], J.R. Hörandel[76,78], P. Horvath[31], M. Hrabovský[31], T. Huege[38,14], J. Hulsman[8,38], A. Insolia[55,45], P.G. Isar[70], J.A. Johnsen[82], J. Jurysek[30], A. Kääpä[36], K.H. Kampert[36], B. Keilhauer[38], J. Kemp[40], H.O. Klages[38], M. Kleifges[39], J. Kleinfeller[9], M. Köpke[37], G. Kukec Mezek[72], B.L. Lago[16], D. LaHurd[81], R.G. Lang[18], N. Langner[40], M.A. Leigui de Oliveira[22], V. Lenok[38], A. Letessier-Selvon[33], I. Lhenry-Yvon[32], D. Lo Presti[55,45], L. Lopes[68], R. López[60], R. Lorek[81], Q. Luce[37], A. Lucero[8], J.P. Lundquist[72], A. Machado Payeras[20], G. Mancarella[53,46], D. Mandat[30], B.C. Manning[12], J. Manshanden[41], P. Mantsch[f], S. Marafico[32], A.G. Mariazzi[4], I.C. Mariş[13], G. Marsella[53,46], D. Martello[53,46], H. Martinez[18], O. Martínez Bravo[60], M. Mastrodicasa[54,44], H.J. Mathes[38], J. Matthews[84], G. Matthiae[58,49], E. Mayotte[36], P.O. Mazur[f], G. Medina-Tanco[64], D. Melo[8], A. Menshikov[39], K.-D. Merenda[82], S. Michal[31], M.I. Micheletti[6], L. Miramonti[56,47], S. Mollerach[1], F. Montanet[34], C. Morello[51,50], M. Mostafá[87], A.L. Müller[8,38], M.A. Muller[20,b,24], K. Mulrey[14], R. Mussa[50], M. Muzio[86], W.M. Namasaka[36], L. Nellen[64], M. Niculescu-Oglinzanu[69], M. Niechciol[42], D. Nitz[85,g], D. Nosek[29], V. Novotny[29], L. Nožka[31], A Nucita[53,46], L.A. Núñez[28], M. Palatka[30], J. Pallotta[2], P. Papenbreer[36], G. Parente[75], A. Parra[60], M. Pech[30], F. Pedreira[75], J. Pękala[65], R. Pelayo[62], J. Peña-Rodriguez[28], J. Perez Armand[19], M. Perlin[8,38], L. Perrone[53,46], S. Petrera[43,44], T. Pierog[38], M. Pimenta[68], V. Pirronello[55,45], M. Platino[8], B. Pont[76], M. Pothast[78,76], P. Privitera[88], M. Prouza[30], A. Puyleart[85], S. Querchfeld[36], J. Rautenberg[36], D. Ravignani[8], M. Reininghaus[38,8], J. Ridky[30], F. Riehn[68], M. Risse[42], P. Ristori[2], V. Rizi[54,44], W. Rodrigues de Carvalho[19], J. Rodriguez Rojo[10], M.J. Roncoroni[8], M. Roth[38], E. Roulet[1], A.C. Rovero[5], P. Ruehl[42], S.J. Saffi[12], A. Saftoiu[69], F. Salamida[54,44], H. Salazar[60], G. Salina[49], J.D. Sanabria Gomez[28], F. Sánchez[8], E.M. Santos[19], E. Santos[30], F. Sarazin[82], R. Sarmento[68], C. Sarmiento-Cano[8], R. Sato[10], P. Savina[53,46,32], C.M. Schäfer[38], V. Scherini[46], H. Schieler[38], M. Schimassek[37,8], M. Schimp[36], F. Schlüter[38,8], D. Schmidt[37], O. Scholten[77,14], P. Schovánek[30], F.G. Schröder[89,38], S. Schröder[36], J. Schulte[40], S.J. Sciutto[4], M. Scornavacche[8,38], R.C. Shellard[15], G. Sigl[41], G. Silli[8,38], O. Sima[69,j], R. Šmída[88], P. Sommers[87], J.F. Soriano[83], J. Souchard[34], R. Squartini[9], M. Stadelmaier[38,8], D. Stanca[69], S. Stanič[72], J. Stasielak[65], P. Stassi[34],

A. Streich[37,8], M. Suárez-Durán[28], T. Sudholz[12], T. Suomijärvi[35], A.D. Supanitsky[8], J. Šupík[31], Z. Szadkowski[67], A. Taboada[37], A. Tapia[27], C. Timmermans[78,76], O. Tkachenko[38], P. Tobiska[30], C.J. Todero Peixoto[17], B. Tomé[68], A. Travaini[9], P. Travnicek[30], C. Trimarelli[54,44], M. Trini[72], M. Tueros[4], R. Ulrich[38], M. Unger[38], L. Vaclavek[31], M. Vacula[31], J.F. Valdés Galicia[64], L. Valore[57,48], E. Varela[60], V. Varma K.C.[8,38], A. Vásquez-Ramírez[28], D. Veberič[38], C. Ventura[25], I.D. Vergara Quispe[4], V. Verzi[49], J. Vicha[30], J. Vink[80], S. Vorobiov[72], H. Wahlberg[4], A.A. Watson[d], M. Weber[39], A. Weindl[38], L. Wiencke[82], H. Wilczyński[65], T. Winchen[14], M. Wirtz[40], D. Wittkowski[36], B. Wundheiler[8], A. Yushkov[30], O. Zapparrata[13], E. Zas[75], D. Zavrtanik[72,73], M. Zavrtanik[73,72], L. Zehrer[72], A. Zepeda[61]

[1] *Centro Atómico Bariloche and Instituto Balseiro (CNEA-UNCuyo-CONICET), San Carlos de Bariloche, Argentina*
[2] *Centro de Investigaciones en Láseres y Aplicaciones, CITEDEF and CONICET, Villa Martelli, Argentina*
[3] *Departamento de Física and Departamento de Ciencias de la Atmósfera y los Océanos, FCEyN, Universidad de Buenos Aires and CONICET, Buenos Aires, Argentina*
[4] *IFLP, Universidad Nacional de La Plata and CONICET, La Plata, Argentina*
[5] *Instituto de Astronomía y Física del Espacio (IAFE, CONICET-UBA), Buenos Aires, Argentina*
[6] *Instituto de Física de Rosario (IFIR) – CONICET/U.N.R. and Facultad de Ciencias Bioquímicas y Farmacéuticas U.N.R., Rosario, Argentina*
[7] *Instituto de Tecnologías en Detección y Astropartículas (CNEA, CONICET, UNSAM), and Universidad Tecnológica Nacional – Facultad Regional Mendoza (CONICET/CNEA), Mendoza, Argentina*
[8] *Instituto de Tecnologías en Detección y Astropartículas (CNEA, CONICET, UNSAM), Buenos Aires, Argentina*
[9] *Observatorio Pierre Auger, Malargüe, Argentina*
[10] *Observatorio Pierre Auger and Comisión Nacional de Energía Atómica, Malargüe, Argentina*
[11] *Universidad Tecnológica Nacional – Facultad Regional Buenos Aires, Buenos Aires, Argentina*
[12] *University of Adelaide, Adelaide, S.A., Australia*
[13] *Université Libre de Bruxelles (ULB), Brussels, Belgium*
[14] *Vrije Universiteit Brussels, Brussels, Belgium*
[15] *Centro Brasileiro de Pesquisas Fisicas, Rio de Janeiro, RJ, Brazil*
[16] *Centro Federal de Educação Tecnológica Celso Suckow da Fonseca, Nova Friburgo, Brazil*
[17] *Universidade de São Paulo, Escola de Engenharia de Lorena, Lorena, SP, Brazil*
[18] *Universidade de São Paulo, Instituto de Física de São Carlos, São Carlos, SP, Brazil*
[19] *Universidade de São Paulo, Instituto de Física, São Paulo, SP, Brazil*
[20] *Universidade Estadual de Campinas, IFGW, Campinas, SP, Brazil*
[21] *Universidade Estadual de Feira de Santana, Feira de Santana, Brazil*
[22] *Universidade Federal do ABC, Santo André, SP, Brazil*
[23] *Universidade Federal do Paraná, Setor Palotina, Palotina, Brazil*
[24] *Universidade Federal do Rio de Janeiro, Instituto de Física, Rio de Janeiro, RJ, Brazil*
[25] *Universidade Federal do Rio de Janeiro (UFRJ), Observatório do Valongo, Rio de Janeiro, RJ, Brazil*
[26] *Universidade Federal Fluminense, EEIMVR, Volta Redonda, RJ, Brazil*
[27] *Universidad de Medellín, Medellín, Colombia*
[28] *Universidad Industrial de Santander, Bucaramanga, Colombia*
[29] *Charles University, Faculty of Mathematics and Physics, Institute of Particle and Nuclear Physics, Prague, Czech Republic*
[30] *Institute of Physics of the Czech Academy of Sciences, Prague, Czech Republic*
[31] *Palacky University, RCPTM, Olomouc, Czech Republic*
[32] *CNRS/IN2P3, IJCLab, Université Paris-Saclay, Orsay, France*
[33] *Laboratoire de Physique Nucléaire et de Hautes Energies (LPNHE), Sorbonne Université, Université de Paris, CNRS-IN2P3, Paris, France*
[34] *Univ. Grenoble Alpes, CNRS, Grenoble Institute of Engineering Univ. Grenoble Alpes, LPSC-IN2P3, 38000 Grenoble, France, France*
[35] *Université Paris-Saclay, CNRS/IN2P3, IJCLab, Orsay, France, France*
[36] *Bergische Universität Wuppertal, Department of Physics, Wuppertal, Germany*
[37] *Karlsruhe Institute of Technology, Institute for Experimental Particle Physics (ETP), Karlsruhe, Germany*
[38] *Karlsruhe Institute of Technology, Institut für Kernphysik, Karlsruhe, Germany*
[39] *Karlsruhe Institute of Technology, Institut für Prozessdatenverarbeitung und Elektronik, Karlsruhe, Germany*
[40] *RWTH Aachen University, III. Physikalisches Institut A, Aachen, Germany*
[41] *Universität Hamburg, II. Institut für Theoretische Physik, Hamburg, Germany*
[42] *Universität Siegen, Fachbereich 7 Physik – Experimentelle Teilchenphysik, Siegen, Germany*
[43] *Gran Sasso Science Institute, L'Aquila, Italy*
[44] *INFN Laboratori Nazionali del Gran Sasso, Assergi (L'Aquila), Italy*
[45] *INFN, Sezione di Catania, Catania, Italy*
[46] *INFN, Sezione di Lecce, Lecce, Italy*
[47] *INFN, Sezione di Milano, Milano, Italy*
[48] *INFN, Sezione di Napoli, Napoli, Italy*
[49] *INFN, Sezione di Roma "Tor Vergata", Roma, Italy*
[50] *INFN, Sezione di Torino, Torino, Italy*
[51] *Osservatorio Astrofisico di Torino (INAF), Torino, Italy*

[52] *Politecnico di Milano, Dipartimento di Scienze e Tecnologie Aerospaziali , Milano, Italy*
[53] *Università del Salento, Dipartimento di Matematica e Fisica "E. De Giorgi", Lecce, Italy*
[54] *Università dell'Aquila, Dipartimento di Scienze Fisiche e Chimiche, L'Aquila, Italy*
[55] *Università di Catania, Dipartimento di Fisica e Astronomia, Catania, Italy*
[56] *Università di Milano, Dipartimento di Fisica, Milano, Italy*
[57] *Università di Napoli "Federico II", Dipartimento di Fisica "Ettore Pancini", Napoli, Italy*
[58] *Università di Roma "Tor Vergata", Dipartimento di Fisica, Roma, Italy*
[59] *Università Torino, Dipartimento di Fisica, Torino, Italy*
[60] *Benemérita Universidad Autónoma de Puebla, Puebla, México*
[61] *Centro de Investigación y de Estudios Avanzados del IPN (CINVESTAV), México, D.F., México*
[62] *Unidad Profesional Interdisciplinaria en Ingeniería y Tecnologías Avanzadas del Instituto Politécnico Nacional (UPIITA-IPN), México, D.F., México*
[63] *Universidad Autónoma de Chiapas, Tuxtla Gutiérrez, Chiapas, México*
[64] *Universidad Nacional Autónoma de México, México, D.F., México*
[65] *Institute of Nuclear Physics PAN, Krakow, Poland*
[66] *University of Łódź, Faculty of Astrophysics, Łódź, Poland*
[67] *University of Łódź, Faculty of High-Energy Astrophysics,Łódź, Poland*
[68] *Laboratório de Instrumentação e Física Experimental de Partículas – LIP and Instituto Superior Técnico – IST, Universidade de Lisboa – UL, Lisboa, Portugal*
[69] *"Horia Hulubei" National Institute for Physics and Nuclear Engineering, Bucharest-Magurele, Romania*
[70] *Institute of Space Science, Bucharest-Magurele, Romania*
[71] *University Politehnica of Bucharest, Bucharest, Romania*
[72] *Center for Astrophysics and Cosmology (CAC), University of Nova Gorica, Nova Gorica, Slovenia*
[73] *Experimental Particle Physics Department, J. Stefan Institute, Ljubljana, Slovenia*
[74] *Universidad de Granada and C.A.F.P.E., Granada, Spain*
[75] *Instituto Galego de Física de Altas Enerxías (IGFAE), Universidade de Santiago de Compostela, Santiago de Compostela, Spain*
[76] *IMAPP, Radboud University Nijmegen, Nijmegen, The Netherlands*
[77] *KVI – Center for Advanced Radiation Technology, University of Groningen, Groningen, The Netherlands*
[78] *Nationaal Instituut voor Kernfysica en Hoge Energie Fysica (NIKHEF), Science Park, Amsterdam, The Netherlands*
[79] *Stichting Astronomisch Onderzoek in Nederland (ASTRON), Dwingeloo, The Netherlands*
[80] *Universiteit van Amsterdam, Faculty of Science, Amsterdam, The Netherlands*
[81] *Case Western Reserve University, Cleveland, OH, USA*
[82] *Colorado School of Mines, Golden, CO, USA*
[83] *Department of Physics and Astronomy, Lehman College, City University of New York, Bronx, NY, USA*
[84] *Louisiana State University, Baton Rouge, LA, USA*
[85] *Michigan Technological University, Houghton, MI, USA*
[86] *New York University, New York, NY, USA*
[87] *Pennsylvania State University, University Park, PA, USA*
[88] *University of Chicago, Enrico Fermi Institute, Chicago, IL, USA*
[89] *University of Delaware, Department of Physics and Astronomy, Bartol Research Institute, Newark, DE, USA*

——

[a] *Fermi National Accelerator Laboratory, USA*
[b] *also at Universidade Federal de Alfenas, Poços de Caldas, Brazil*
[c] *Max-Planck-Institut für Radioastronomie, Bonn, Germany*
[d] *School of Physics and Astronomy, University of Leeds, Leeds, United Kingdom*
[e] *also at Radboud Universtiy Nijmegen, Nijmegen, The Netherlands*
[f] *Fermi National Accelerator Laboratory, Fermilab, Batavia, IL, USA*
[g] *also at Karlsruhe Institute of Technology, Karlsruhe, Germany*
[h] *Colorado State University, Fort Collins, CO, USA*
[i] *now at Hakubi Center for Advanced Research and Graduate School of Science, Kyoto University, Kyoto, Japan*
[j] *also at University of Bucharest, Physics Department, Bucharest, Romania*

* Correspondence:
spokesperson@auger.org.ar

Abstract

The Pierre Auger Observatory was built to study cosmic rays of the highest energies. It is installed in the Departments of Malargüe and San Rafael in the Province of Mendoza, Argentina. The Observatory is based on a hybrid design, comprised by two detector systems: a surface array of 1660 water Cherenkov detectors is complemented with 27 fluorescence telescopes which overlook the atmosphere above the surface array. Covering a total area in excess of 3000 km^2, it is the largest and most precise observatory of its kind. It has been in full operation for over a decade now. In this article we review the objectives and design properties of the Pierre Auger Observatory, present its performance and the main scientific results obtained so far, and we describe the Upgrade that is well underway to enhance its capabilities for the next decade of measurements.

Keywords:
cosmic rays, Pierre Auger Observatory

1. Cosmic rays and their spectrum

The discovery of cosmic rays is attributed to Viktor Hess, who in 1912 demonstrated the extraterrestrial origin of the very penetrating ionising radiation that had already been measured years before. Although it was soon established that this energetic radiation originated beyond the solar system, it was hard to discern if it was caused by photons or massive particles. It took nearly two decades of intense research and after heated debates among the top scientists in the field, it could be concluded that cosmic rays are composed of massive, charged particles, mostly high energy protons and, to a lesser degree, heavier atomic nuclei.

Cosmic ray physics was a very active field of research in the first half of the XXth century. The main breakthroughs in the dawn of particle physics were possible thanks to the existence of this cosmic radiation of very high energy. Through its study, the foundations of elementary particle physics were laid, when the positron, the muon, the pions and many other subatomic particles were discovered as by-products of interactions of cosmic rays.

At the end of the 1930s, Pierre Auger operated a number of Geiger-Müller counters in coincidence at high altitude sites in the Alps, and concluded that the penetrating radiation detected at ground level is due to so called extensive air showers (EAS), i.e., secondary particles produced by the interaction of very high energy cosmic rays with the atoms of the atmospheric air. Fig. 1 shows an artistic view of an Extensive Air Shower. In his studies, Auger concluded that the cosmic radiation must include particles with energies in excess of 10^{15} eV. Following Pierre Auger's discovery, systematic effort was invested in the study of cosmic air showers, their development and characteristics. Pioneering work by Bethe, Heitler, Greisen, Hillas, Nishimura and many others set the foundations for their description. For a historical review, see [1].

In the 1950s, surface detectors for the study of Extensive Air Showers became a widely used tool. The first measurements of energy and arrival direction of cosmic rays above 10^{15} eV were carried out in 1954 by the cosmic ray group of Bruno Rossi at MIT, using an array of 11 scintillation detectors arranged in a circle of 230 m radius. Between 1954 and 1957, the cosmic ray spectrum was explored to energies beyond 10^{18} eV with data provided by the Agassiz Station at Harvard [2]. In 1962, Volcano Ranch in Albuquerque, New Mexico, would be the first giant array to register an ultra-energetic event of 1.4×10^{20} eV [3, 4].

After the discovery of the cosmic microwave background radiation (CMBR) by Penzias and Wilson in 1964 [5], Kenneth Greisen [6] and independently Georgiy Zatsepin and Vadim Kuz'min [7] demonstrated that for protons with energies above $\sim 5 \times 10^{19}$ eV, the cross section for the interaction with the CMB photons has a sharp increase due to the Δ resonance for production of pions:

$$\begin{aligned} \mathrm{p} + \gamma_{\mathrm{cmb}} &\to \triangle^{+} \to \mathrm{n} + \pi^{+}\,, \\ \mathrm{p} + \gamma_{\mathrm{cmb}} &\to \triangle^{+} \to \mathrm{p} + \pi^{0}\,. \end{aligned} \tag{1}$$

This interaction degrades the proton energy, preventing particles with energies greater than $\sim 5 \times 10^{19}$ eV to be observed

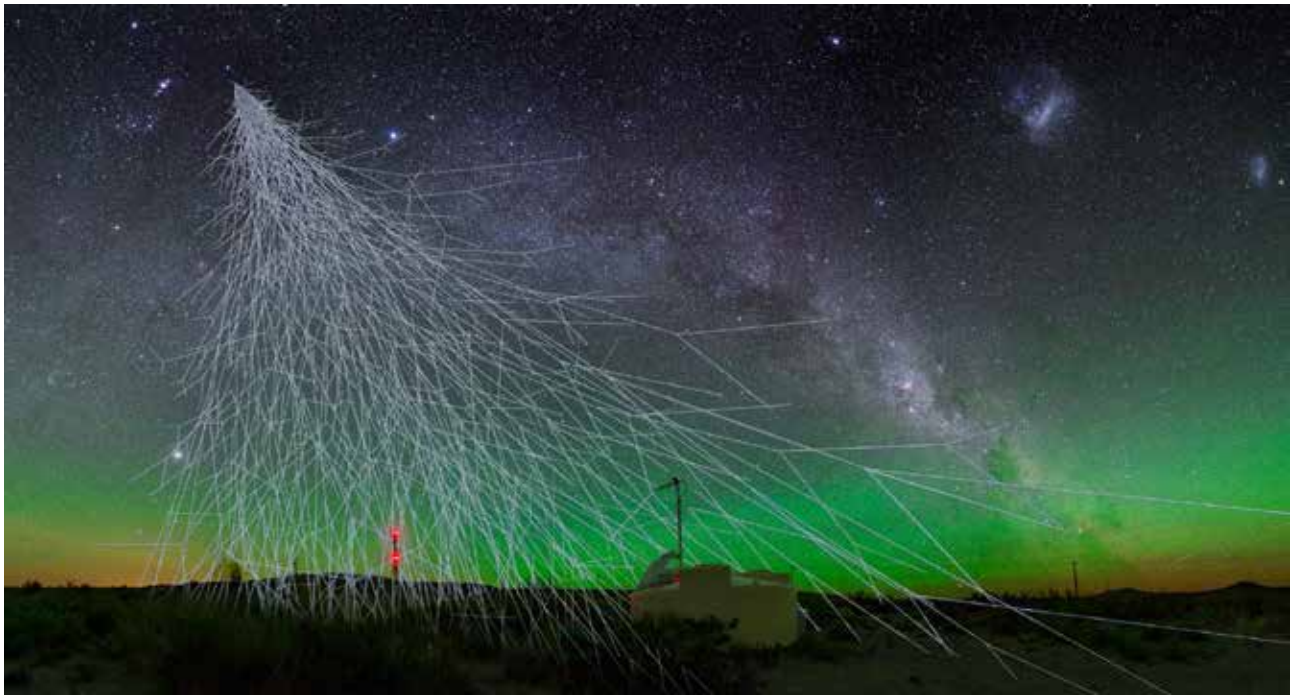

Figure 1. Artistic view of an Extensive Air Shower. Ultra high energy cosmic rays produce Extensive Air Showers with $\sim 10^{11}$ energetic secondary particles, spread over tens of km^2.

at distances larger than ~ 100 Mpc. Therefore, if cosmic rays originate at cosmological distances, the flux above this energy should be largely suppressed, giving rise to a sharp decrease in the cosmic ray energy spectrum, known as the GZK cut-off.

Similarly as for protons, for primary cosmic rays with mass number $A > 1$ the photodisintegration process comes into play, both with the microwave and the infra-red background. This leads to the ejection of one or several nucleons N from the nucleus [8, 9]. Given that the energy of the primary nuclei is shared between nucleons, the threshold energy for these processes is typically higher than for protons, but producing a similar suppression in the flux at high energies.

Therefore, a series of experiments were set up to study the upper end of the spectrum of cosmic rays. Casa Mia in USA [10], SUGAR in Australia [11], Haverah Park in England [12], Yakutsk in the USSR [13], KASCADE and Kascade-Grande in Germany [14], AGASA in Japan [15] and Fly's Eye - HiRes in the USA [16, 17, 18] recorded high energy cosmic ray events and contributed to the determination of their spectrum. In 1990, there were already a few dozens of events detected with estimated energies above the GZK cut-off, including the remarkable event with an energy of $E = 3 \times 10^{20}$ eV detected by the Fly's Eye detector in 1991 [19]. Fly's Eye was a fluorescence detector that operated from 1981 to 1993 in Utah, and was later replaced by the "High Resolution Fly's Eye" (HiRes) detector.

However, a notorious discrepancy was observed between the spectra reported by the two largest observatories, AGASA [20] and HiRes [21]. While HiRes observed a suppression at the highest energies, AGASA did not. It was conjectured that systematic errors could be the cause, as AGASA was composed of a surface array of 111 scintillator detectors and 27 muon detectors, covering some 100 km^2, while HiRes was an observatory based on the atmospheric fluorescence technique. The AGASA results seemed to contradict the expectations from the GZK suppression. If these events had an astrophysical origin, due to the GZK effect they would necessarily need to have a nearby origin (of the order of $\sim$100 Mpc). This conclusion created a tension with the expectation that in this case their arrival directions should suffer small deviations and should therefore point backwards to identifiable sources, which was not the case.

1.1. The need for a giant array

The question about the existence of the GZK cut-off was one of the main reasons for the design of a new observatory that would be able to gather enough statistics at the highest energies where the cosmic ray flux is below 1 km^{-2} century^{-1}. This piece of the cosmic ray puzzle, together with the fact that the sources of the highest energy cosmic rays had not yet been identified, were the main arguments that led to the construction of the Pierre Auger Observatory.

Due to the very low flux of cosmic rays above 10^{20} eV, vast areas need to be monitored to collect a large statistical sample. Already in 1992, James Cronin and Alan Watson had proposed the idea of building a huge array of detectors to answer the question of the origin of the cosmic rays of the highest energies, their composition, source distribution and propagation. The proposal found support and encouragement from the scientific community and, in 1995, a 6-month workshop was held at Fermilab to refine the proposal and prepare the Design Report. From the originally called "Giant Array Project", the "Pierre Auger Observatory" was born.

To get a full-sky coverage, two 3000 km^2 hybrid observatories, one in each terrestrial hemisphere, were planned, with the objective of giving a definite answer to the question of the high energy end of the cosmic ray spectrum, to individualize their sources, to study other primaries rather than nuclei (photons and neutrinos), reveal the chemical composition of primaries, and study hadronic interactions at the highest energies.

One of the key ingredients of Auger was its *hybrid detection* concept: a large-scale observatory that would combine the surface detection technique as exploited by AGASA or Haverah Park, and the fluorescence technique as pioneered by Fly's Eye and employed in HiRes. The Surface Detector (SD) is an array of detectors that are sensitive to the secondary particles of the EAS (muons, electrons, positrons and photons) as they reach the surface of the Earth, providing information on their arrival times and lateral distribution. The Fluorescence Detector (FD) consists of a set of telescopes that measure the UV light emitted by the atmospheric nitrogen which is excited by the particles of the shower as they traverse the atmosphere. The FD provides data on the longitudinal development of the EAS. While the SD is operational 24 hours per day, all year long, the FD can only operate on clear, moonless nights, with a duty cycle of $\sim$15%. The combination of information from the two detection systems enhances the reconstruction capability with respect to the individual detector reconstruction. A *"hybrid event"* is an EAS that is simultaneously detected by the FD and the SD.

Several aspects were taken into account for the choice of the observatory's location, related to the scientific goals and the construction feasibility [22]. These include the need of a site at $\sim 500-1500$ m above sea level to optimize the detection of showers produced by cosmic rays of 10^{19} eV. In addition, the communications and deployment requirements call for a relatively flat site with scarce vegetation and population.

The need to detect the faint fluorescence signals produced by the EAS requires a location with optical characteristics close to those sought for astronomical telescopes. Small elevations at the periphery of the site are required to install fluorescence telescopes above the dusty lower layers of the atmosphere. The availability of preexisting infrastructure and human resources was a requirement to guarantee a smooth construction, operation and maintenance of the observatory for at least 20 years.

A broad sky coverage was one of the important considerations for the selection of water-Cherenkov detectors (WCDs) for the surface detector array. WCDs can be relatively deep (e.g. 1.2 m at Haverah Park), while scintillators commonly used in arrays are much thinner. As such, a WCD allows the detection of much more inclined particles from the EAS. To optimise the uniformity in exposure of the sky with detectors that can reconstruct showers with a zenith angle up to 60°, two observatories are required at latitudes between 30° and 45° in both hemispheres.

2. The Pierre Auger Observatory

In 1996, after a world-wide survey for suitable sites for installation of the observatories, including Argentina, South Africa and Australia in the Southern Hemisphere, the International Collaboration agreed to install the Southern Pierre Auger Observatory in Argentina. This decision was based on the fact that Argentina could provide suitable sites, but also political, scientific and technological support. Main candidate sites in Argentina that were considered more seriously were Pampa Amarilla in the Departments of Malargüe and San Rafael in the Province of Mendoza, and the Meseta de Somuncura in Rio Negro Province [22]. In 1998 the Pampa Amarilla site was chosen, located at 35.0° – 35.3° S, 69.0° – 69.4° W and $1340-1610$ m above sea level. The observatory spans a total area of approximately 3000 km^2. It is the first hybrid observatory combining a surface array of water-Cherenkov detectors and a set of fluorescence detectors at the periphery of the array.

Although later on a decision was made to build the Northern Auger Observatory in Lamar, Colorado, USA, this plan was never fulfilled. However, the Telescope Array collaboration built a hybrid detector expanding the HiRes site in Utah, USA, and covering 762 km^2 [23].

The baseline design of the Pierre Auger Observatory [24] consists of 1600 surface detectors in a triangular grid with 1500 m between adjacent detectors. Twenty four fluorescence telescopes, located in four buildings at the periphery of the surface array, overlook the atmosphere above the array and record the fluorescence light produced by the cosmic air showers.

Additionally, an "Infill array" covering an area of 23.5 km^2 is composed of the regular array with added detectors at half-spacing between them, i.e., forming an array with 750 m distance between detectors. This denser array allows to trigger on smaller showers, caused by lower energy cosmic rays. This infill permits to lower the trigger threshold by one decade in energy and to detect with full efficiency cosmic rays down to 3×10^{17} eV. Given that at these lower energies the cosmic ray flux is considerably higher, the smaller surface is sufficient. To access even lower energies, some additional detectors have been placed at the central point of the 750 m-triangles, forming a 433 m-array. Furthermore, for timing and calibration studies, some array positions have been equipped with two or even three detectors. This brings the total number of detectors in the field to approximately 1660 units.

Also, to complement the FD, three additional fluorescence telescopes were installed to observe lower energy showers. These instruments are dubbed "HEAT", which stands for High Elevation Atmospheric Telescopes. As the maximum development of lower energy showers occurs higher in the atmosphere, the HEAT telescopes have a field of view with an elevation between 30° and 60°.

A full, detailed description of the Pierre Auger Observatory can be found in [24]. Fig. 2 shows one of the WCDs of the SD in front of the Los Leones FD building. Fig. 3 shows the layout of the Observatory.

Figure 2. One surface detector deployed in the field, in the background one of the FD buildings and the communications tower.

The construction of Auger began in 2001 with an Engineering Array consisting of two fluorescence telescopes and 32 WCDs deployed within the fields of view of the two telescopes. The construction and operation of the Engineering Array allowed to optimise the techniques related to the production and deployment of the detector components, the trigger algorithms, the data acquisition, monitoring software and telecommunications for both detection systems [25]. In 2004, the project entered into the production phase and in 2008 the construction of the Observatory was concluded.

2.1. The surface detector array

The principle of operation of the SD stations [24, 26] is based on the Cherenkov light emission in water. When relativistic secondary particles from an air shower propagate in water, they produce Cherenkov light. This is true for charged particles such as electrons, positrons and muons of the air shower when their speed exceeds the speed of light in water. Also, when high energy photons interact with the water, they produce electron-positron pairs which can also be detected by their Cherenkov emission.

Each WCD consists of a volume of 12,000 litres of ultra-pure water contained in a liner within a rotomolded polyethylene tank. The tanks are 3.6 m in diameter and 1.5 m high. The liner is black on the outside, for light tightness, and covered with a highly reflective and diffusive inner surface, provided by a Tyvek film, to distribute uniformly the Cherenkov light within the water volume.

The ultra-pure water (resistivity above 12 MΩ-cm) is produced in a water purification plant that was installed in the Auger Central Station in Malargüe. Once deployed at their correct positions in the field, the tanks are filled with ultra-pure water transported in clean specialized transport tanks. Because of its high purity, the water maintains its clarity without significant degradation during the lifetime of the observatory. Periodic bacteriological tests have indicated that the ultra-pure water and the environment free of light and organic residues does not support bacterial growth which could lead to reduced water clarity.

The SD stations are completely autonomous. Electrical power is provided by two 55 Wp (Watt-peak) solar panels and a pair of 12V, 105 Ah batteries, which provide a 24 V power system. Batteries are charged through a commercial charge controller. The electronics assembly at each SD station possesses a Tank Power Control Board (TPCB) which monitors the power system operation. The batteries are accommodated in a rotationally molded polyethylene battery box, protected from direct sunlight at the southern side of the tank. The solar panels are mounted on aluminium brackets, which also support a mast. Antennas for radio communications and GPS reception are mounted at the top of this mast.

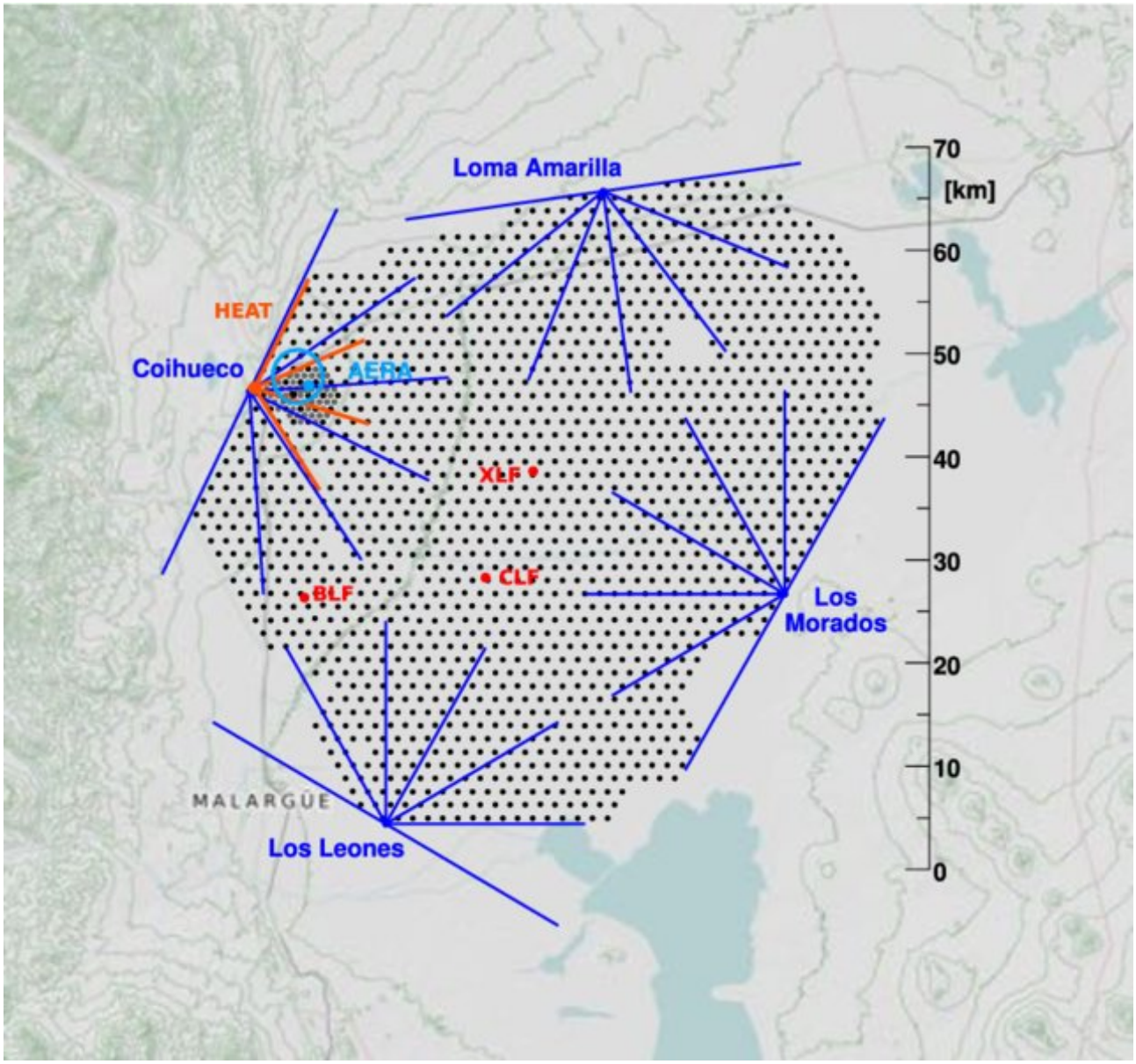

Figure 3. The layout of the Pierre Auger Observatory. Each black dot represents a WCD. The scale can also be inferred from the distance of 1500 m between adjacent detectors. Lines from the FD buildings represent the field of view of each of the fluorescence telescopes.

2.2. SD electronics

The Cherenkov light produced in the detector is collected by three 9-inch photomultiplier tubes (PMTs) which view the water volume from above, through three window domes integrated to the liner. Each PMT has two outputs. An AC coupled anode signal is provided. In addition, the signal at the last dynode is amplified and inverted by the PMT base electronics to provide a signal with 32 times the charge gain of the anode.

Six identical channels of electronics are provided to digitize the anode and amplified dynode signals from each of the PMTs. The analog signals from the PMTs are fed to Analog Devices AD9203 10 bit 40 MHz semi-flash analog to digital converters (ADCs), corresponding to time bins of 25 ns for the signals. The use of two 10 bit ADCs with a gain difference of 32 extends the dynamic range of the system to 15 bits. The maximum signal recorded before saturation corresponds to

about 650 times the peak current from a vertical muon traversing the tank, which corresponds to the signal from a 10^{20} eV cosmic ray at about 500 m from the shower core.

Each SD station contains a GPS receiver with its corresponding antenna mounted at the top of the communications mast for event timing and communication synchronization. The absolute timing of the signals in individual WCDs is relevant for reconstructing the shower front and computing the arrival directions of the incoming cosmic rays. The time-tagging system allows to adjust the ADC data to GPS time within 10 ns RMS.

Communications with the Central Station is done through a WLAN customs radio network operating in the 902-928 MHz band. Four concentrators located at the FD buildings collect the data from the field and transfer it through a dedicated microwave link to the Central Station. This microwave link also transports the FD data. Communications with the individual WCDs is bidirectional, so that the full trigger information can be requested from the WCD by the Central Data Acquisition System (CDAS) on demand, and software updates and reset commands can be sent to the individual detectors.

2.3. SD trigger, calibration and event reconstruction

The SD trigger system is hierarchical. The first two triggers (T1 and T2) are at the local level of each WCD, whereas the third level trigger, T3, occurs at a global level [27]. The first level trigger, T1, has different independent modes. It triggers either when all three PMT signals exceed a threshold value, or on lower signals extended in time. The second trigger level, called T2, decreases the global rate of the T1 trigger down to about 23 Hz. All T2s send their timestamp to CDAS for the global trigger (T3) determination.

To identify real EAS, a coincident T2 trigger in adjacent WCDs is required. For example, at the highest energies, above 10^{19} eV, the footprint of the air shower on the ground extends over more than 25 km^2. To apply the main trigger condition, the central trigger processor is used to identify groups of locally triggered stations clustered in time and space. At least three stations in a compact configuration and in a compatible time window are required to form a T3 trigger. With the arrangements described above, the total T3 trigger rate of the observatory is presently of the order of 0.1 Hz and about 3 million SD events are recorded yearly. The T3 trigger is the shower trigger that results in the recording of 768 samples (19.2 μs) of the six signals (anode and last dynode signal from each of the three PMTs).

The SD array has full trigger efficiency for events of energy above 2.5×10^{18} eV. The Infill array allows to reduce the threshold for full acceptance by more than a full order of magnitude in energy.

Calibration of the SD stations is performed during routine operation of the detector. The total bandwidth available from each SD station to the central station requires that the calibration be done by the local electronics. Also, the remoteness of the detectors requires the calibration procedure to be robust.

The Cherenkov light recorded by a surface detector is measured in units of the signal produced by a muon traversing the tank on a vertical trajectory through its centre. This unit is termed the “vertical equivalent muon” (VEM). The goal of the surface detector calibration is to measure the value of 1 VEM in hardware units (i.e., in integrated FADC channels). The conversion to units of VEM is done both to provide a common reference level between tanks and to calibrate against the detector simulations.

For this purpose, each station has a trigger mode which allows to record small signals, which are mostly due to single muons and other single particles traversing the detector. A histogram of the total charge produced by these signals has a characteristic peak which is related to the total signal deposited by omnidirectional atmospheric muons. The relation between this histogram peak and the signal produced by a single, through-going vertical muon can be established from measurements with muon hodoscopes. Ref.[28] describes in detail the calibration method of the surface detector.

To ensure good quality of the data used for physics analysis, two additional off-line “triggers” are implemented. One of them, called T4, selects real showers and discards random coincidences of nearby detectors which have triggered on low energy showers. This trigger is mainly based on a coincidence between adjacent detector stations within the propagation time of the shower front. Additionally, a fiducial cut is applied to preserve events whose shower core is within an area well enclosed by functioning detectors. This cut is required both to make sure that the reconstruction is not biased and to define a precise volume for acceptance calculations.

The reconstruction of the energy and the arrival direction of the cosmic rays producing air showers that have triggered the surface detector array is based on the signal sizes and start times of the traces registered by individual stations. For a recent summary, see [29]. The total signal recorded by the WCDs, which is a measure of the total energy transferred to Cherenkov light inside the detector, is converted into units of VEM. Reconstruction of showers with the SD requires fitting the signals observed in each of the triggered detectors to a lateral distribution function, and the arrival times to a shower front shape. This allows to reconstruct the impact point of the shower core, the azimuthal and zenith angle of the shower axis, and the lateral spread of the signal as a function of the distance to the shower axis. From the information on the lateral spread of the shower, the signal expected at a reference distance of 1000 m from the shower axis, $S(1000)$, can be interpolated. The reference distance of 1000 m is chosen because it minimises the fluctuations in the expected signal for the array geometry with a spacing of 1500 m between adjacent detectors. However, this value of $S(1000)$ needs to be corrected for the dependence of the atmospheric attenuation with zenith angle. For this correction, a Constant Intensity Cut method is used, which is based on the fact that the flux of cosmic rays above a certain energy is independent of the arrival zenith angle. A correction factor is applied to the $S(1000)$ as a function of zenith angle and energy, so that the fluxes are

equalized in all zenith angle bins. The zenith angle-corrected $S(1000)$, normalized to its value at the median angle of 38° is called S_{38°. The assignment of the absolute energy scale to S_{38° is based on the hybrid data acquired in conjunction with the FD and will be mentioned in the following section.

The accuracy in the evaluation of the arrival direction of the shower depends on the start times of the individual stations. Timing precision with the WCDs is of 10 ns. The overall angular reconstruction accuracy of the WCDs can be derived by means of simulations, and at the highest energies it results to be better than 1° for all simulated primary masses and shower axis directions.

Fig. 4 shows a typical event recorded by the Auger SD in 2020.

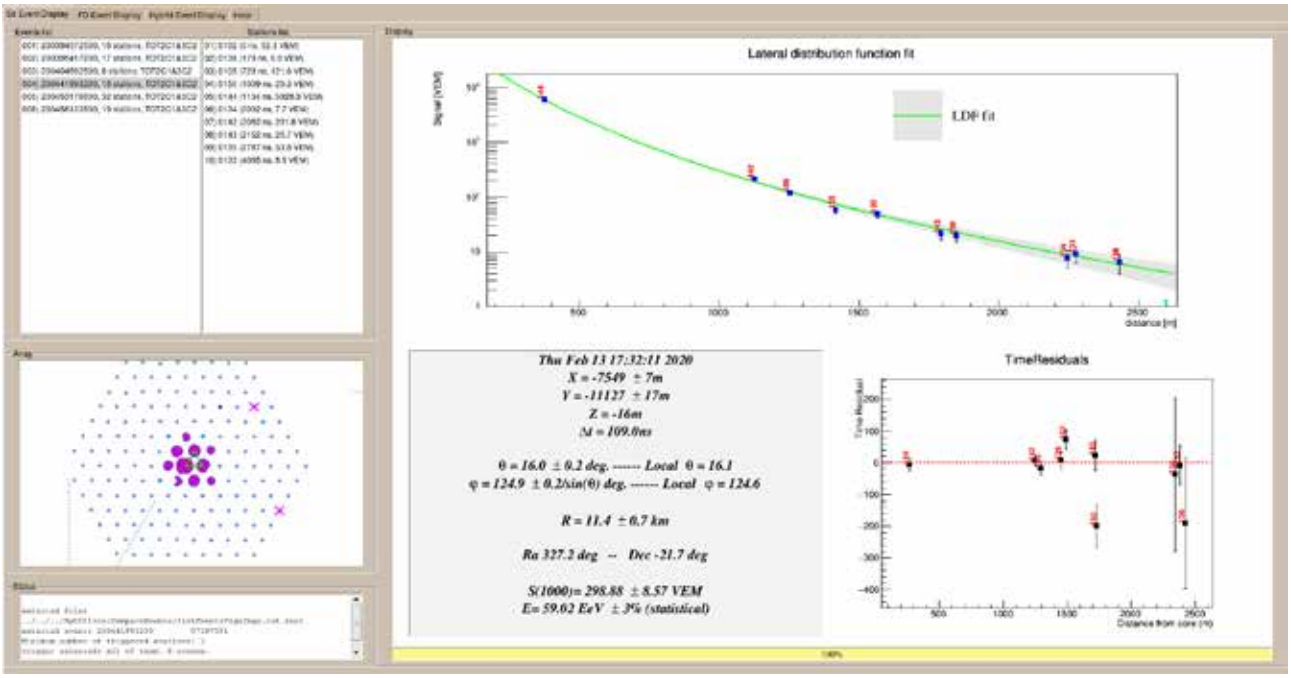

Figure 4. A typical event recorded with the Surface Detector Array, as visualized with the Auger Event Display. The lateral distribution of signals in the intervening SD is shown as a function of the distance to the shower core, together with the fitted lateral distribution function.

2.4. The fluorescence telescopes

The 24 fluorescence telescopes [24, 30] are located in four buildings at the periphery of the SD array, on small elevations named Los Leones, Coihueco, Loma Amarilla and Los Morados. Each site hosts six telescopes, in six independent bays within a building with controlled climate. Each telescope has a field of view from 1° to 31° in elevation and covering 30° in azimuth.

Nitrogen fluorescence light, emitted isotropically by an air shower, enters through a circular diaphragm of 1.1 m radius covered with a filter glass window which only allows the passage of UV light, to reduce the background light. The filter also serves as a window over the aperture. The telescopes are based on Schmidt optics to reduce the coma aberration of large optical systems. A shutter system and fail-safe curtains protect the telescope when not in operation or when excessive outside light or weather effects are detected. A simplified annular lens to correct spherical aberration and eliminate coma aberration is mounted in the outer part of the aperture.

The fluorescence light is collected by a segmented spherical mirror of 3400 mm radius of curvature onto a spherical focal surface with radius of curvature 1700 mm. The primary mirror has an area of 13 m^2. The camera consists of an array of 440 photomultiplier tubes of 40 mm diameter each. These are arranged in a matrix of 22 rows by 20 columns. The field of view of each pixel corresponds to an angular size of 1.5°.

The FD electronics must provide a large dynamic range and strong background rejection, while accepting any physically plausible air shower. Moreover, the electronics includes capabilities for antialias filtering, digitizing, and storing signals from the PMTs. The signal is shaped and digitized in the front-end electronics (FE) unit, where threshold and geometry triggers are also generated. Analog boards in the FE unit are designed to handle the large dynamic range required for air fluorescence measurements; this means a range of 15 bits and 100 ns timing.

As the PMT data are processed, they are passed through a flexible three-stage trigger system implemented in firmware and software. The trigger rate of each pixel in a camera (first level trigger) is kept around 100 Hz by adjusting the pixel threshold level. The algorithm of the second level trigger searches for track segments at least five pixels in length within a camera. The typical trigger rate per camera fluctuates between 0.1 and 10 Hz. The third level trigger is a software algorithm

designed to clean the air shower data stream of noise events that survive the low-level hardware triggers. It is optimized for the fast rejection of triggers caused by lightning, triggers caused by cosmic ray muon impacts on the camera and randomly triggered pixels. Data from an event that survives all three trigger levels is merged between all the telescopes and generates a hybrid trigger (FD-T3) for the surface array. The event rate is about 0.012 Hz per site for the 24 baseline telescopes.

It should be noticed that unlike the SD, for the FD the energy threshold for detection depends on the distance and the relative geometry of the shower with respect to the FD building.

The precise reconstruction of air shower longitudinal profiles requires the conversion of an ADC count to a light flux for each pixel that receives a portion of the signal from a shower. To this end, the absolute calibration of the detector response is essential. In the first years of operation, a calibrated, large diameter, drum-shaped light source provided an absolute, end-to-end calibration for each pixel of the fluorescence telescopes, with independent verification for some pixels by atmospheric Rayleigh scattering from vertical laser pulses. For these absolute methods, the flux of photons on the telescope aperture is independently measured. The effects of diaphragm area projection, optical filter transmittance, mirror reflectivity, pixel light collection efficiency and area, cathode quantum efficiency, PMT gain, preamplifier and amplifier gains, and digital conversion are all included in the end-to-end calibration procedure. Presently, a new calibration method is being implemented, based on a calibrated point-like UV light source, which is movable and scans all the front surface of the aperture of the telescopes.

Hybrid events are those recorded simultaneously by FD and SD systems. Hybrid events allow a very precise timing of arrival of the shower, which is required for a precise geometric reconstruction. Events that trigger three or more SDs, so that an independent reconstruction can be made with SD alone, are named “Golden hybrid”. These are of particular importance for the energy calibration of the SD events.

2.5. Energy calibration

Once the geometry of the shower is known, the light collected at the aperture as a function of time can be converted to the energy deposited by the shower as a function of the traversed atmospheric depth X. For this purpose, the light attenuation from the shower to the detector needs to be accounted for, and all contributing light sources need to be disentangled: fluorescence light, direct and scattered Cherenkov light as well as multiply scattered light. The proportionality between the fluorescence intensity and the energy deposit is given by the fluorescence yield. A good knowledge of its absolute value as well as its dependence on wavelength, temperature, pressure and humidity is essential to reconstruct the longitudinal profile.

The full longitudinal profile of the energy deposit and its maximum $(dE/dX)_{\max}$ at depth $X = X_{\max}$ are estimated by fitting an asymmetric bell-shaped Gaisser–Hillas function to the time profile of photoelectrons detected in the PMTs of the FD cameras. For this purpose, a log-likelihood fit is used in which the number of photoelectrons detected by the PMTs of the FD cameras is compared to the expectation from the Gaisser-Hillas function after folding it with the light yield, atmospheric transmission, lateral distributions and detector response.

Finally, the calorimetric energy of the shower is obtained by integrating over the total longitudinal profile and the total energy is estimated by correcting for the “invisible energy” carried away by neutrinos and high energy muons.

To assign the energy to the showers detected with the SD, the “golden hybrid” events are used for cross-calibration. High-quality hybrid events with reconstructed zenith angles less than 60° are used to relate the shower size from SD to the almost-calorimetric measurement of the shower energy from FD, E_{FD}. For the FD part of the event, we require an accurate fit of the longitudinal profile. Furthermore, the depth of the shower maximum $\mathrm{X_{max}}$ must be contained within the telescope field-of-view and measured with an accuracy better than 40 g/cm^2. The uncertainty on the reconstructed E_{FD} is required to be less than 18%. The final criteria for defining the calibration data sample include a selection of data with clear atmospheric conditions.

The final step in the calibration analysis leads to a relation between S_{38° and E_{FD}. The correlation between the two variables is obtained from a maximum likelihood method which takes into account the evolution of uncertainties with energy, as well as event migrations due to the finite energy resolution of the SD. The relation between S_{38° and E_{FD} is well described by a single power law function, as shown in Fig. 5 [34].

Systematic uncertainties in the energy scale add up to 14%, the major contribution arising from the absolute calibration of the telescopes, with a value of 9.9%, the other contributions arising from fluorescence yield, atmosphere, profile reconstruction, estimation of invisible energy and energy scale stability.

The recorded dataset extends up to larger angles approaching 90°. For the inclined events, with zenith angles larger than 60°, we employ a different reconstruction method, yielding to the energy estimator N_{19}, the relative muon content with respect to simulated proton showers at 10^{18} eV. The energy range of full efficiency of the surface detector has been extended down to 3×10^{16} eV using the events recorded by the infill array. For infill events, the analogous energy estimator is S_{35°.

2.6. Complementary equipment and infrastructure

Other vital components and equipment relevant to the functioning of the Observatory are described in [24] and in references therein. These include the full communications system, the Central Data Acquisition System (CDAS), the data handling and storing, the monitoring tools and the Offline framework for data processing and analysis.

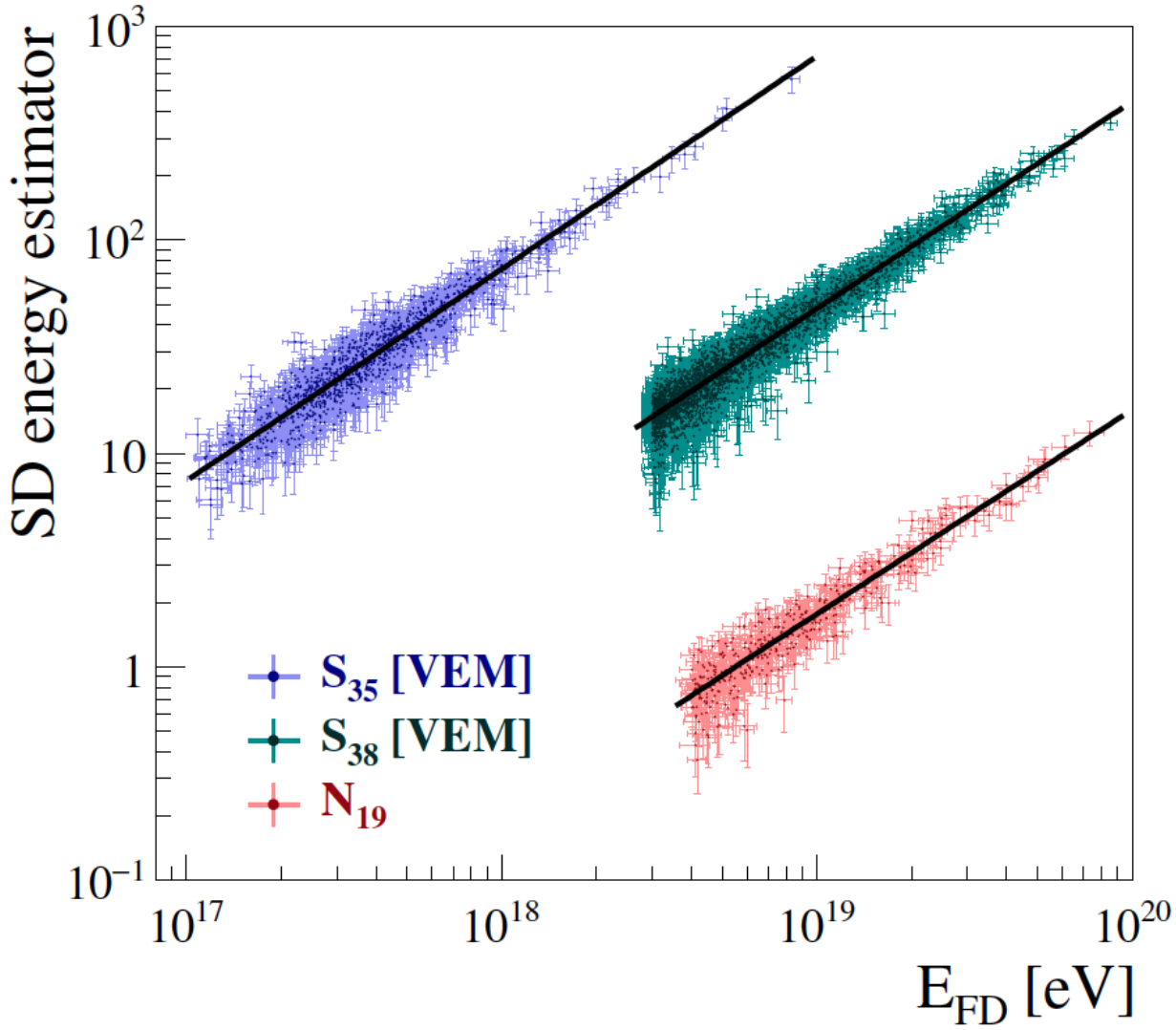

Figure 5. Relation between the SD energy estimator S_{38° and the calorimetric FD energy E_{FD} for good quality golden hybrid events. Also shown is the relation with the energy estimator S_{35° for lower energy showers detected with the 750 m infill array, and the energy estimator N_{19} for inclined showers.

The Pierre Auger Observatory runs an extensive atmospheric monitoring program for characterizing the atmosphere,both to understand the light absorption for FD and to obtain the input parameters for the weather correction of SD events (pressure, temperature, air density).

The knowledge of the vertical atmospheric profile is of paramount importance for understanding the shape of the longitudinal shower development in the atmosphere. In the first years of operation of the Observatory, radiosondes were launched from the observatory site to measure air properties as a function of height. This information was used to calibrate the atmosphere to the information provided by the Global Data Assimilation System (GDAS), which is now used as input for shower reconstructions.

The observatory additionally uses five ground-based weather stations to monitor the ground-level pressure, temperature, humidity, and wind velocity with a time resolution of 5 min.

The atmospheric monitoring includes two laser facilities, dubbed CLF and XLF, installed at 12km from each other in the centre of the array, from which vertical UV laser pulses are fired. This laser light is registered by the FD telescopes in order to determine the light attenuation in the atmosphere. At the CLF station there is also a Raman LIDAR system, which is used to make three measurements of the vertical aerosol profile each night: before, during, and after the FD observations.

LIDARs located near the FD buildings record the back-scattered light in order to determine cloud levels and aerosol layers. Cloud monitoring cameras, photometric robotic telescopes for star tracking, and aerosol samplers complete the available equipment.

3. Main scientific results

3.1. Spectrum

The Pierre Auger Observatory allows to determine the spectrum of Ultra-High-Energy cosmic rays at the highest energies with unprecedented precision.

The regular surface detector array (SD array with a spacing of 1500 m between adjacent detectors), after calibration with the hybrid data acquired together with the FDs as explained before, allows to reconstruct the spectrum spanning the energy interval starting from 2.5×10^{18} eV up to the highest energies. At the lower limit, the SD array still has full acceptance, therefore the determination of the aperture is based only on the array geometry and the uptime of the WCDs. The most recent dataset contains more than 215,000 events with reconstructed zenith angle $\theta < 60^{\circ}$, corresponding to an exposure of (60,400 ± 1,810) km^2 sr yr. The addition of "inclined" events with $60^{\circ} < \theta < 80^{\circ}$ allows to increase the exposure by roughly 30%.

The Pierre Auger Observatory has capabilities to extend the spectrum below the energy range described above (see [31] and references therein). To determine the spectrum below the full aperture of the 1500 m SD, hybrid events recorded by the FD in combination with one of the SD, allow to go down in energy to $E > 10^{18}$ eV. Even lower energies, $E > 10^{17}$ eV, can be achieved with the SD infill, where WCDs have a spacing of 750 m. Using events detected with the HEAT telescopes, which are dominated by Cherenkov light, allows to study the spectrum at energies as low as $E > 10^{16.5}$ eV [33, 34].

The full, combined spectrum, is depicted in Fig. 6. Given that the flux is a steep function of the energy, is is customary to plot the flux multiplied by a power of the energy (in this case, E^3), to highlight the features of the spectrum.

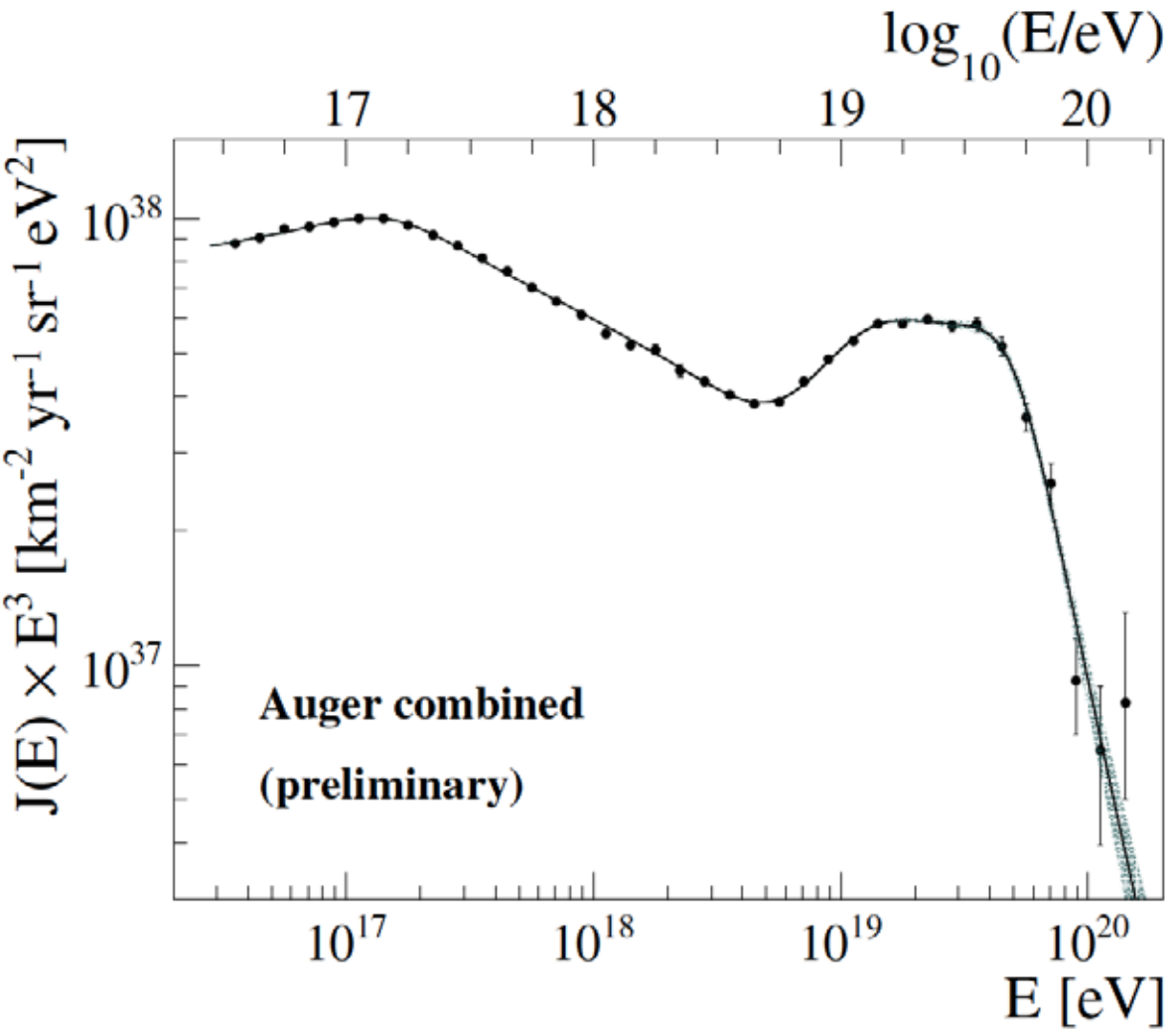

Figure 6. The combined spectrum of the Pierre Auger Observatory, multiplied by E^3 to emphasize its features.

The spectrum above 2.5×10^{18} eV can be well fitted with a broken power law in four intervals, as described in [32]. In each interval, the functional form is assumed to be $dN/dE \sim E^{-\gamma}$, where γ is the spectral index in the corresponding

interval. The high-energy suppression has been clearly identified above an energy of $E_{34} = (46 \pm 3 \pm 6) \times 10^{18}$ eV with a slope given by $\gamma_4 = 5.1 \pm 0.3 \pm 0.1$, confirming with the highest precision the previous reports of the strong attenuation of the flux at these energies [21, 35, 36]. Determining whether this suppression is a GZK-like effect arising from the propagation of cosmic rays in the intergalactic medium, or due to an exhaustion of the injection power of the astrophysical sources is as yet not clear. To find an answer to this question is one of the main goals of the Upgrade, described further on in this review.

The "ankle" is a known spectral feature described by a rollover at $E_{12} = (5.0 \pm 0.1 \pm 0.8) \times 10^{18}$ eV, marking a hardening of the spectrum from $\gamma_1 = 3.29 \pm 0.02 \pm 0.10$ to $\gamma_2 = 2.51 \pm 0.03 \pm 0.05$. This ankle has been widely reported in the literature [21, 37, 38]. Different possible explanations have been suggested for this feature, e.g. the transition from a galactic to an extragalactic origin of cosmic rays, or a dip due to the contribution of e^+- e^- pair production resulting from cosmic ray proton interactions with the cosmic microwave background. The Auger measurements favor instead the interpretation that it results from the transition from an extragalactic component dominated by light elements for lower energies to one with intermediate and heavier masses at higher energies.

A novel feature that also has to be accounted for in an integrated description of the spectrum is the break at $E_{23} = (13 \pm 1 \pm 2) \times 10^{18}$ eV, where the spectrum softens from γ_2 to $\gamma_3 = 3.05 \pm 0.05 \pm 0.10$.

At lower energies, the spectrum shows a clear inflection point corresponding to the so-called "second knee" around 10^{17} eV, which is normally explained as related to the maximum energy at which the Fe group galactic cosmic rays can be accelerated.

3.2. Composition

The determination of the mass composition of the primary cosmic rays is a major experimental challenge. The most precise and straightforward determination is based on the analysis of the atmospheric depth at which the shower exhibits its maximum development, X_{max}. Showers initiated by protons and other light primaries develop deeper in the atmosphere, leading to larger values of X_{max}. Also, the number of muons N_μ in the shower is a good proxy for studying the composition: showers from light primaries contain less muons than showers initiated by heavier nuclei, as will be described in Section 4. From a simple superposition model (see, e.g., [39]), the $\langle X_{max} \rangle$ of the showers varies linearly with $< \ln A >$, being A the atomic mass of the primary, and it is therefore a sensitive parameter for mass composition. Although more complex to interpret for mixed compositions, the behaviour of the fluctuations of X_{max}, i.e., $\sigma(X_{max})$, also gives information of the primary mass.

The direct measurement of X_{max} can only be achieved with the fluorescence technique. The HEAT telescopes provide the adequate field of view to record the low energy showers that develop higher in the atmosphere.

Comparing X_{max} and its standard deviation to results from simulations based on different hadronic interaction models allows us to interpret its evolution with energy. The latest results can be found in [34, 33] and are displayed in Fig. 7. Based on 47,000 hybrid events, this analysis shows a trend towards lighter composition as energy increases up to 2×10^{18} eV and then to a heavier composition at higher energies.

The elongation rate is defined as the variation of the average X_{max} with energy, $d\langle X_{max} \rangle / d \log E$. The values obtained are 77 ± 2 (stat) g cm^{-2}/decade below $E_0 = 10^{18.32 \pm 0.03}$ eV and 26 ± 2 (stat) g cm^{-2}/decade above this energy. This result suggests a composition getting lighter up to E_0 and going towards intermediate-heavy masses above it. As can be seen in the comparison to results from simulations, the observed elongation rate is not compatible with a constant composition, which would require instead an elongation rate of ~ 60 g cm^{-2}/decade in the whole energy range. The results reported for $\sigma(X_{max})$ at the highest energies strongly suggest a pure and heavy composition, while in the lower energy range they are compatible with both a light or mixed composition.

Other more indirect methods for the determination of the primary mass have also been explored [40]. Although not so precise, given the higher statistics they allow to measure composition in a broader energy interval.

Any integral astrophysical interpretation of the Auger data has to describe both the spectral features and the composition evolution with energy. A combined fit of spectrum, mass composition and its fluctuations has been described in [32, 41]. The fit has been performed for energies above 5×10^{18} eV, i.e. the region above the "ankle" of the all-particle spectrum. The astrophysical model consists of identical sources uniformly distributed in comoving volume, where nuclei are accelerated through a rigidity-dependent mechanism. The fit results suggest that the sources are characterized by relatively low maximum rigidity of the particles at the acceleration site, hard spectra and mixed chemical composition, with heavier elements becoming dominant as the energy increases. The steepening of the spectrum at $\sim 10^{19}$ eV suggests the interplay between the flux contributions of the helium and carbon-nitrogen-oxygen components injected at the source with their distinct cut-off energies, combined with photodisintegration effects during the propagation. However, uncertainties about physical quantities relevant to cosmic ray propagation and shower development have a non-negligible impact on the fit results. To make progress along these lines of research, a more precise determination of the mass composition on an event-by-event basis is required, with high statistics to reach the upper end of the spectrum where events are scarce. This program is pursued with the Upgrade of the Auger Observatory described in Section 4.

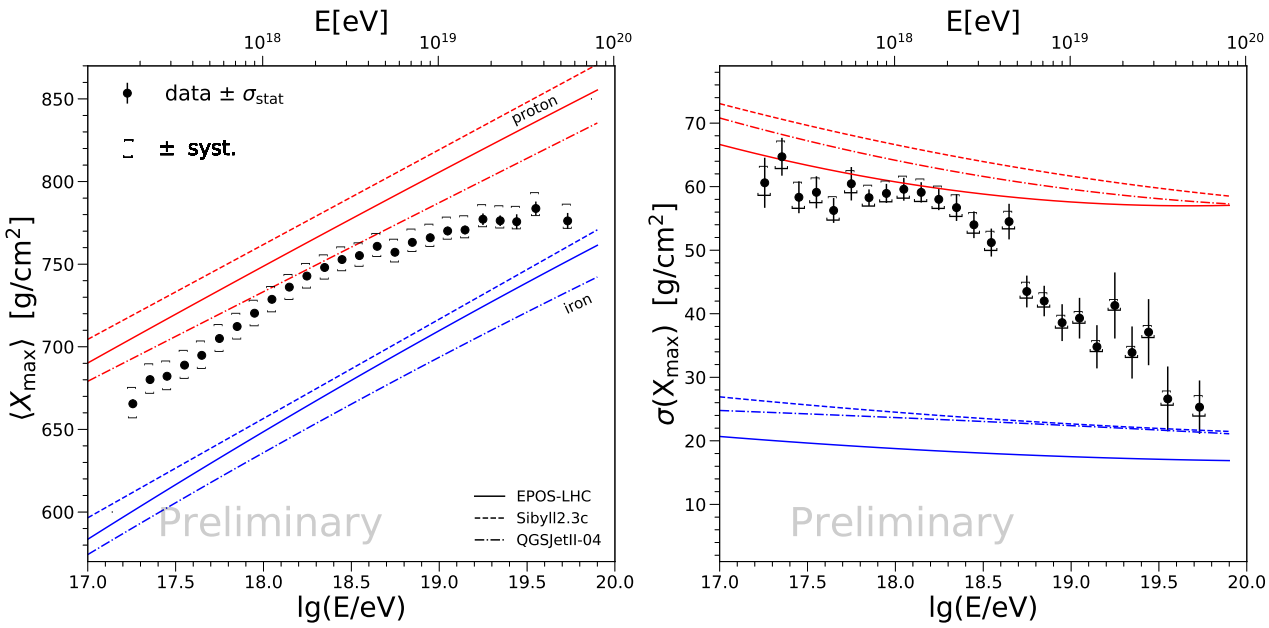

Figure 7. X_{max} (left) and $\sigma(X_{max})$ (right) as a function of primary energy, and comparison to the expectations from simulated showers with different hadronic models for proton (red) and iron (blue) primaries.

3.3. Arrival direction anisotropies

A basic objective in the study of cosmic rays and in the quest to determine their origin is the search for anisotropies in the arrival directions. These anisotropies might manifest themselves at different angular scales and energy ranges.

At higher energies, cosmic rays are expected to come from nearby, as the flux from far away sources is suppressed due to energy losses suffered during propagation. On the other hand, the particles with larger rigidity are expected to suffer smaller deflections by the galactic and intergalactic magnetic fields. Therefore, at the highest energies, tracing backwards the arrival directions should hint to the sources, or at least reveal anisotropies correlated with the directions of the sources. Searches for anisotropies on small and intermediate angular scales have been performed by exploiting 15 years of data, reaching an unprecedented exposure of ∼100,000 km^2 sr yr in a declination range between $-90°$ and $+45°$. One strategy for searching for anisotropies is based on scanning the sky for an excess in the flux of particles in different angular scale windows. The advantage of this search is that it is model independent and does not require any assumption on the possible sources. This search was performed over the whole field of view, in a wide energy threshold range $E_{thr} = 32\text{-}80 \times 10^{18}$ eV, using a 1×10^{18} eV step and scanning circular regions of radius Ψ from 1° to 30° in steps of 1°. The most significant excess was found for $E > 3.8 \times 10^{19}$ eV in an angular window of 27° centered in the direction ($\alpha = 202°$, $\delta = -45°$) [34]. This direction corresponds to a region densely populated with extragalactic objects, among which is Centaurus A, our closest radio galaxy. Indeed, the excess of events in its direction, already pointed out in the past [42], reached a one-sided post-trial significance of 3.9σ for energies above $E_{thr} = 3.7 \times 10^{19}$ eV and for $\Psi = 28°$.

The arrival directions of ultrahigh energy cosmic rays were also studied by searching for correlations with the distribution of nearby extragalactic matter. This has been modelled by using different catalogs of possible sources up to a distance of ∼250 Mpc. In [34, 42], the following sources were considered: (a) a sample of 32 starburst galaxies (SBGs) selected based on their continuum emission at 1.4 GHz, used as a proxy for their UHECR flux; (b) a selection of γAGNs from the 3FHL catalog, weighting the sources with the integral flux from 10 GeV to 1 TeV; (c) the 2MRS catalog of nearby matter farther than 1 Mpc; (d) a selection of Swift-BAT radio-loud and radio-quiet AGNs.

In this analysis, we exploited the source directions and also the possible scenarios for the relative UHECR fluxes from source candidates provided by the observations from Fermi-LAT. Furthermore, our current knowledge of the cosmic ray composition could be used to evaluate the attenuation in intensity due to the energy losses during propagation. A likelihood ratio analysis allowed us to evaluate the smearing angle and the fraction of anisotropic cosmic rays for each case. The highest significance is obtained for the case of SBGs, where we found an anisotropic fraction of (11±5)% of events with energy above 3.8×10^{19} eV in a smearing angle of 15°. Note that the attenuation of particles in the case of the nearby SBGs is much less important than for more distant blazars. After penalization for the scanning in energy, the significance of the correlation results to be 4.5σ.

In 2017, the Pierre Auger Collaboration announced the observation of a large-scale anisotropy in the arrival directions of cosmic rays above 8×10^{18} eV [43]. This analysis was extended in [44] to a broader energy range, using about 15 years of data. For energies above 4×10^{18} eV, data from the fully efficient 1500 m SD array were used, reaching a total exposure of 92,500 and 60,700 km^2 sr yr for events with $\theta \leq 80°$ and $\theta \leq 60°$ respectively. Under the assumption that

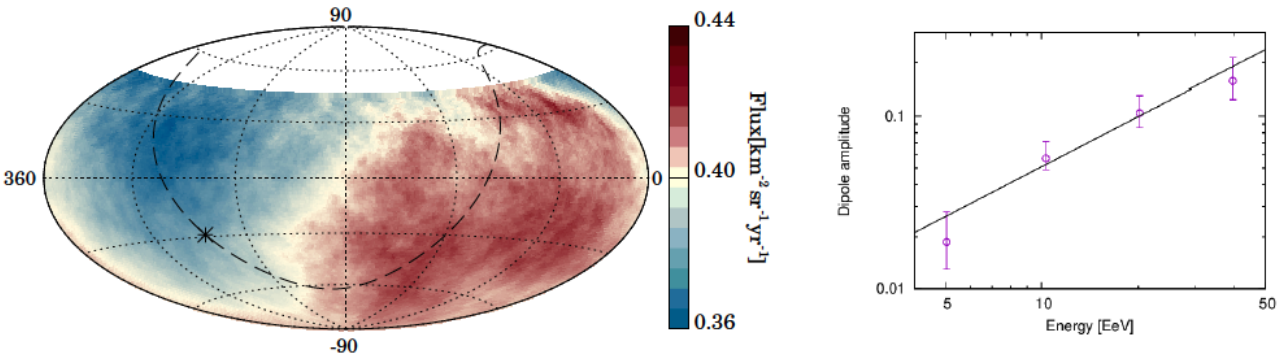

Figure 8. Left: Map of the flux of cosmic rays above 8×10^{18} eV, in equatorial coordinates. The Galactic plane and the Galactic centre are indicated by a dashed line and a star, respectively. The flux is averaged on windows of 45° radius. Right: Energy dependence of the dipolar amplitude measured in four energy bins above 4×10^{18} eV.

higher multipoles are negligible, we found a total dipolar amplitude for $E \leq 8 \times 10^{18}$ eV of $d = 0.066 \pm 0.012$, with a 6σ significance, pointing $\sim 125^{\circ}$ away from the direction of the Galactic centre, as shown in Fig. 8. This result strongly indicates an extragalactic origin of the modulation.

3.4. Search for neutrinos and photons

The Pierre Auger Observatory possesses the capability of recording and identifying extensive air showers initiated by neutrinos or photons. The interaction of UHECRs with the radiation background during their propagation is expected to produce a diffuse flux of neutrinos and photons, caused by the decay of charged and neutral pions respectively, produced in the photon-nucleon collisions. The resulting neutrino and photon fluxes depend critically on the cosmological evolution of the cosmic ray sources, and on their composition and injection spectra [45].

In FD, high energy photons can be identified because they are more penetrating than nuclei, therefore producing a much larger X_{max}. With SD, photon showers are characterised by a very low muonic content in the shower and by its steeper lateral distribution.

The search for neutrinos is based on the study of horizontal showers. When initiated by nuclei, very inclined showers traverse a large amount of air, thus producing a shower development in which the electromagnetic component has been very much attenuated, therefore the shower is dominated by energetic muons. Contrarily, showers initiated by neutrinos are expected to develop much deeper in the atmosphere, therefore still containing a large electromagnetic component when reaching the SD. Also, Earth-skimming tau-neutrinos can give rise to upwards pointing showers that are a characteristic signature for neutrinos. It turns out that Auger has an aperture for the detection of neutrinos at the highest energies that is comparable to that of other neutrino observatories.

Photons and neutrinos propagate through space in lightlike paths, therefore no time delays are expected with respect to gamma or radio emissions. This capacity positions the Auger Observatory as an important partner in multimessenger astronomy.

Present Auger limits on photon and neutrino fluxes at ultra-high energy can be found in [46, 47]. The upper limits on the photon flux have been relevant to exclude some "top-down" source scenarios, such as those in which ultrahigh energy cosmic rays originate from the decay of super-heavy particles. The limits above 10^{18} eV energies also constrain the most optimistic models of photon production from the interaction of protons with the Cosmic Microwave Background. Present bounds on neutrinos and photons will be further improved as statistics increases with increased aperture.

3.5. Additional results

3.5.1. Hadronic interactions

Collisions of cosmic ray protons of energies of 10^{20} eV with air nuclei have a centre of mass energy $\sqrt{s}$ larger than 400 TeV, which is more than 30 times beyond the reach of human-made accelerators. Therefore, the observation of the development of showers in the atmosphere can provide valuable information about high-energy hadronic interactions in an energy range not yet accessible with particle colliders. The shower development depends on many different features of the hadronic interactions. In particular, by measuring the depth of maximum development of the EAS, X_{max}, we obtain information about the cross-section of the first interaction. The determination of the muonic component at the ground is more sensitive to the details of the hadronic interactions along many steps of the cascade, like the multiplicity of the secondaries and the fraction of electromagnetic component with respect to the total signal. On the contrary, the intrinsic muon fluctuations mostly depend on the first interactions. Clear evidence for a deficit of the number of muons predicted by the models was reported by the Auger Collaboration by exploiting different techniques such as the study of inclined showers [48], comparison of the development of the lateral and longitudinal profiles of showers with models [49], the study of the muon production depth [50] and of the time profiles of the signals recorded with SD [40].

More recently and at lower energies, the deficit of muons in the models was also confirmed by directly measuring the muon content in EAS with an array of underground muon detectors (AMIGA project, see Section 4), while comparing with the X_{max} obtained from FD [55]. The resulting predicted muon content is 38% too low when the hadronic interaction model EPOS-LHC is used, the mismatch increasing to 50% - 53% at the two energies in the case of QGSJetII-04.

Shower-to-shower fluctuations of the muonic component could also be measured with hybrid inclined showers [56], at the same time updating the results on the mean muon number. The expectations for the relative fluctuations are compatible with the experimental results, while models and data show a significant discrepancy in the average muon scale. These results thus suggest that models are describing reasonably well the distribution of energy going into the electromagnetic component after the first interaction, while the discrepancy in the overall muon number should be explained by changes in the characteristics of hadronic interactions at all shower stages.

3.5.2. Atmospheric phenomena: ELVES

ELVES is an acronym for "Emissions of Light and Very low frequency perturbations due to Electromagnetic pulse Sources". They are transient luminous events produced at the base of the ionosphere by the intense electromagnetic pulses emitted during lightning discharges. These intense flashes of light appear in the night sky as rapidly expanding quasi-circular fronts; generated at 80–95 km altitudes, they are visible at distances of several hundred kilometers. The original pulse lasts less than 20 μs, but the propagating light front is visible for a few milliseconds.

The first clear observation of ELVES was made using a high-speed photometer from the Space Shuttle. More recently such phenomena were studied using photometers either based at the ground or on satellites.

After the first serendipitous observation of an ELVES event during an FD shift, further studies, done on a sample of data taken in the period 2008–2011, have shown that the FD is ideally suited for detailed studies of ELVES. A new, modified third level trigger algorithm was implemented in March 2013 to increase the detection and recording efficiency of these events. Since then, a large fraction of these events is regularly recorded, and a new dedicated readout scheme has been gradually improved to allow recording of the light emission, from farther and farther distances [51].

Auger has detected thousands of ELVES events with an unprecedented time resolution of 100 ns. These observations facilitate the study of the frequency of such events and of the correlation with other atmospheric phenomena.

3.5.3. Space weather

Every second, the Pierre Auger surface detectors record the rate of low energy particles detected and report this information to the central data acquisition system. This event rate is related to the flux of low energy Galactic cosmic rays reaching the Earth, which is modulated by the solar activity. Therefore, by measuring with great precision the flux variations, and after correction for atmospheric effects, the Pierre Auger Observatory is able to contribute to the Space Weather program, in a way similar to neutron monitors.

A description of the Pierre Auger low energy detection mode can be found in [52]. More information about Space Weather and cosmic rays can be found on the webpage http://www.spaceweather.com/.

4. AugerPrime: The upgrade of the Pierre Auger Observatory

4.1. Science case for the upgrade

So far, the Pierre Auger Observatory has provided important results regarding the upper end of the cosmic ray spectrum, the spectral features at lower energy, the search for anisotropies at different angular scales and the composition of the primaries. However, these findings open up new questions and a full, integrated picture is still missing. Having established the existence of a sharp steepening of the cosmic ray spectrum at the highest energies, it is natural to inquire about the origin of this suppression. It may be due to energy losses during propagation of the cosmic rays from their sources to the Earth, but it could also be an indication of the upper limit of the power of the accelerating sources. Also, the spectral features at lower energy could be an indication of the transition from galactic to extragalactic origin or it may be due to propagation losses. Therefore, for a full understanding of the observations, a combined analysis of the spectrum and the composition is required. Although anisotropies in the arrival directions have been found, the search for the sources is still not concluded. Hints towards a heavier composition at higher energies suggest greater magnetic deflections, which hinders the search for point sources. If, however, even a small fraction of cosmic rays of the highest energies is composed of protons, identifying these protons might lead to a possible indication of the sources. The measurement of the fraction of protons is a decisive ingredient for assessing the prospects for proton astronomy with future ultra-large detectors.

Determining the mass composition of ultra-high energy cosmic rays is closely related to, and crucially depends on understanding extensive air showers and hadronic interactions. When estimating the number of muons in air showers from Auger data, a discrepancy is currently found between the observed and expected muon numbers. The study of extensive air showers and hadronic multiparticle production is a further open field of research, including the exploration of fundamental particle physics at energies well beyond those accessible at terrestrial accelerators as well as the derivation of constraints on new physics phenomena, such as Lorentz invariance violation or extra dimensions.

In 2015, the Pierre Auger Collaboration agreed to design and build an upgrade of the Observatory to address the open science questions described above. The Upgrade is described in [53, 54]. To accomplish its science objectives, it will be of paramount importance to improve the composition sensitivity and to extend it into the energy region of the flux suppression. This will allow us to:

- measure the composition-discriminated flux in the range from about 10^{18} eV up to the highest energies,
- carry out composition-enhanced anisotropy searches based on event-by-event estimates of the primary mass,
- search for GZK secondaries as tracers of proton primaries,
- search for ultra-high energy secondary photons produced in or near cosmic ray sources,
- understand the muon deficit in shower simulations,
- test our understanding of hadronic interactions at c.m.s. energies near and beyond 60 TeV.

Presently, determinations of the cosmic ray mass composition are performed by direct observations of the shower maximum X_{max} with the FD, and indirectly by measuring X_{max} using the surface detectors. Optical observations of X_{max} can currently be performed with a duty cycle of only 13% to 15%. Another good indicator of the primary composition is the number of muons N_μ present in the shower. Therefore, disentangling the muonic and electromagnetic component of the EAS at the ground provides the largest boost in performance towards the aforementioned science goals. This can be achieved either with a muon detector or a detector which has differential sensitivity to both EAS components.

The Pierre Auger Observatory Upgrade, named "AugerPrime", will be based on the following improvements:

- A complementary measurement of the shower particles will be provided by plastic Surface Scintillator Detectors (SSD) placed above the existing 1660 water-Cherenkov Detectors (WCD).
- The surface detector stations will be upgraded with new electronics that will process both WCD and SSD signals. The new electronics will also provide faster sampling of ADC traces, better timing accuracy, increased dynamic range, and enhanced triggers.
- To increase the dynamic range, each WCD will be equipped with an additional "small PMT", i.e., a smaller low gain photomultiplier tube, to register large pulses from very close showers that saturate the signal of the large PMTs.
- An Underground Muon Detector (UMD) will provide important direct measurements of the shower muon content and its time structure, while serving as verification and fine-tuning of the methods used to extract muon information with the SSD and WCD measurements.
- The operation mode of the Fluorescence Detector (FD) will be changed to extend measurements into periods with higher night sky background and twilight. This will allow an increase in the current $\sim$15% duty cycle of the FD to over $\sim$20%.
- Each Surface Detector station will be complemented with an antenna for radio detection of cosmic ray showers.

Both the scintillator planes, the new electronics and the radio antennas can be deployed over the full 3000 km^2 area of the Pierre Auger Surface Detector, with minimal impact on the continuous data taking and maintenance of the existing detectors. Except for the Infill area, the current communication systems for the Surface Detector will remain unchanged. The solar power system will be upgraded with larger, more efficient solar panels. Only minor software changes are required for the central data acquisition system (CDAS) and for the monitoring system.

Prototyping of the Upgrade began in 2015 and its complete installation is planned for 2022. It is expected to operate and provide data for over a decade, nearly doubling the statistics with respect to the presently available one.

4.2. Scintillator Surface Detector (SSD)

The key element of the upgrade is the installation of a new detector consisting of a plastic scintillator plane above each of the existing water-Cherenkov detectors. These scintillation detectors will provide a complementary measurement of the shower particles: as the SSD and the WCD have different responses to muons and electromagnetic particles, this allows for the disentangling of the different shower components. Whereas in a WCD the signal deposited by electromagnetic particles (e^+, e^-, γ) is proportional to their energy and the signal from muons is proportional to their track length, in the SSD each particle contributes essentially one MIP (Minimum Ionizing Particle) to the signal. The SSD array will also map the lateral footprint of EAS at the surface, being more sensitive to the electromagnetic component than to muons.

The design of the surface scintillator detectors is simple and reliable [53]. The SSD unit consists of a box of 3.8 m $\times$ 1.3 m, housing two scintillator panels, each covering an area of 1.9 m^2. Each panel is composed of 24 bars of 10 mm thick, 50 mm wide and 1.6 m long scintillator made of extruded polystyrene. The bars are co-extruded with a TiO2 outer

Figure 9. The Pierre Auger Observatory Upgrade: a prototype of an upgraded Auger Surface Detector, including the SSD on top of the tank and the SALLA antenna for the Radio Upgrade. Left: schematics. Right: the detector in the field.

layer for reflectivity and have two holes in which the wavelength-shifting fibres can be inserted. The fibres are 1 mm in diameter and are disposed in a "U" configuration that maximizes light yield and uniformity. The response over the area of the scintillator has been characterised and found to be uniform within 5%. All ends of the fibres are bundled towards one single photomultiplier in the centre of the module. A PMT of 38 mm in diameter, eight stages, fast time response and high linearity was chosen. The triggering of the SSDs is done in slave mode, i.e. the SSD data is read out every time the corresponding WCD reports a trigger.

The SSD modules are easily deployed in the field with a truck and crane. They are fixed to an aluminium frame mounted on top of the WCD tanks of the SD.

Calibration of the SSDs is performed in a similar way as for the WCDs. In a histogram of background signals, a clean peak is observed corresponding to Minimum Ionizing Particle (MIP) signals.

An engineering array of ten detectors was installed at the Auger site in September 2016. First, very encouraging results can be found in [34]. Additional 70 SSDs were installed in the field in 2018 and are collecting data since then. As of August 2020, all of the 1500 SSDs for the Upgrade have already been built at laboratories in Germany, Italy, Poland, Netherlands and France. More than half of them have already been shipped to Malargüe, where they were assembled and installed in the field, awaiting the delivery of the optical modules and electronics. Fig. 9 shows a detector in the field with the SSD installed on top.

4.3. Upgraded electronics

The surface detector stations will be upgraded with new electronics that will process both WCD and SSD signals [53]. It will increase the data quality with faster sampling of ADC traces (120 MHz), giving a better timing accuracy, and increased dynamic range (12 bits). To enhance the local trigger and processing capabilities a more powerful local station processor and FPGA have been implemented. This upgrade also improves calibration and monitoring capabilities of the surface detector stations. The surface detector electronics upgrade (SDEU) can be easily deployed and will have only minimal impact on the continuous data taking of the Surface Detector.

To increase the dynamic range of the WCD, a fourth PMT, 1 inch in diameter, corresponding to 1/9th of the WCD PMTs, will be added in each detector. With this solution, the total dynamic range of the SD will correspond to 22 effective ADC bits, ranging from fractions of 1 VEM (energy from one Vertical Equivalent Muon) to 20,000 VEM. This amplitude in ranges is achieved by splitting and amplifying the anode signal of the three large PMTs of the WCD and by using the single channel of the small additional PMT. This leads to less than 2% saturated events at the highest energies and unambiguous determination of the particle density down to less than 300 m from the shower core.

4.4. AMIGA: Auger muons and infill for the ground array

4.4.1. Underground muon detectors

In addition to the SD array of 1600 WCDs with a 1500 m spacing and the denser array of 61 WCDs with a 750 m spacing (SD-750), more recently the SD energy threshold has been further extended down to $10^{16.5}$ eV thanks to the installation of an even denser 1.9 km^2 array in which detectors are spaced by 433 m (SD-433). To provide a direct measurement of the muon content in air showers, an underground muon detector (UMD) [53] is also being deployed. Both arrays, the "infilled" array of WCDs working jointly with the UMD, form "AMIGA".

The UMD will consist of an array of scintillator detectors co-located at the position of each infill WCD: three 10 m^2 scintillation modules are buried at a distance of at least 7 m from the WCD, at a depth of 2.3 m underground. The separation from the surface detector guarantees that even particles with zenith angles up to 45° hit the underground scintillators without passing through the WCD, while probing the same point in the shower front. The chosen depth, which corresponds to 540 g/cm^2 of overburden as determined by the local soil density, ensures that the electromagnetic component of extensive air showers is largely absorbed while muons with energy greater than 1 GeV can reach the buried detectors. Each underground module is composed of 64 plastic-scintillation strips of 400 cm × 1 cm × 4 cm, similar to those of the SSD. They carry embedded wavelength-shifting (WLS) optical fibres which are optically coupled to an array of 64 silicon photomultipliers (SiPMs) [57, 58]. The light produced in the plastic scintillation bars is absorbed by the WLS optical fibre. The excited molecules of the fibre decay by emitting photons, some of which are propagated along the fibres towards a single pixel of the array of optical sensors.

Using data of the UMD engineering array that was operative until the end of 2017, it was determined for the first time with direct measurements of the muons, that the muonic densities in data are larger than those expected from simulations of showers between $10^{17.5}$ eV and 10^{18} eV [59], even after the update of the simulations to the latest hadronic interaction models, which include the data from the Large Hadron Collider. After the engineering array phase, modifications in the design were implemented to optimize the detector performance based on the experience gained with the operation of the prototypes. In particular, the optical devices were changed. The formerly used photomultiplier tubes were replaced by silicon photomultipliers to improve the detection efficiency, lower the costs and reduce the power consumption. Additionally, upgraded electronics with a novel acquisition mode to extend the dynamic range were adopted. It was also decided to work with a segmentation per position corresponding to 192 channels total, by splitting the 30 m^2 module into three 10 m^2 units.

A scheme of the layout of an AMIGA station as deployed during the engineering phase is shown in Fig. 10. For the full array, only three buried modules per position will be installed. As of the time of writing this review, the modules at 20 positions were already deployed at the Observatory site, and 15 of them are acquiring data. The completion of the UMD is foreseen for 2022.

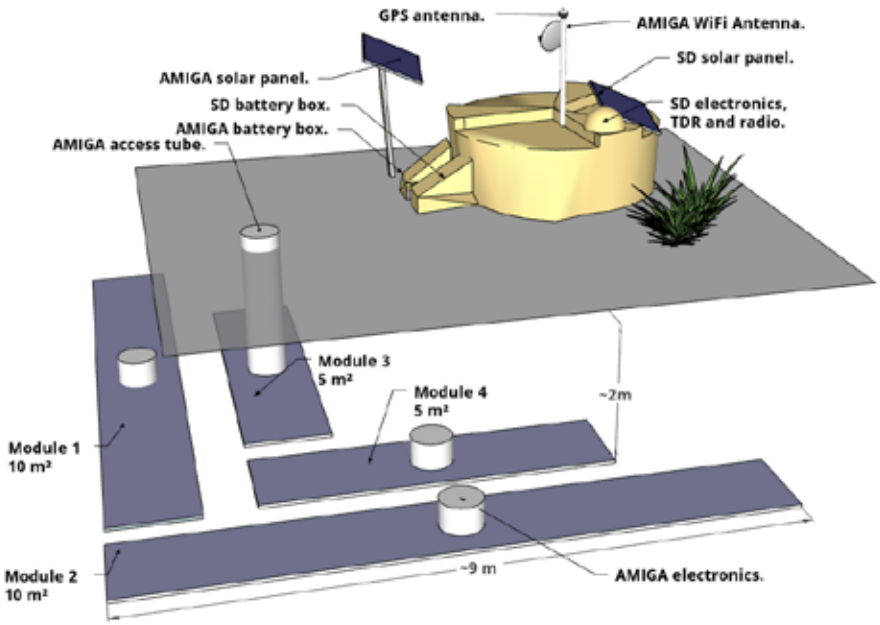

Figure 10. AMIGA station general overview. Both surface and underground detectors are shown in their arrangement during the prototyping phase. For the final design, the 30 m^2 detection area will be reached with three 10 m^2 units with 64 segments each, totalling 192 channels.

4.4.2. Mechanics and electronics of the underground muon detectors

Much effort was invested in developing the buried scintillator detectors that act as muon counters. As can be seen in the left panel of Fig. 11, in each module of the UMD, the scintillator strips are laid in two groups of 32 scintillator bars mounted at opposite sides of a central dome, which houses the optical sensors and the underground electronics. The scintillation light transported by the WLS optical fibre (Saint-Gobain BCF-99-29AMC) is fed to the array of 64 SiPMs, which converts the light pulses into a measurable electrical signal.

Each SiPM of the UMD (Hamamatsu S13361-2050) is composed of 1584 avalanche photodiodes (also referred as *cells*) operated in Geiger mode. The cells are distributed over an area of 2 mm^2 [58]. An electronics board acquires the signals from the photo-sensor and, at the same time, provides control, monitoring and communications to the UMD station.

Figure 11. (Left) A 10 m^2 module being assembled and (Right) its deployment at the Observatory site.

The UMD aims at measuring a broad range of muon densities, from 0.03 m^{-2}, typical for distances far from the shower core, to more than 20 m^{-2} in regions closer to the core where the muon flux is very high. This ample dynamic range is attained by *binary* and *ADC* acquisition modes working simultaneously. The former is optimized to count a small number of particles, the latter is designed to cope with large muon densities.

The binary mode benefits from the detector segmentation: muons can be directly counted as pulses above a certain threshold. This mode is very robust since it neither relies on deconvoluting the total number of particles from a single integrated signal, nor on the precise optical device gain or its fluctuations, and is almost completely independent of the hitting position of the particle on the scintillator strip and the corresponding light attenuation along the fibre. Another advantage is that it does not require a thick scintillator to control Poissonian fluctuations in the number of photons per impinging muon. However, the binary acquisition is limited by the segmentation itself: two muons arriving at the same strip simultaneously will be indistinguishable and, therefore, only counted as one. This undercounting feature is known as *pile-up* effect. As long as the number of strips with coincident signal is less than the segmentation, the pile-up effect can be statistically treated and corrected for, but when the number of particles is similar to the number of channels (64 in this case), the binary mode is saturated and the correction is no longer feasible.

On the other hand, knock-on electrons from the soil or from inclined muons might produce signals in two neighbouring strips resulting in an over-count of particles as well as an increased probability of saturating the detector. Therefore, being limited in the number of muons that can be detected at the same time, the binary mode is limited in the distance to the shower core that can be probed.

To overcome this difficulty, the ADC mode is well-suited to measure a higher number of particles. This mode provides a single, integrated signal from all 64 strips in a module. Contrary to the binary acquisition, in the ADC mode the fluctuations in the signal charge decrease with the number of hitting muons. The disadvantage of the ADC channel, when used to estimate the number of particles, is that it relies on an averaged charge estimation and therefore the signal fluctuations are propagated to uncertainties in the estimation of the muon densities.

In the binary acquisition mode, the 64 SiPM signals are handled independently through a pre-amplifier, a fast shaper, and a discriminator, built within each channel of two 32-channel Application-Specific Integrated Circuits (ASICs). The discriminator signal is sampled at 320 MHz (3.125 ns sample time) with the FPGA into 64 traces of 2048 bits. In each trace, a "1"-bit results if the fast-shaper output is above a fixed discriminator threshold, and a "0"-bit otherwise. The threshold is defined, as last step of the calibration procedure, to significantly reject the noise due to the SiPM dark-counts [58] while keeping a high efficiency.

The data acquisition system of each UMD module is fully synchronized with its associated SD station. Each module works as a slave detector and, therefore, follows the SD trigger chain [27]. The buried scintillators are synchronized at the first-level trigger: when such a condition is met, the WCD sends a signal with a timestamp to all the underground detector modules associated to it. Upon arrival of such signal, the traces of both, binary and ADC modes, as well as the timestamp of the trigger, are stored in an internal memory which can accommodate data up to 2048 triggers. Therefore, the rate of triggers determines that, at each position, the data is retrievable up to $\sim$20 s after its occurrence. Each triggered event in the UMD is composed, in turn, of 2048 samples of 64 single end lines measured at 320 MHz and 1024 samples of two 14-bit ADCs (high and low gain) measured at 160 Msps. The temporal length of each event is 6.4 microseconds and occupies 184 Kbits of memory. When a shower trigger takes place, all first- and second-level triggers from the WCDs, along with the muon detector traces, are sent to the central data acquisition server for higher level physical analysis.

4.5. Radio detection array

Extensive air showers are composed of charged particles undergoing acceleration in the atmosphere and are therefore known to produce radio emission in the frequency range of tens to hundreds of MHz. Radio emission from cosmic rays is due to two effects: the radiation arising from time-varying transverse currents induced by the geomagnetic field and the Askaryan effect related to a time-varying net negative charge. At the Auger Observatory, radio emission was first studied with the Auger Engineering Radio Array (AERA), an array of more than 150 radio detector stations, covering an area of about 17 km^2, co-located with the infill array, see [60, 61] and references therein.

The Auger Upgrade will also include a radio-detector array the size of the SD [62]. Each of the 1660 WCDs will carry a radio antenna on top of it, forming a radio-array covering 3000 km^2 and measuring in coincidence with the SD, the FD (during its uptime fraction of $\sim$15%) and the AMIGA underground muon detectors in the infill area. Fig. 9 shows the layout of the WCD with the SSD and the radio antenna on top of it.

With the combination of water-Cherenkov detector and Surface Scintillator Detector, the electron-to-muon ratio (e/μ) is measured for vertical showers. In a similar way, the combination of WCD and Radio Detector will be used to measure the ratio of the electromagnetic energy content and the number of muons for horizontal air showers. Thus, the Radio Detector will increase the aperture of the Observatory for mass-sensitive investigations, allowing the e/μ separation for showers with a broad zenith angle range, from zenith with the Surface Scintillator Detector to the horizon with the Radio Detector. Horizontal air showers have a large footprint of the radio emission on the ground, covering areas of the order of 100 km^2 for very inclined showers. This has already been confirmed experimentally with AERA. Thus, the radio emission from such showers can be recorded with a sparse antenna array with 1.5 km spacing.

The chosen design proposes the use of a short aperiodic loaded loop antenna (SALLA) to detect the radio emission from air showers in the frequency range 30 to 80 MHz. The SALLA realizes a Beverage antenna as a dipole loop of 1.2 m diameter. The SALLA has been developed to provide a minimal design that fulfills the need for both, ultra-wideband sensitivity, and low costs for production and maintenance of the antenna in a large-scale radio detector. The compact structure of the SALLA makes the antenna robust and easy to manufacture. Beverage antennas include a resistor load within the antenna structure to give a specific shape to the directivity. In the case of the SALLA, a resistance of 500 Ω connects the ends of the dipole arms at the bottom of the antenna. The antenna is read out at the top which is also the position of the Low-Noise Amplifier (LNA). While signals coming from above will induce a current directly at the input of the amplifier, the reception from directions below the antenna is strongly suppressed as the captured power is primarily consumed within the ohmic resistor rather than amplified by the LNA. The resulting strong suppression of sensitivity towards the ground reduces the dependence of the antenna on structures installed below it (like the Surface Scintillator Detector and the water-Cherenkov detector) and on environmental conditions which might vary as a function of time and are thus a source of systematic uncertainty. With the inclusion of an ohmic resistor, the SALLA especially challenges its amplifier as only $\sim$10% of the captured signal intensity is available at the input of the LNA. Proper matching between the antenna structure and the LNA is realized with a 3:1 transmission line transformer. The structure of the SALLA creates a sensitivity which is flat as a function of frequency. The antenna measures along two polarization directions oriented orthogonal to each other. The signals of the two analogue channels will be pre-amplified in a LNA at the antenna. The signals are transmitted through shielded coaxial cables to the filter amplifier on the front-end board. They will be digitized with a sampling frequency of 200 Msps. A FPGA controls the data flow and the communication with the existing electronics of each Surface Detector station.

The water-Cherenkov detector will provide a trigger signal when energy deposition is detected. The data from the radio antenna will be passed to the read-out electronics of the Surface Scintillator Detector/water-Cherenkov detector system (UUB) and will be transmitted together with all data from the station to the central data acquisition of the Auger Observatory.

The expected number of cosmic rays for the envisaged lifetime of the Radio Detector of ten years is of more than 3000 cosmic rays at energies exceeding 10^{19} eV, and approximately of 300 air showers with an energy in excess of $10^{19.5}$ eV. It is to be noticed that an increase of the assumed detection threshold mostly affects detection efficiencies and thus event rates at energies below 10^{19} eV. The Radio Detector will be a powerful tool to study the muon content in inclined air showers. The almost pure separation of the muon content (water-Cherenkov detectors) and electromagnetic energy (radio antennas) of inclined air showers will allow us to determine the energy dependence of the number of muons in inclined air showers, as has previously been done with the combination of water-Cherenkov Detectors and Fluorescence Detectors (FD). The Radio Detector, however, will achieve an order of magnitude higher event statistics: To date, a few hundreds of hybrid FD-SD events above $10^{18.8}$ eV have been collected for this analysis. Over the lifetime of the Radio Detector, roughly 6500 air showers can be collected in that energy range.

Prototypes of all components are installed in the field and evaluation of their performance is ongoing. Mass production of some components has already begun in 2020. The plan foresees to complete the deployment of the almost 1700 units of the 3000 km^2 Radio Detector at the beginning of 2022. The Radio Detector will improve the science capabilities of the Auger Observatory, by providing electron-muon separation for inclined air showers up to the highest energies. This implies also a larger mass-sensitive set of cosmic rays, measured by the Auger Observatory in the overlap region on the sky with the Telescope Array. The Auger Radio Detector is a natural next step towards future cosmic ray experiments,

applying the radio technique on even larger scales, such as GRAND [63] or a next-generation cosmic ray experiment, or applying hybrid detection techniques by combining radio antennas with e.g. segmented water-Cherenkov detectors. The Auger Radio Detector will be the biggest array for the next decade, and it will allow to evaluate the detector technology, establish reconstruction methods, and study the physics performance of such large radio arrays.

Conclusions

The construction of the Pierre Auger Observatory was completed in 2008. It has been running smoothly with nearly full aperture, and has now accumulated more than 12 years of data with the full-size observatory, which allowed to confirm previous results and to provide new insights about the spectrum, arrival directions and mass composition of ultra-high energy cosmic rays. It has also contributed to the understanding of cosmic ray shower physics, high-energy particle interactions, atmospheric phenomena and instrumentation development. The main scientific results have been described in Section 3.

The day-to-day operation of the Observatory demands 34 people on site, mostly highly qualified engineers and technicians. Night shifts for running the Fluorescence Detectors are covered by members of the international collaboration, both on site in Malargüe, as well as in the different control rooms set up at many participating institutions.

A major upgrade of the Auger Observatory is now underway. Presently, more than half of the 1500 SSD have been installed in the field, most of the remaining ones are already in Malargüe awaiting deployment. Their PMTs are being fabricated and tested in Europe and will soon be shipped to the site for installation. Small PMTs for increased dynamic range of the WCDs are ready to be deployed together with the new electronics. An engineering array of more than 70 SSD is running for more than a year in the field, using the original electronics kits. Their performance indicates that they respond according to design. The first batch of the preproduction series of upgraded electronics is being tested and will be installed at the site in the coming months. The upgrade of the Pierre Auger Observatory is expected to be completed in 2022.

AugerPrime, the Upgrade of the Pierre Auger Observatory, will provide a multi-hybrid cosmic ray detector, that will allow simultaneous measurement of a shower with water-Cherenkov detectors, surface scintillator detectors, radio detectors, muon counters and fluorescence detectors. As an illustration of the potentiality of this approach, in Fig. 12 a real event with the measured signals of all the surface techniques is shown. Operation of the upgraded Observatory is expected for at least 10 years.

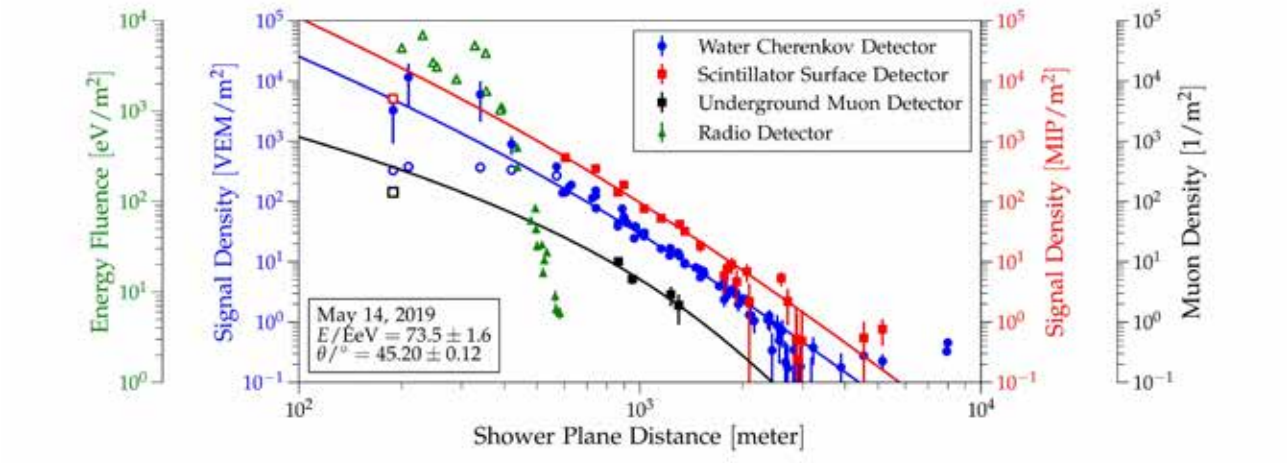

Figure 12. Lateral distribution of signals from SD, SSD, UMD and RD of a real event, as a function of the distance to the reconstructed shower core, including a fit (solid red, blue and black lines) to the measured data.

Outreach to the local community is important for the Auger Collaboration. The Visitor Centre in the town of Malargüe has already received more than 120,000 visitors, including many schoolchildren from the town of Malargüe and the Province of Mendoza. A webpage www.auger.org is maintained to provide updated news and information on the Observatory. Public data for outreach and educational purposes is also provided through that page.

Acknowledgments

The successful installation, commissioning, and operation of the Pierre Auger Observatory would not have been possible without the strong commitment and effort from the technical and administrative staff in Malargüe. We are very grateful to the following agencies and organizations for financial support:

Argentina – Comisión Nacional de Energía Atómica; Agencia Nacional de Promoción Científica y Tecnológica (ANPCyT); Consejo Nacional de Investigaciones Científicas y Técnicas (CONICET); Gobierno de la Provincia de Mendoza;

Municipalidad de Malargüe; NDM Holdings and Valle Las Leñas; in gratitude for their continuing cooperation over land access; Australia – the Australian Research Council; Brazil – Conselho Nacional de Desenvolvimento Científico e Tecnológico (CNPq); Financiadora de Estudos e Projetos (FINEP); Fundação de Amparo à Pesquisa do Estado de Rio de Janeiro (FAPERJ); São Paulo Research Foundation (FAPESP) Grants No. 2019/10151-2, No. 2010/07359-6 and No. 1999/05404-3; Ministério da Ciência, Tecnologia, Inovações e Comunicações (MCTIC); Czech Republic – Grant No. MSMT CR LTT18004, LM2015038, LM2018102, CZ.02.1.01/0.0/0.0/16_013/0001402, CZ.02.1.01/0.0/0.0/18_046/0016010 and CZ.02.1.01/0.0/0.0/17_049/0008422; France – Centre de Calcul IN2P3/CNRS; Centre National de la Recherche Scientifique (CNRS); Conseil Régional Ile-de-France; Département Physique Nucléaire et Corpusculaire (PNC-IN2P3/CNRS); Département Sciences de l'Univers (SDU-INSU/CNRS); Institut Lagrange de Paris (ILP) Grant No. LABEX ANR-10-LABX-63 within the Investissements d'Avenir Programme Grant No. ANR-11-IDEX-0004-02; Germany – Bundesministerium für Bildung und Forschung (BMBF); Deutsche Forschungsgemeinschaft (DFG); Finanzministerium Baden-Württemberg; Helmholtz Alliance for Astroparticle Physics (HAP); Helmholtz-Gemeinschaft Deutscher Forschungszentren (HGF); Ministerium für Innovation, Wissenschaft und Forschung des Landes Nordrhein-Westfalen; Ministerium für Wissenschaft, Forschung und Kunst des Landes Baden-Württemberg; Italy – Istituto Nazionale di Fisica Nucleare (INFN); Istituto Nazionale di Astrofisica (INAF); Ministero dell'Istruzione, dell'Universitá e della Ricerca (MIUR); CETEMPS Center of Excellence; Ministero degli Affari Esteri (MAE); México – Consejo Nacional de Ciencia y Tecnología (CONACYT) No. 167733; Universidad Nacional Autónoma de México (UNAM); PAPIIT DGAPA-UNAM; The Netherlands – Ministry of Education, Culture and Science; Netherlands Organisation for Scientific Research (NWO); Dutch national e-infrastructure with the support of SURF Cooperative; Poland -Ministry of Science and Higher Education, grant No. DIR/WK/2018/11; National Science Centre, Grants No. 2013/08/M/ST9/00322, No. 2016/23/B/ST9/01635 and No. HARMONIA 5–2013/10/M/ST9/00062, UMO-2016/22/M/ST9/00198; Portugal – Portuguese national funds and FEDER funds within Programa Operacional Factores de Competitividade through Fundação para a Ciência e a Tecnologia (COMPETE); Romania – Romanian Ministry of Education and Research, the Program Nucleu within MCI (PN19150201/16N/2019 and PN19060102) and project PN-III-P1-1.2-PCCDI-2017-0839/19PCCDI/2018 within PNCDI III; Slovenia – Slovenian Research Agency, grants P1-0031, P1-0385, I0-0033, N1-0111; Spain – Ministerio de Economía, Industria y Competitividad (FPA2017-85114-P and FPA2017-85197-P), Xunta de Galicia (ED431C 2017/07), Junta de Andalucía (SOMM17/6104/UGR), Feder Funds, RENATA Red Nacional Temática de Astropartículas (FPA2015-68783-REDT) and María de Maeztu Unit of Excellence (MDM-2016-0692); USA – Department of Energy, Contracts No. DE-AC02-07CH11359, No. DE-FR02-04ER41300, No. DE-FG02-99ER41107 and No. DE-SC0011689; National Science Foundation, Grant No. 0450696; The Grainger Foundation; Marie Curie-IRSES/EPLANET; European Particle Physics Latin American Network; and UNESCO.

References

[1] K.-H. Kampert and A. Watson, "Extensive Air Showers and Ultra High-Energy Cosmic Rays: A Historical Review", EPJ-H 37 (2012) 359

[2] G. W. Clark et al, Phys. Rev. 122 (1961) 637

[3] J. Linsley, L. Scarsi and B. Rossi, Phys. Rev. Lett. 6 (1961) 485

[4] J. Linsley, Phys. Rev. Lett. 10 (1963) 146

[5] A. A. Penzias and R. W. Wilson, "A Measurement of Excess Antenna Temperature at 4080 Mc/s", Astrophysical Journal, 142 (1965) 419

[6] K. Greisen, "End to the Cosmic-Ray Spectrum?", Physical Review Letters 16 (1966) 748

[7] G. T. Zatsepin and V. A. Kuz'min,"Upper Limit of the Spectrum of Cosmic Rays", Journal of Experimental and Theoretical Physics Letters 4 (1966) 78

[8] F. W. Stecker and M. H. Salamon, "Photodisintegration of Ultra–High-Energy Cosmic Rays: A New Determination", The Astroph. Journal 512 (1999) 521

[9] L. N. Epele and E. Roulet, "Comment on "On the Origin of the Highest Energy Cosmic Rays"" Phys. Rev. Lett. 81 (1998) 3295

[10] See, for example, http://www.astro.ucla.edu/ rene/talks/Cronin-Fest-Ong-Writeup.pdf

[11] M.M. Winn et al., J.Phys.G: Nucl.Phys., 12 (1986) 653

[12] R. M. Tennent, "The Haverah Park extensive air shower array", Proceedings of the Physical Society 92(2002) 622

[13] A. A. Ivanov et al., New Journal of Physics 11 (2009) 065008

[14] The KASCADE-Grande Collaboration, Nuclear Instruments and Methods in Physics Research A 620 (2010) 202

[15] N. Hayashida et al., Astropart. Phys. 10 (1999) 303

[16] R. M. Baltrusaitis et al., "The Utah Fly's Eye detector", Nuclear Instruments and Methods in Physics Research A 240 (1985) 410

[17] T. Abu-Zayyad et al., Proc. 26th ICRC, 4 (1999) 349

[18] J. H. Boyer et al., Nucl. Inst. Meth. A 482 (2002) 457

[19] D. J. Bird et al., "Detection of a cosmic ray with measured energy well beyond the expected spectral cutoff due to cosmic microwave radiation", The Astrophysical Journal 441 (1995) 144

[20] M. Takeda et al., Astropart. Phys. 19 (2003) 447

[21] R. U. Abbasi et al., Physical Review Letters 100 (2008) 101101; R. U. Abbasi et al., Astroparticle Physics 32 (2009) 53

[22] I. Allekotte et al. [The Pierre Auger Collaboration], "Site survey for the Pierre Auger observatory", J. Phys. G: Nucl. Part. Phys. 28 (2002) 1499

[23] H. Kawai et al., "Telescope Array Experiment", Nuclear Physics B Proceedings Supplements 175–176 (2008) 221

[24] The Pierre Auger Collaboration, "The Pierre Auger Cosmic Ray Observatory", Nuclear Instruments and Methods in Physics Research A 798 (2015) 172

[25] The Pierre Auger Collaboration, "Properties and performance of the prototype instrument for the Pierre Auger Observatory", Nuclear Instruments and Methods in Physics Research A: 523 (2004) 50

[26] I. Allekotte et al. [The Pierre Auger Collaboration], "The surface detector system of the Pierre Auger Observatory", Nuclear Instruments and Methods in Physics Research A 586 (2008) 409

[27] The Pierre Auger Collaboration, "Trigger and aperture of the surface detector array of the Pierre Auger Observatory", Nuclear Instruments and Methods in Physics Research A 613 (2010) 29

[28] X. Bertou et al., Nuclear Instruments and Methods in Physics Research A 568 (2006) 839

[29] The Pierre Auger Collaboration, "Reconstruction of Events Recorded by the Surface Detector of the Pierre Auger Observatory", accepted by JINST (2020)

[30] J. Abraham et al. [The Pierre Auger Collaboration], "The fluorescence detector of the Pierre Auger Observatory", Nuclear Instruments and Methods in Physics Research A 620 (2010) 227

[31] V.Verzi [Pierre Auger Collaboration], "Measurement of the energy spectrum of ultra-high energy cosmic rays using the Pierre Auger Observatory", PoS(ICRC2019) (2019) 450

[32] The Pierre Auger Collaboration, "Features of the energy spectrum of cosmic rays above 2.5×10^{18} eV using the Pierre Auger Observatory", to be published in Phys. Rev. Letters (2020) ; "A measurement of the cosmic ray energy spectrum above 2.5×10^{18} eV using the Pierre Auger Observatory", to be published in Phys. Rev. D (2020).

[33] A. Castellina [Pierre Auger Collaboration], "Highlights from the Pierre Auger Observatory", PoS(ICRC2019) (2019)

[34] The Pierre Auger Collaboration, "Contributions to the 36th International Cosmic Ray Conference (ICRC 2019)", arXiv:1909.09073 (2019)

[35] Telescope Array Collaboration, Astrophys. J. 768 (2013) L1

[36] The Pierre Auger Collaboration, Phys. Rev. Lett. 101 (2008) 061101

[37] D. J. Bird et al. [HiRes Collaboration], Phys. Rev. Lett. 71, 3401 (1993)

[38] The Pierre Auger Collaboration, Phys. Lett. B685 (2010) 239, arXiv:1002.1975 [astro-ph.HE]

[39] T. K. Gaisser, "Cosmic Rays and Particle Physics", Cambridge University Press, Cambridge, 1990

[40] The Pierre Auger Collaboration, "Inferences on mass composition and tests of hadronic interactions from 0.3 to 100 EeV using the water-Cherenkov detectors of the Pierre Auger Observatory", Phys. Rev. D 96 (2017) 122003

[41] The Pierre Auger Collaboration, "Combined fit of spectrum and composition data as measured by the Pierre Auger Observatory", JCAP04 (2017) 038

[42] The Pierre Auger Collaboration, Astrop. J. Lett. 853 (2018) L29

[43] The Pierre Auger Collaboration, Science 357 (2017) 1266

[44] E. Roulet [The Pierre Auger Collaboration], "Large-scale anisotropies above 0.03 EeV measured by the Pierre Auger Observatory", PoS(ICRC2019) (2019) 408

[45] R. Engel, D. Seckel and T. Stanev, "Neutrinos from propagation of ultrahigh energy protons", Phys. Rev. D 64 (2001) 093010

[46] The Pierre Auger Collaboration, "Limits on point-like sources of ultra-high-energy neutrinos with the Pierre Auger Observatory", JCAP 11 (2019) 004; F. Pedreira [The Pierre Auger Collaboration], "Bounds on diffuse and point source fluxes of ultra-high energy neutrinos with the Pierre Auger Observatory" PoS (ICRC2019) (2019) 979

[47] J. Rautenberg [The Pierre Auger Collaboration], "Limits on ultra-high energy photons with the Pierre Auger Observatory", PoS(ICRC2019) (2019) 398

[48] The Pierre Auger Collaboration, Phys. Rev. D91 (2015) 032003

[49] The Pierre Auger Collaboration, Phys. Rev. Lett. 117 (2016) 192001

[50] The Pierre Auger Collaboration, Phys. Rev. D 90 (2014) 012012; D90 (2014) 039904(A); D92 (2015) 019903(E)

[51] The Pierre Auger Collaboration, "A Three Year Sample of Almost 1600 Elves Recorded Above South America by the Pierre Auger Cosmic Ray Observatory", Earth Space Sci. 7 (2020) e2019EA000582

[52] The Pierre Auger Collaboration, "The Pierre Auger Observatory scaler mode for the study of solar activity modulation of galactic cosmic rays", Journal of Instrumentation, 6 (2011) P01003 (open access)

[53] The Pierre Auger Collaboration, "The Pierre Auger Observatory Upgrade - Preliminary Design Report", arXiv:1604.03637 (2016)

[54] A.Castellina [The Pierre Auger Collaboration], "AugerPrime: the Pierre Auger Observatory Upgrade", EPJ Web Conf. 210 (2019) 06002

[55] F.Sanchez [The Pierre Auger Collaboration], "The muon component of extensive air showers above $10^{17.5}$ eV measured with the Pierre Auger Observatory", PoS (ICRC2019) (2019) 411; Pierre Auger Collaboration, "Direct measurement of the muonic content of extensive air showers between 2×10^{17} and 2×10^{18} eV at the Pierre Auger Observatory", Eur. Phys. J. C (2020) .

[56] F. Riehn [The Pierre Auger Collaboration], "Measurement of the fluctuations in the number of muons in inclined air showers with the Pierre Auger Observatory", PoS(ICRC2019) 404

[57] The Pierre Auger Collaboration, JINST 11 (2016) P02012

[58] The Pierre Auger Collaboration, JINST 12 (2017) P03002

[59] The Pierre Auger Collaboration, "Direct measurement of the muonic content of extensive air showers between 2×10^{17} and 2×10^{18} eV at the Pierre Auger Observatory", Eur. Phys. J. C (2020) to be published

[60] The Pierre Auger Collaboration, "Observation of inclined EeV air showers with the radio detector of the Pierre Auger Observatory " JCAP 10 (2018) 026

[61] T. Huege [The Pierre Auger Collaboration], "Radio detection of cosmic rays with the Auger Engineering Radio Array", EPJ Web Conf. 210 (2019) 05011

[62] B. Pont [The Pierre Auger Collaboration], "A large radio detector at the Pierre Auger Observatory - measuring the properties of cosmic rays up to the highest energies", POS(ICRC2019) (2019) 434

[63] J. Alvarez-Muñiz, et al., Science China: Phys., Mech. & Astron., 63 (2020) 219501; http://arxiv.org/abs/1810.09994

Bio

The Pierre Auger Collaboration is a scientific collaboration with more than 400 scientists, engineers and technicians from over 80 institutions from 17 countries: Argentina, Australia, Belgium, Brazil, Colombia, Czech Republic, France, Germany, Italy, Mexico, Poland, Portugal, Romania, Slovenia, Spain, The Netherlands and USA. The collaboration has built and operates the largest cosmic ray observatory worldwide, the Pierre Auger Observatory, located in the Province of Mendoza, Argentina.

Science Reviews
from the end of the world

Vol. 1, No. 4, September 2020 // pp. 34-46 /

Large Latin American Millimeter Array

Gustavo E. Romero

Instituto Argentino de Radioastronomía (CONICET, CICPBA), Villa Elisa, Argentina.

Abstract

The Large Latin American Millimeter Array (LLAMA) is a multipurpose single-dish 12 m radiotelescope with VLBI capability under construction in the Puna de Atacama desert in the Province of Salta, Argentina. In this paper I review the project, the instrument, the current status, and the scientific goals of this astronomical collaboration beween Argentina and Brazil.

Keywords:
radio astronomy, telescopes, astrophysics, submillimeter astronomy

Introduction

Astronomy is concerned with the detection and measurement of natural signals emitted from astrophysical sources in the Universe. During most of its long history astronomy was restricted to a very narrow kind of signals: optical radiation. After the work of James Clerk Maxwell in the 1860s, it became clear that light is a phenomenon based on electric and magnetic perturbations and that a continuum of electromagnetic radiation should exist. Between 1886 and 1889 Heinrich Hertz, a young physicist researching at Karlsruhe University, conducted a series of experiments that would prove the existence of electromagnetic waves.

Quite soon radio waves were being used for communications. The discovery in 1902 that these waves are reflected by the ionosphere led physicists to think that astronomical radio signals would not penetrate the atmosphere. Bouncing waves, however, might be used for overseas communication. In the early 1930s, Karl Jansky, an engineer working for Bell Telephone Laboratories, was investigating the static that interfered with short wave transatlantic voice transmissions when serendipitously discovered cosmic radio waves coming from the Galactic center region. He published his results [1] but was not allowed to continue with his astronomical research by the Bell Labs. Grote Reber, an engineer and radio aficionado, followed Jansky's path and built the first orientable radio telescope[1] in the backyard of his house in Wheaton, Illinois. He confirmed Jansky's discovery, found additional astronomical radio sources, and by 1944 published the first radio map of the sky at 160 MHz [2].

Until the end of World War II, Reber remained the world's only radio astronomer. During the late 1940s and early 1950s the field of radio astronomy exploded with the development of new technologies based upon the radio and radar techniques. In 1946 Sir Martin Ryle and D. D. Vonberg made the first astronomical observation using a pair of radio antennas as an interferometer. In 1951 the 21-cm line associated with the emission of hydrogen due to the spin flip of the electron, was detected at Harvard University. Many discoveries followed, including the spiral structure of the Galaxy, extragalactic radio sources, supernova remenants, pulsars, quasars, and more.

In Argentina these discoveries did not go unnoticed. In 1958 a Commission for Radio Astronomy was created at the

[1] The instrument had a 9.5-m parabolic dish.

University of Buenos Aires (UBA). Soon things were ready for the establishment of the first radio telescope of South America. The Instituto Argentino de Radioastronomía[2] (IAR) was created in 1962 by Nobel laureate Dr. Bernardo Houssay, then President of the National Research Council of Argentina (CONICET) through an agreement with the Carnegie Institution of Washington. The latter would provide a radio telescope and train engineers that would work on the receiver. The primary goal of the instrument was to survey the HI line in the galactic plane. As first Director of the institute was appointed Carlos Varsavsky, an Argentine physicist who got his PhD at Harvard University and was well-known as the translator to English of Shklovskii's classic book on radio astronomy [3]. The IAR was originally thought as a radio observatory but eventually evolved into a full institute with research staff, students, offices, labs, library, and other facilities (see Figure 1). Till this day it operates two 30-m single-dish radio telescopes, observing at wavelengths of 21 cm in line, timing, or continuum modes.

Figure 1. View of the Instituto Argentino de Radioastronomía, with one of its two 30-m radio telescopes.

In the late 1960s, while the IAR first telescope commenced to produce results of scientific interest, the Astronomy Committee of the UK's Science Research Council started to analyze the importance of astronomical observations at submillimeter and millimeter wavelengths. In 1975 it was concluded that it would be possible to construct a 15-meter diameter telescope capable of observing at wavelengths down to 750 μm (Terahertz radiation or THz). The submillimeter radio window (from far infrared to microwaves) is particularly challenging because this radiation is absorbed in the atmosphere by water vapor. At low elevations, where most water vapor resides, the atmosphere is very opaque at submillimeter wavelengths; the abundant water vapor absorbs any incoming submillimeter photons before they can reach the telescope. At higher elevations, however, the water content decreases substantially. By minimizing the atmospheric water vapor, one improves the transparency of the atmosphere and makes astronomical observations possible. It is for this reason that infrared and submillimeter observatories should be built as high as possible and in very dry places: by being above some of the atmosphere, the radiation from astronomical sources is much less attenuated.

There are only a handful sites identified on the Earth that are suitable for submillimeter radio observatories. These include, Mauna Kea (Hawaii, United States), the Atacama Plateau (in the Northwest of Argentina and Northeast of Chile), the South Pole, and Ladakh, India.

The submillimeter telescope recommended by the British Science Research Council would be eventually constructed in Mauna Kea and named the James Clerk Maxwell Telescope. The telescope saw first light in 1987. Since then, many other submillimeter telescopes have been built in the few available sites. The most notorious is the Atacama Large Millimeter Array (ALMA), an astronomical interferometer of 66 radio telescopes in the Atacama Desert (on the Chilean side). At a cost of about USD 1.4 billion, ALMA is the most expensive ground-based telescope in operation in the world. It is a joint enterprise of partners in Europe, the United States, Canada, Japan, South Korea, Taiwan, and Chile. ALMA has a higher sensitivity and higher resolution than any existing submillimeter facility. This is achieved thanks to the large number of antennas and the fact that they can be separated up to 16 km to determine long baselines for interferometry.

At a basic level, interferometry is simply the combining of signals from two different sources. If the two signals are similar then they will combine to make a stronger signal, and if they are not, they will tend to cancel out. This becomes

[2] Argentine Instituite for Radio Astronomy.

useful for astronomy when two signals are out of synchronicity: then it is possible to shift them (correlate them) so that they will be synchronized. When the signal is strongest, the signals are correctly lined up.

When two radio antennas are aimed in the same direction, they receive the same basic signal, but the signals are out of synchronicity because it takes a bit longer to reach one antenna than the other. That difference depends on the direction of the antennas and their spacing apart from each other. By correlating the two signals, it is possible to determine the location of the signal in the sky very precisely.

Two antennas only give one point in the sky, but dozens of antennas (such as the array at ALMA) can get lots of points, one for each pairing of antennas, creating an image. But this will be a discretely sampled image. If the Earth were fixed in relation to the sky, then a radio image would look like a pointillist painting. Since the Earth rotates with respect to the sky, so as time goes by the relative positions of the antennas shift with respect to an astronomical signal. As the observations are done, the gaps between antennas are filled to create a more solid image. It takes lots of observations and lots of computing power to combine the images in the right way. At ALMA there is a supercomputer that spends all its time correlating signals. The results are superb.

By the time when ALMA started operations in 2011, both Argentina and Brazil had embarked into a joint project to build a submillimeter observatory that might be used to extend ALMA baselines more than 100 km, with the consequent increase in angular resolution. Such project was named Large Latin America Millimeter Array (LLAMA). It is described in the pages that follows.

Figure 2. LLAMA building for administration, lodging, and labs in San Antonio de los Cobres, Salta. Credit: Gobierno de la Provincia de Salta.

1. The project

Campaigns to characterize the potential of the astronomical sites for short wavelengths radio astronomy in the North of Argentina started in the early 2000s. These campaigns were conducted by the IAR and consisted of meteorological (especially measurements of atmospheric opacity) and topographical data collection. In 2007, discussions between scientists from Argentina and Brazil started to shape a joint project for the installation of a submillimeter facility in the Argentine extension of the Atacama desert. Such a facility should be able to operate both in single-dish mode or as a component of a

large interferometer array with ALMA or other telescopes. The project was presented to the Argentine scientific community in 2008, during the Annual Meeting of the Argentine Astronomical Society held in San Juan [4]. The formal presentation before the Argentine Science Ministry (MinCyT) was in 2010, while a meeting held at the offices of the Brazilian agency FAPESP, based on São Paulo, in August 2011, marked the formal entrance of Brazil in the project [5]. In 2011 MinCyT ranked LLAMA as its main astronomical project and in 2012 FAPESP approved a grant of about USD 9 M. The final agreement, between MinCyT, FAPESP, and the University of São Paulo (USP), was signed in June 2014.

The site chosen for the telescope was located in the region of Alto Chorrillos, in Salta province. The site is at 4832.5 meters above sea level and about 16 km away from the small town of San Antonio de los Cobres (longitude 66° 28' 29.4" (W), −24° 11' 31.4"(S)). At the end of 2016 construction work on the route to the top of the mountain started. By the end of 2018 the building of the project in San Antonio de los Cobres was completed (see Fig. 2).

Regarding the telescope, it was decided to acquire an antenna and receivers similar to those ones used in ALMA. The antenna was provided by Vertex, the same company that built some of ALMA antennas. It is described in the next section.

2. The instrument

Since LLAMA is expected to be a multipurpose instrument that should operate either as a stand-alone telescope or as a part of a larger interferometer, an obvious option was to base the project on the design of an existing and well-tested antenna. An apparent choice was the design of the Atacama Pathfinder Experiment (APEX), a very successful instrument used to test technologies later used in ALMA, see Figures 3 and 4. The APEX telescope is a modified ALMA prototype antenna and is at the site of the ALMA observatory. APEX is designed to work at submillimeter wavelengths, in the 0.2 to 1.5 mm range and its primary goal is to find targets that ALMA will be able to study in greater detail.

Figure 3. The APEX antenna. APEX, the Atacama Pathfinder Experiment, is a collaboration between Max Planck Institut f ur Radioastronomie (MPIfR), Onsala Space Observatory (OSO), and the European Southern Observatory (ESO) aimed at constructing and operating a modified ALMA prototype antenna as a single dish on the high altitude site of Llano Chajnantor in Chile. This instrument essentially operates with the same antenna design that will be used in LLAMA. Credit: ESO.

The antenna for LLAMA was commissioned to the German company Vertex Antennentechnik, GmbH. It is quite similar to APEX. The basic design is shown in Figure 5. The operating frequency range of the antenna will be from 30 GHz to 950 GHz. The antenna has a symmetric paraboloidal reflector with a diameter of 12 m, mounted on an elevation over an azimuth mount. The overall optical layout of the antenna is a Cassegrain configuration with the parameters as shown

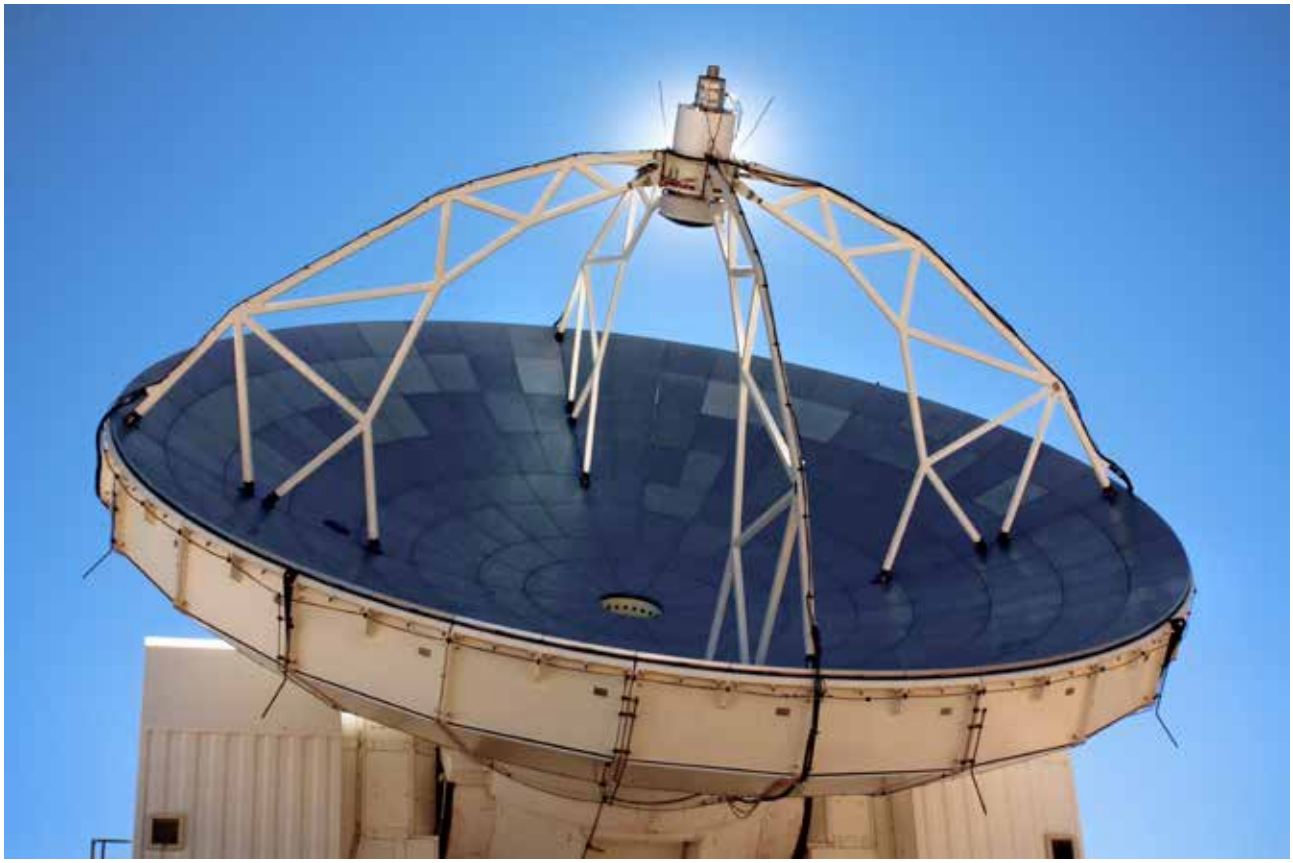

Figure 4. Detail of the Vertex antenna. Credit: ESO.

in Table 1. There are two Nasmyth cabins for single pixel receivers on both sides of the instrument. These heterodyne receivers are listed in Table 2.

Table 1. Optical parameters of LLAMA telescope[6]

Name		
Parameter	Symbol	Value
D	Primary Apperture	12.0 m
f_p	Focal Length of Primary	4.8 m
D_s	Secondary Aperture	0.75 m
M	Magnification Factor	20.0
θ_p	Primary Angle of Illumination	128.02°
θ_s	Secondary Angle of Illumination	7.16°
$2c$	Distance between Primary and Secondary Focus	6.177 m
H	Depth of Primary	1.875 m
V	Primary Vertex Hole Clear Aperture	0.75 m
W	Total Weight	125 tons

Major design specifications of the telescope are:

- Capability to operate at an altitude of $\sim$ 5000 m.
- Pointing accuracy 2 arcsec (absolute) and 0.6 arcsec (offset pointing).
- Reflector surface accuracy $< 25\ \mu$m.
- Temperature stability of $\pm 1^\circ$ C in receiver cabin.
- Design lifetime > 20 years.

The main dish consists of 264 aluminium panels in 8 rings fixed on a carbon fiber reinforced plastic backup structure of 24 sandwich shell segments. Each panel is supported by five vertical (four corners and center) and three horizontal

Table 2. Single pixel receivers of LLAMA telescope[7]

Name		
Band	Frequency (GHz)	Average noise
1	35 – 50	17 K
3	84 – 116	35 K
5	163 – 211	45 K
6	211 – 275	55 K
7	275 – 373	70 K
9	602 – 720	160 K

adjustment elements. The panels have been chemically etched to scatter visible and IR radiation and thus allow for daytime observations. To operate at the shorter submillimeter wavelengths, the antenna should have a surface of exceedingly high quality. After a series of high precision adjustments, the surface of the primary mirror will have remarkable precision. Over the 12 m diameter of the antenna, the rms deviation from the perfect parabola is less than 17 thousandths of a millimeter . This is smaller than one fifth of the average thickness of a human hair.

The optical system is designed to be as versatile as possible. A maximum of two simultaneous receivers, with dual polarization each, could be used at any given time. Though the optical design of the telescope will not allow Cassegrain/Nasmyth simultaneous observations to be carried out, the system will have the capability of making a fast swap (within a few minutes) between instruments located at the Cassegrain focus (e.g. a MKID camera or an heterodyne array at a given frequency) and those located at a Nasmyth focus.

The different receivers will be contained in cartridges within a cryostat that will cool the electronics to ~ 4 K (see Figure 6). In the Cassegrain focus area there will be a bolometric array. At present, the most promising technology for bolometric cameras employs 300 mK cooled microwave kinetic inductance detectors (MKIDs). These type of extremely cooled arrays of bolometers are similar to those used in the nearby QUBIC telescope [8]. The low frequency receivers are currently being under construction by NOVA[3]. NOVA is also in charge of LLAMA back-end. The cryostat where the cartridges with the receivers are inserted was developed by the National Astronomical Observatory of Japan (NAOJ). It will accommodate up to three ALMA compatible receivers. The cryostat is currently in NOVA for integration. For first light LLAMA is expected to count with receivers operating in Bands 5 and 9 (see Table 2).

In the Cassegrain focus a Water Vapor Radiometer (WVR) could also be located tuned to a frequency of 183 GHz. The WVR would be used to measure the water vapor content of the atmosphere at the time of observation. With this measurement, the observation frequency band can be programmed in real time and the effects of the distortion caused by the atmosphere on the signal phase can be obtained for its later removal, with digital techniques, in the detected signal.

3. Science

Much of the electromagnetic radiation in the local Universe arrives in the far-infrared and submillimeter band as thermal radiation from dust. The microwave electromagnetic window in astronomy is particularly suitable for investigations of star forming regions and protostars. Molecular outflows associated with the formation of stars and their winds can be traced by line observations of molecules such as CO, HCN, HCO+, N2H+, CS, and NH3. Interstellar gas clouds are heated by starlight. When they collapse under gravity, they heat up. However, the clouds need to cool in order to form the next generation of stars. The spectral lines that are in the far-infrared and submillimeter bands are the primary coolants for the neutral gas that form stars. Some of the most important cooling lines include H2O, SO2, and CO rotational lines, [CI] [CII], and [NII] fine structure lines. All these lines can be investigated with LLAMA telescope.

ALMA, with its high resolution, has obtained extraordinary images of young stars with protoplanetary disk (see Figure 8). These images reveal the gaps open in the disks by the forming planets. LLAMA can contribute to this kind of studies either observing as a single dish, measuring the rotational velocity of disks in young stellar objects, or as a part of a larger interferometer array helping to increase the angular resolution of the images.

As APEX, LLAMA can be used for the Event Horizon Telescope (ETH), a collaboration that applies submillimeter telescopes to image the supermassive black hole in the galactic center (Figure 7). In the future, this array is also expected to map the black hole in nearby radio galaxies. In 2019 it already has obtained the first image of the shadow of a supermassive black hole at the centered of M87 [9].

LLAMA will also be capable of observing the Sun. Frequencies near the submillimeter range are produced in the lower solar chromosphere or even in the photosphere. LLAMA observations can gather information on the lower solar atmosphere and particle acceleration there. If working in interferometric mode with ALMA or APEX, the array might

[3]NOVA stands for 'Nederlandse Onderzoekschool Voor Astronomie', i.e., the 'Netherlands Research School for Astronomy'. It is the alliance of the astronomical institutes of the universities of Amsterdam, Groningen, Leiden, and Nijmegen.

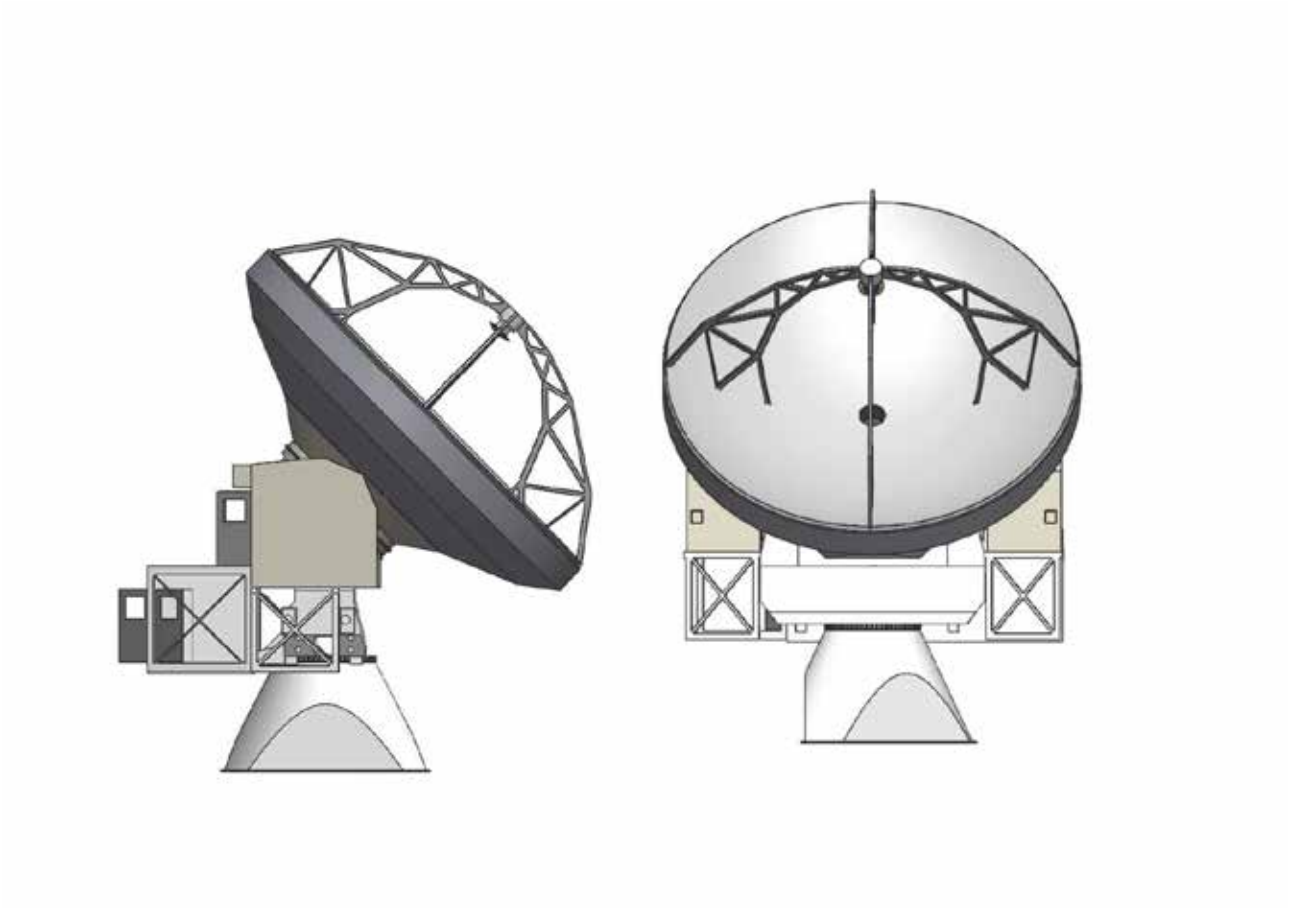

Figure 5. Sketch of LLAMA antenna produced by Vertex Antennentechnik, GmbH. Lateral and front views. Credit: Vertex.

achieve a spatial resolution of 0.001″ at wavelengths of about 1 mm. This is tantamount to about 700 m over the solar surface.

Outside the Galaxy, LLAMA can be used to investigate outflows in starbursts, the chemical enrichment of the intergalactic medium around galaxies, dusty Active Galactic Nuclei, and galaxy formation at high redshifts. Dusty star-forming galaxies reprocess stellar light in dust, which radiates in the far-infrared and submillimeter bands. The Milky Way emits about half of its light in this range. The most luminous galaxies in the local Universe, called Ultra-luminous Infrared Galaxies (ULIGS) emit most (up to 99%) of their energy at millimeter and submillimeter wavelengths. These galaxies are natural targets for LLAMA.

Finally, LLAMA also offers a unique opportunity to make research in cosmology. The Cosmic Microwave Background Radiation (CMBR) stems from about 300.000 years after the Big Bang, when the Universe had expanded and cooled to an extent such that atoms could form; leaving light waves to travel freely through space. Until that point, the Universe was ionized, and too dense and hot for light to travel far without interacting with matter. The so-called "last scattering surface" marks the epoch when the Universe became transparent . The radiation from this epoch has been shifted in wavelength because of the continued expansion of the Universe, now appearing in the microwave region of the spectrum, and is observable with millimeter and submillimeter receivers. A major challenge is to detect the polarization of this radiation, in particular the kind of polarization created by gravitational waves traveling through the primordial plasma. This type of polarization is known as the "B mode". Several telescopes, including QUBIC and the Atacama Cosmology Telescope (ACT), are devoted to the detection of this feature in the CMBR. The latter instrument is a six-meter telescope located on Cerro Toco in the Atacama Desert in the north of Chile, near the Llano de Chajnantor Observatory. LLAMA, with its larger surface, might obtain information of CMB fluctuations on smaller scales than these instruments, if an appropriate array of bolometers is located in one of the focus.

4. Management

The project is funded by the Secretary of Scientific-Technological Articulation of the Ministry of Science, Technology and Productive Innovation (MINCYT) of Argentina and the Foundation for Research of the State of São Paulo (FAPESP) of Brazil. The construction was supervised by a Steering Committee formed by 6 Argentine and 6 Brazilian scientists, headed

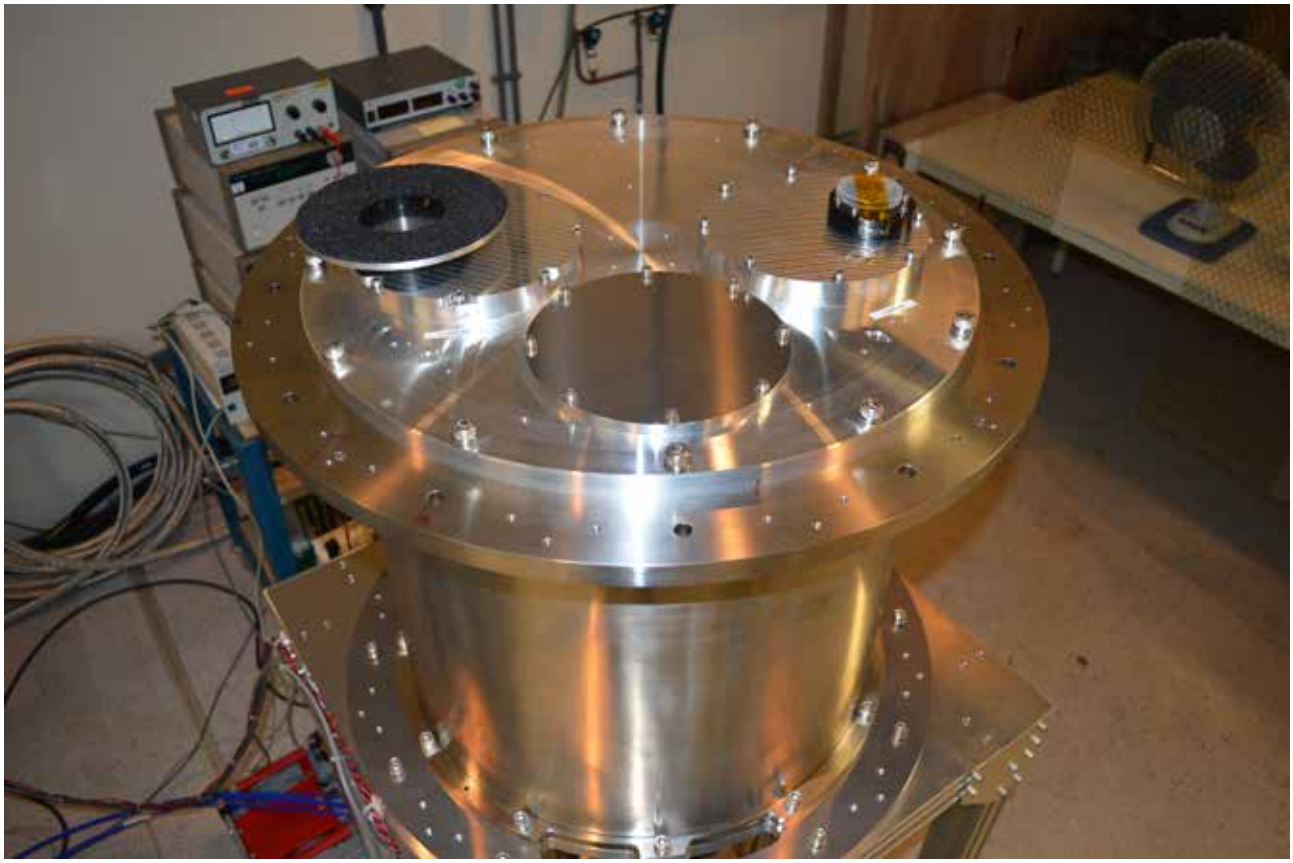

Figure 6. Cryostat for the bolometers. Credit: NOVA/ALMA.

by a Director. The first director resigned in late 2017, after the arrival of the telescope to Argentina. The deputy director also resigned in mid 2018, after the instrument was transported to Alto Chorrillos (see Figure 9). The yoke of the antenna was damaged during an accident with one of the trucks. This has produced a delay in the original schedule. Currently the management is being redefined in order to adequately face the final stage of construction and the integration of the telescope. First light is expected in 3-4 years.

5. Synergy with other instruments

LLAMA will be part of a larger astronomical center in Salta. In the same summit of the mountain another telescope will be located a few hundred meters away: the Q&U Bolometric Interferometer (QUBIC) [8]. QUBIC is a hybrid telescope of innovative technology for studies of the polarization of the Cosmic Microwave Background (see the article about QUBIC in this same issue). It consists of two arrays of bolometers and an array of horns that allow for observations in two bands: 150 GHz and 220 GHz. The cryostats require similar temperatures to those of LLAMA's receivers (4 and 0.3 K). Both experiments, then, can share supporting infrastructure and personnel.

A number of lower frequency single dish instruments in Argentina can perform observations complementary to those made with LLAMA. ESA's Deep Space Antenna 3 (DSA 3), located in Malarg ue, Province of Mendoza, is a 35-m antenna that incorporates state-of-the-art technology[10]. Its technical facilities comprise Ka-band reception (31.8 – 32.3 GHz) and X-band transmission and reception. It is prepared to host Ka-band transmission (34.3 – 34.7 GHz) and K-band reception (25.5 – 27 GHz). An agreement between ESA and the Argentine Space Agency (CONAE) grants 10 % of the observing time to Argentina, and part of this time is available to the local astronomical community. Both IAR and the University of Rio Negro are working on a new digital receiver for astronomical purposes. A similar antenna has been built by China in the southern province of Neuquén, and it is also partially available for astronomical uses[11].

Another mm instrument will be located soon in Argentina: the China-Argentina Radio Telescope (CART)[4]. It is a 40-m single dish that will operate at the Felix Aguilar Observatory in San Juan Province. The instrument will be used at low frequencies for VLBI with application to geodesy, but in its final configuration it will be able to operate up to 45 GHz. At such frequencies it will be possible to implement interferometric observations with LLAMA.

A major goal of LLAMA is to form part of a larger array with the ALMA, see Figure 10. In order to operate as a piece in a larger interferometer LLAMA needs an ultra-precise timekeeping. ALMA uses for this purpose an atomic clock

[4] http://cart.unsj.edu.ar/index.php.

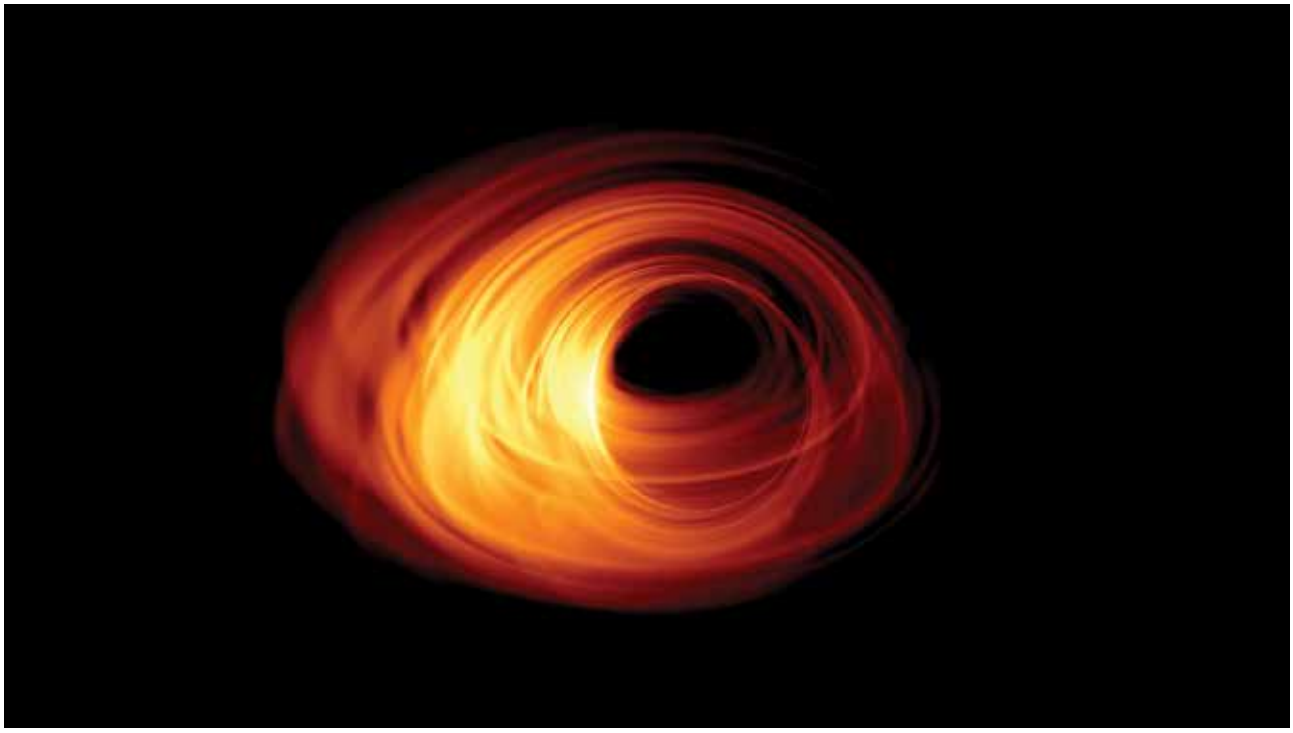

Figure 7. Simulated image of an accreting black hole. The event horizon is in the middle of the image, and the shadow can be seen with a rotating accretion disk surrounding it.. Credit: Bronzwaer/Davelaar/Moscibrodzka/Falcke/Radboud University.

powered by a hydrogen maser. A similar device should be implemented in LLAMA to link with other observatories. Also, formal agreements should be signed with ALMA in order to make possible an adequate integration of LLAMA in the array.

Conclusions

LLAMA telescope is a great challenge for Argentina and Brazil. It represents the most advanced astronomical instrument ever attempted by these countries. Once in operation, it will be a versatile facility that will be used as a single telescope for molecular line and continuum observations and as a component of a larger interferometer for high-resolution imaging of astrophysical sources. This latter utility is by far the most challenging one. It requires to implement technical and scientific methods never tried before in these countries. Advice from and collaboration with ALMA, ESO, NRAO, and other observatories with greater experience in this field will be essential to achieve success. The result, hopefully, will be the formation of a new generation of Latin American radio astronomers and many exciting contributions to our understanding of the Universe.

Acknowledgments

I thank Dr. Leonardo Pellizza, Dr. Paula Benaglia, and Dr. A. Etchegoyen for support and illuminating discussions about the project and Eng. Juan J. Larrarte for valuable information and help with the multiple tasks associated with the relationship between LLAMA and IAR. I am also grateful to Dr. Paula Benaglia, Eng. Leandro Gracía, Eng. Emiliano Rasztocky, Eng. J.J. Larrarte, Tech. Guillermo Gancio, and Tech. Fernando Hauscarriaga for their contributions to the project. The author was supported by the Argentine agency CONICET (PIP 2014-00338) and the Spanish Ministerio de Economía y Competitividad (MINECO/FEDER, UE) under grant AYA2016-76012-C3-1-P while writing this review.

References

[1] K. G. Jansky. Radio Waves from Outside the Solar System. *Nature*, 132:66, July 1933.

[2] G. Reber. Cosmic Static. *ApJ*, 100:279, November 1944.

[3] I. S. Shklovskii. *Cosmic radio waves*. Cambridge, Harvard University Press, 1960.

[4] E. M. Arnal, I. F. Mirabel, R. Morras, G. E. Romero, Z. Abraham, E. M. de Gouveira Dal Pino, and J. Lepine. Proyecto "LLAMA". *Boletin de la Asociacion Argentina de Astronomia La Plata Argentina*, 52:357–366, 2009.

[5] E. M. Arnal, R. Morras, G. M. Dubner, E. Giacani, I. F. Mirabel, G. E. Romero, J. R. D. Lepine, Z. Abraham, and E. M. de Gouveia dal Pino. Hacia una integración radioastronómica con Brasil: Proyecto LLAMA (Long Latin American Millimetre Array). *Boletin de la Asociacion Argentina de Astronomia La Plata Argentina*, 54:435–438, 2011.

[6] Vertex Antennentechnik GmbH. *Large Latin-American Millimetric Array Telescope LLAMA – Antenna with Nasmyth Focus – Technical proposal*. Vertex Antennentechnik GmbH, Duisburg, 2014, VA Proj-No.: 21/09087.

[7] LLAMA Collaboration Argentina. *Large Latin America Millimeter Array White Paper*. Preprint (undated).

[8] A. Mennella, P. Ade, G. Amico, D. Auguste, J. Aumont, S. Banfi, G. Barbaràn, P. Battaglia, E. Battistelli, A. Baù, B. Bélier, D. Bennett, L. Bergé, J. Bernard, M. Bersanelli, M. Sazy, N. Bleurvacq, J. Bonaparte, J. Bonis, E. Bunn, D. Burke, D. Buzi, A. Buzzelli, F. Cavaliere, P. Chanial, C. Chapron, R. Charlassier, F. Columbro, G. Coppi, A. Coppolecchia, R. D'Agostino, G. D'Alessandro, P. Bernardis, G. Gasperis, M. Leo, M. Petris, A. Donato, L. Dumoulin, A. Etchegoyen, A. Fasciszewski, C. Franceschet, M. Lerena, B. Garcia, X. Garrido, M. Gaspard, A. Gault, D. Gayer, M. Gervasi, M. Giard, Y. Héraud, M. Berisso, M. González, M. Gradziel, L. Grandsire, E. Guerard, J. Hamilton, D. Harari, V. Haynes, S. Versillé, D. Hoang, N. Holtzer, F. Incardona, E. Jules, J. Kaplan, A. Korotkov, C. Kristukat, L. Lamagna, S. Loucatos, T. Louis, A. Lowitz, V. Lukovic, R. Luterstein, B. Maffei, S. Marnieros, S. Masi, A. Mattei, A. May, M. McCulloch, M. Medina, L. Mele, S. Melhuish, L. Montier, L. Mousset, L. Mundo, J. Murphy, J. Murphy, C. O'Sullivan, E. Olivieri, A. Paiella, F. Pajot, A. Passerini, H. Pastoriza, A. Pelosi, C. Perbost, M. Perciballi, F. Pezzotta, F. Piacentini, M. Piat, L. Piccirillo, G. Pisano, G. Polenta, D. Prêle, R. Puddu, D. Rambaud, P. Ringegni, G. Romero, M. Salatino, A. Schillaci, C. Scóccola, S. Scully, S. Spinelli, G. Stankowiak, M. Stolpovskiy, F. Suarez, A. Tartari, J. Thermeau, P. Timbie, M. Tomasi, S. Torchinsky, M. Tristram, C. Tucker, G. Tucker, S. Vanneste, D. Viganò, N. Vittorio, F. Voisin, R. Watson, F. Wicek, M. Zannoni, and A. Zullo. QUBIC: Exploring the Primordial Universe with the Q&U Bolometric Interferometer. *Universe*, 5:42, January 2019.

[9] Event Horizon Telescope Collaboration, Kazunori Akiyama, Antxon Alberdi, Walter Alef, Keiichi Asada, Rebecca Azulay, Anne-Kathrin Baczko, David Ball, Mislav Baloković, John Barrett, Dan Bintley, Lindy Blackburn, Wilfred Boland, Katherine L. Bouman, Geoffrey C. Bower, Michael Bremer, Christiaan D. Brinkerink, Roger Brissenden, Silke Britzen, Avery E. Broderick, Dominique Broguiere, Thomas Bronzwaer, Do-Young Byun, John E. Carlstrom, Andrew Chael, Chi-kwan Chan, Shami Chatterjee, Koushik Chatterjee, Ming-Tang Chen, Yongjun Chen, Ilje Cho, Pierre Christian, John E. Conway, James M. Cordes, Geoffrey B. Crew, Yuzhu Cui, Jordy Davelaar, Mariafelicia De Laurentis, Roger Deane, Jessica Dempsey, Gregory Desvignes, Jason Dexter, Sheperd S. Doeleman, Ralph P. Eatough, Heino Falcke, Vincent L. Fish, Ed Fomalont, Raquel Fraga-Encinas, William T. Freeman, Per Friberg, Christian M. Fromm, José L. Gómez, Peter Galison, Charles F. Gammie, Roberto García, Olivier Gentaz, Boris Georgiev, Ciriaco Goddi, Roman Gold, Minfeng Gu, Mark Gurwell, Kazuhiro Hada, Michael H. Hecht, Ronald Hesper, Luis C. Ho, Paul Ho, Mareki Honma, Chih-Wei L. Huang, Lei Huang, David H. Hughes, Shiro Ikeda, Makoto Inoue, Sara Issaoun, David J. James, Buell T. Jannuzi, Michael Janssen, Britton Jeter, Wu Jiang, Michael D. Johnson, Svetlana Jorstad, Taehyun Jung, Mansour Karami, Ramesh Karuppusamy, Tomohisa Kawashima, Garrett K. Keating, Mark Kettenis, Jae-Young Kim, Junhan Kim, Jongsoo Kim, Motoki Kino, Jun Yi Koay, Patrick M. Koch, Shoko Koyama, Michael Kramer, Carsten Kramer, Thomas P. Krichbaum, Cheng-Yu Kuo, Tod R. Lauer, Sang-Sung Lee, Yan-Rong Li, Zhiyuan Li, Michael Lindqvist, Kuo Liu, Elisabetta Liuzzo, Wen-Ping Lo, Andrei P. Lobanov, Laurent Loinard, Colin Lonsdale, Ru-Sen Lu, Nicholas R. MacDonald, Jirong Mao, Sera Markoff, Daniel P. Marrone, Alan P. Marscher, Iván Martí-Vidal, Satoki Matsushita, Lynn D. Matthews, Lia Medeiros, Karl M. Menten, Yosuke Mizuno, Izumi Mizuno, James M. Moran, Kotaro Moriyama, Monika Moscibrodzka, Cornelia Müller, Hiroshi Nagai, Neil M. Nagar, Masanori Nakamura, Ramesh Narayan, Gopal Narayanan, Iniyan Natarajan, Roberto Neri, Chunchong Ni, Aristeidis Noutsos, Hiroki Okino, Héctor Olivares, Gisela N. Ortiz-León, Tomoaki Oyama, Feryal Özel, Daniel C. M. Palumbo, Nimesh Patel, Ue-Li Pen, Dominic W. Pesce, Vincent Piétu, Richard Plambeck, Aleksandar PopStefanija, Oliver Porth, Ben Prather, Jorge A. Preciado-López, Dimitrios Psaltis, Hung-Yi Pu, Venkatessh Ramakrishnan, Ramprasad Rao, Mark G. Rawlings, Alexander W. Raymond, Luciano Rezzolla, Bart Ripperda, Freek Roelofs, Alan Rogers, Eduardo Ros, Mel Rose, Arash Roshanineshat, Helge Rottmann, Alan L. Roy, Chet Ruszczyk, Benjamin R. Ryan, Kazi L. J. Rygl, Salvador Sánchez, David Sánchez-Arguelles, Mahito Sasada, Tuomas Savolainen, F. Peter Schloerb, Karl-Friedrich Schuster, Lijing Shao, Zhiqiang Shen, Des Small, Bong Won Sohn, Jason SooHoo, Fumie Tazaki, Paul Tiede, Remo P. J. Tilanus, Michael Titus, Kenji Toma, Pablo Torne, Tyler Trent, Sascha Trippe, Shuichiro Tsuda, Ilse van Bemmel, Huib Jan van Langevelde, Daniel R. van Rossum, Jan Wagner, John Wardle, Jonathan Weintroub, Norbert Wex, Robert Wharton, Maciek Wielgus, George N. Wong, Qingwen Wu, Ken Young, André Young, Ziri Younsi, Feng Yuan, Ye-Fei Yuan, J. Anton Zensus, Guangyao Zhao, Shan-Shan Zhao, Ziyan Zhu, Juan-Carlos Algaba, Alexander Allardi, Rodrigo Amestica, Jadyn Anczarski, Uwe Bach, Frederick K. Baganoff, Christopher Beaudoin, Bradford A. Benson, Ryan Berthold, Jay M. Blanchard, Ray Blundell, Sandra Bustamente, Roger Cappallo, Edgar Castillo-Domínguez, Chih-Cheng Chang, Shu-Hao Chang, Song-Chu Chang, Chung-Chen Chen, Ryan Chilson, Tim C. Chuter, Rodrigo Córdova Rosado, Iain M. Coulson, Thomas M. Crawford, Joseph Crowley, John David, Mark Derome, Matthew Dexter, Sven Dornbusch, Kevin A. Dudevoir, Sergio A. Dzib, Andreas Eckart, Chris Eckert, Neal R. Erickson, Wendeline B. Everett, Aaron Faber, Joseph R. Farah, Vernon Fath, Thomas W. Folkers, David C. Forbes, Robert

Freund, Arturo I. Gómez-Ruiz, David M. Gale, Feng Gao, Gertie Geertsema, David A. Graham, Christopher H. Greer, Ronald Grosslein, Frédéric Gueth, Daryl Haggard, Nils W. Halverson, Chih-Chiang Han, Kuo-Chang Han, Jinchi Hao, Yutaka Hasegawa, Jason W. Henning, Antonio Hernández-Gómez, Rubén Herrero-Illana, Stefan Heyminck, Akihiko Hirota, James Hoge, Yau-De Huang, C. M. Violette Impellizzeri, Homin Jiang, Atish Kamble, Ryan Keisler, Kimihiro Kimura, Yusuke Kono, Derek Kubo, John Kuroda, Richard Lacasse, Robert A. Laing, Erik M. Leitch, Chao-Te Li, Lupin C. C. Lin, Ching-Tang Liu, Kuan-Yu Liu, Li-Ming Lu, Ralph G. Marson, Pierre L. Martin-Cocher, Kyle D. Massingill, Callie Matulonis, Martin P. McColl, Stephen R. McWhirter, Hugo Messias, Zheng Meyer-Zhao, Daniel Michalik, Alfredo Montaña, William Montgomerie, Matias Mora-Klein, Dirk Muders, Andrew Nadolski, Santiago Navarro, Joseph Neilsen, Chi H. Nguyen, Hiroaki Nishioka, Timothy Norton, Michael A. Nowak, George Nystrom, Hideo Ogawa, Peter Oshiro, Tomoaki Oyama, Harriet Parsons, Scott N. Paine, Juan Peñalver, Neil M. Phillips, Michael Poirier, Nicolas Pradel, Rurik A. Primiani, Philippe A. Raffin, Alexandra S. Rahlin, George Reiland, Christopher Risacher, Ignacio Ruiz, Alejandro F. Sáez-Madaín, Remi Sassella, Pim Schellart, Paul Shaw, Kevin M. Silva, Hotaka Shiokawa, David R. Smith, William Snow, Kamal Souccar, Don Sousa, T. K. Sridharan, Ranjani Srinivasan, William Stahm, Anthony A. Stark, Kyle Story, Sjoerd T. Timmer, Laura Vertatschitsch, Craig Walther, Ta-Shun Wei, Nathan Whitehorn, Alan R. Whitney, David P. Woody, Jan G. A. Wouterloot, Melvin Wright, Paul Yamaguchi, Chen-Yu Yu, Milagros Zeballos, Shuo Zhang, and Lucy Ziurys. First M87 Event Horizon Telescope Results. I. The Shadow of the Supermassive Black Hole. *The Astrophysical Journal*, 875(1):L1, Apr 2019.

[10] P. Benaglia, N. Casco, S. Cichowolski, A. Cillis, B. García, D. Ravignani, E. M. Reynoso, and G. de la Vega. The antenna DSA 3 and its potential use for Radio Astronomy. *Boletin de la Asociacion Argentina de Astronomia La Plata Argentina*, 54:447–450, 2011.

[11] M. Colazo. Las antenas de espacio profundo en la Argentina. *Boletin de la Asociacion Argentina de Astronomia La Plata Argentina*, 60:65–66, August 2018.

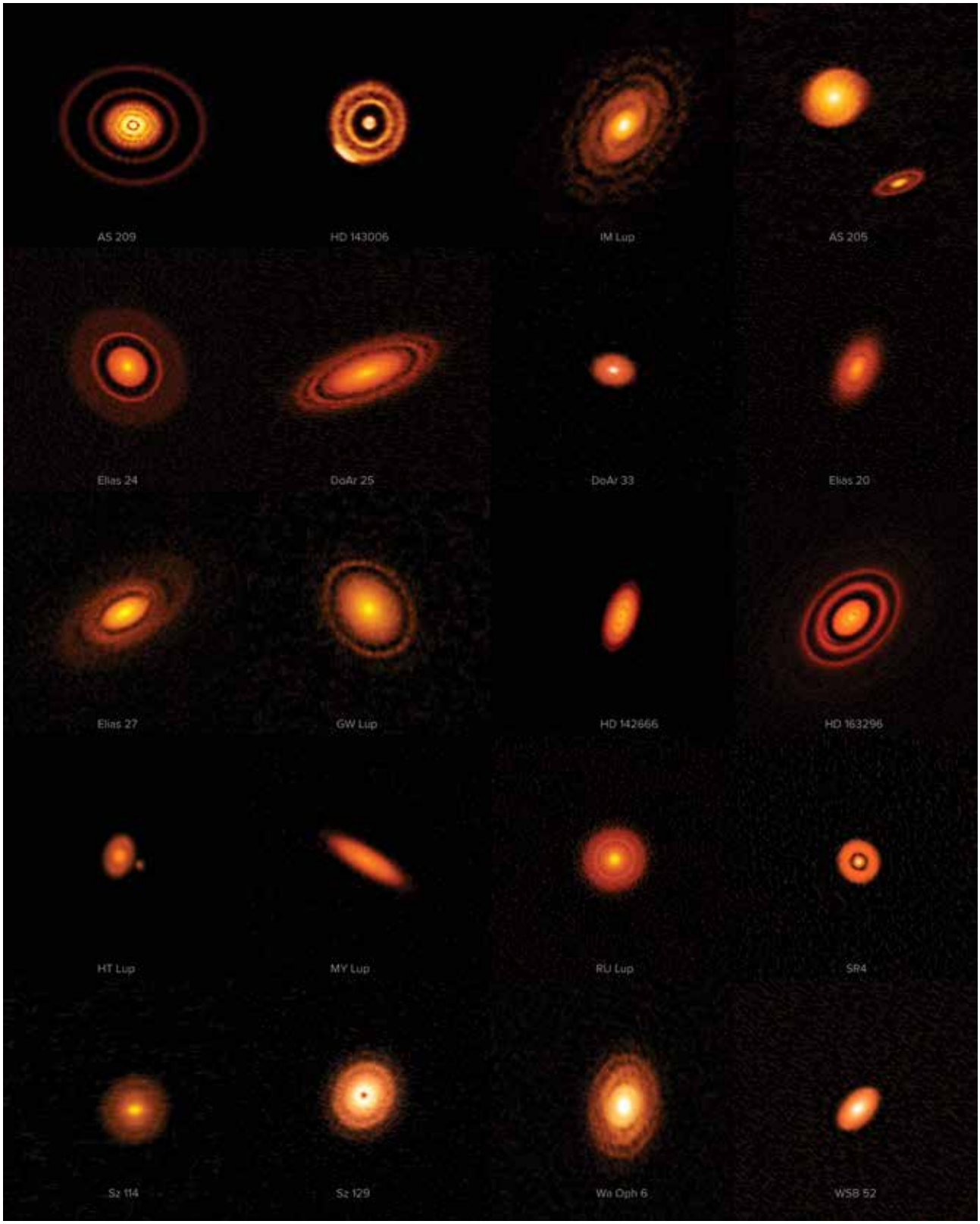

Figure 8. Protoplanetary discs around young stars captured by ALMA's first Large Program, known as the Disk Substructures at High Angular Resolution Project (DSHARP). Credit: ALMA (ESO/NAOJ/NRAO), S. Andrews et al.; NRAO/AUI/NSF, S. Dagnello .

Figure 9. View of the installation of different components of LLAMA antenna in Alto Chorrillos . Credit: Fundación CAPACIT-AR and Instituto Geonorte, INENCO (CONICET).

Figure 10. View of the Atacama Large Millimeter Array (ALMA). Credit: Y. Beletsky/ESO

Bio

Gustavo E. Romero

Gustavo E. Romero is a Full Professor of Relativistic Astrophysics at the University of La Plata and Superior Researcher of the National Research Council of Argentina (CONICET). He is a former President of the Argentine Astronomical Society and is the current Director of the Argentine Institute for Radio Astronomy (IAR). Romero is one of the most frequently cited scientists of Argentina. He has published more than 450 papers on astrophysics, gravitation, the foundations of physics, philosophy, and 12 books. Most of his research focuses on black hole physics, gamma-ray astrophysics, gravitation, cosmic rays, and ontological problems of spacetime theories. He has received numerous awards in recognition of his work, including the Houssay Prize (twice), the Gaviola Award from the National Academy of Sciences of Argentina, and the Helmholtz International Award. Among his books we can mention *Introducción a la Astrofísica Relativista* (Universitat de Barcelona Press, 2011 in collaboration with J.M. Paredes), *Introduction to Black Hole Astrophysics* (Springer, 2013 in collaboration with G. Vila) and *Scientific Philosophy* (Springer, 2018).

Science Reviews
from the end of the world

Vol. 1, No. 4, September 2020 // pp. 47-65 /

QUBIC: Observing the Polarized Microwave Sky over the Puna

QUBIC Collaboration:

Beatriz García[1], Diego Harari[2*], Claudia Scóccola[3], Peter Ade[4], José G. Alberro[3], Alejandro Almela[1], Giorgio Amico[5], Horacio Arnaldi[2], Didier Auguste[6], Jonathan Aumont[7], Susanna Azzoni[8], Stefano Banfi[9,10], Paola Battaglia[11], Elia Battistelli [5,12], Alessandro Baú[9,10], Benoit Bélier[13], David G. Bennett[14], Laurent Bergé[15], Jean-Philippe Bernard[16], Marco Bersanelli[17,18], Marie-Anne Bigot Sazy[19], Nathan Bleurvacq[19], Juan Bonaparte[20], Julien Bonis[6], Asdrúbal Bottani[3], Emory Bunn[21], David Burke[14], Daniele Buzi[5], Alessandro Buzzelli[22,23], Francesco Cavaliere[17,18], Pierre Chanial[19], Claude Chapron[19], Romain Charlassier[19], Fabio Columbro[5,12], Gabriele Coppi[24], Alessandro Coppolecchia[5,12], Giuseppe D'Alessandro[5,12], Paolo de Bernardis[5,12], Giancarlo De Gasperis[22,23], Stéphane Dheilly[19], Michele De Leo[5,25], Marco De Petris[5,12], Andrés Di Donato[20], Louis Dumoulin[15], Alberto Etchegoyen[1], Adrián Fasciszewski[20], Luciano P. Ferreyro[1], Diego Fracchia[1], Cristian Franceschet[17,18], Martín Miguel Gamboa Lerena[3], Kenneth Ganga[19], Manuel E. García Redondo[1], Michel Gaspard[6], Amanda Gault[26], Donnacha Gayer[14], Massimo Gervasi [9,10], Martin Giard[16], Valerio Gilles[5], Yannick Giraud Héraud[19], Mariano Gómez Berisso[2], Manuel González[2], Marcin Gradziel[14], Laurent Grandsire[19], Jean-Christophe Hamilton[19], Vic Haynes[8], Sophie Henrot-Versillé[6], Duc Thuong Hoang[19,27], Federico Incardona[17,18], Eric Jules[6], Jean Kaplan[19], Andrei Korotkov[28], Christian Kristukat[20,29], Luca Lamagna[5,12], Sotiris Loucatos[19], Thibaut Louis[6], Raúl Horacio Luterstein[20], Bruno Maffei[7], Stefanos Marnieros[15], Silvia Masi,[5,12], Angelo Mattei[12], Andrew May[8], Mark McCulloch[8], Maria Clementina Medina[30], Lorenzo Mele[5], Simon J. Melhuish[8], Aniello Mennella[17,18], Ludovic Montier[16], Louise Mousset[19], Luis Mariano Mundo[3], John Anthony Murphy[14], James David Murphy[14], Federico Nati[9,10], Créidhe O'Sullivan[14], Emiliano Olivieri[15], Alessandro Paiella[5,12], François Pajot[16], Andrea Passerini[9,10], Hernan Pastoriza[2], Alessandro Pelosi[12], Camille Perbost[19], Maurizio Perciballi[12], Federico Pezzotta[17,18], Francesco Piacentini[5,12], Michel Piat[19], Lucio Piccirillo[8], Giampaolo Pisano[4], Manuel Platino[1], Gianluca Polenta[31], Damien Prêle[19], Roberto Puddu[32], Damien Rambaud[16], Pablo Ringegni[3], Gustavo E. Romero[30], Maria Salatino[33], Juan M. Salum[1], Alessandro Schillaci[34], Stephen P. Scully[14,35], Sebastiano Spinelli[9], Guillaume Stankowiak[19], Michail Stolpovskiy[19], Federico Suarez[1], Andrea Tartari[36], Jean Pierre Thermeau[19], Peter Timbie[26], Maurizio Tomasi[17,18], Steve A. Torchinsky[19], Matthieu Tristram[6], Carole E. Tucker[4], Gregory S. Tucker[28], Sylvain Vanneste[6], Daniele Viganó[17], Nicola Vittorio[22,23], Fabrice Voisin[19], Robert Watson[8], Francois Wicek[6], Mario Zannoni[9,10] and Antonio Zullo[12]

[1] *Instituto de Tecnologías en Detección y Astropartículas (CNEA-CONICET-UNSAM), Buenos Aires B1650, Argentina*
[2] *Centro Atómico Bariloche and Instituto Balseiro, CNEA, San Carlos de Bariloche R8402AGP, Argentina*
[3] *Universidad Nacional de la Plata, La Plata B1900FWA, Argentina*
[4] *School of Physics and Astronomy, Cardiff University, Cardiff CF10 3AT, UK*
[5] *Department of Physics, Università di Roma La Sapienza, 00185 Roma, Italy*
[6] *Laboratoire de l'Accélérateur Linéaire (CNRS-IN2P3), 91898 Orsay, France*
[7] *Institut d'Astrophysique Spatiale (CNRS-INSU), 91405 Orsay*
[8] *School of Physics & Astronomy, University of Manchester, Manchester M13 9PL, UK*
[9] *Department of Physics, Università di Milano Bicocca, 20126 Milano, Italy*

[10] *Istituto Nazionale di Fisica Nucleare Milano Bicocca Section, 20126 Milano, Italy*
[11] *Istituto Nazionale di Astrofisica/OAS Bologna, 40129 Bologna, Italy*
[12] *Istituto Nazionale di Fisica Nucleare Roma 1 Section, 00185 Roma, Italy*
[13] *Centre de Nanosciences et de Nanotechnologies, 91120 Palaiseau, France*
[14] *Department of Experimental Physics, National University of Ireland, Mariavilla, Maynooth 99MX+QH, Ireland*
[15] *Centre de Spectrométrie Nucléaire et de Spectrométrie de Masse (CNRS-IN2P3), 91405 Orsay, France*
[16] *Institut de Recherche en Astrophysique et Planétologie (CNRS-INSU), 31028 Toulouse, France*
[17] *Dipartimento di Fisica, Università degli Studi di Milano, 20133 Milano, Italy*
[18] *Istituto Nazionale di Fisica Nucleare Milano 1 Section, 20133 Milano, Italy*
[19] *AstroParticule et Cosmologie (CNRS-IN2P3), 75013 Paris, France*
[20] *Comisión Nacional De Energia Atómica, C1429BNP Buenos Aires, Argentina*
[21] *Department of Physics, Richmond University, Richmond, VA 23173, USA*
[22] *Dipartimento di Fisica, Università di Roma Tor Vergata, 00133 Roma, Italy*
[23] *Istituto Nazionale di Fisica Nucleare Roma Tor Vergata section, 00133 Roma, Italy*
[24] *Department of Physics and Astronomy, University of Pennsylvania, Philadelphia 19104, USA*
[25] *Department of Physics, University of Surrey, Guildford GU2 7XH, UK*
[26] *Department of Physics, University of Wisconsin, Madison, WI 53706, USA*
[27] *University of Science and Technology of Hanoi (USTH), Vietnam Academy of Science and Technology (VAST), Hanoi 10000, Vietnam*
[28] *Department of Physics, Brown University, Providence, RI 02912, USA*
[29] *Escuela de Ciencia y Tecnología, Universidad Nacional de San Martín, San Martin 1650, Argentina*
[30] *Instituto Argentino de Radioastronomía, Berazategui 1880, Argentina*
[31] *Agenzia Spaziale Italiana, 00133 Rome, Italy*
[32] *Instituto de Astrofísica and Centro de Astro-Ingeniería, Pontificia Universidad Católica de Chile, Santiago 782046, Chile*
[33] *Kavli Institute for Particle Astrophysics and Cosmology and Physics Department, Stanford University, Stanford, CA 94305 USA*
[34] *Department of Physics, California Institute of Technology, Pasadena, California 91125, USA*
[35] *Institute of Technology Carlow, Ireland*
[36] *Istituto Nazionale di Fisica Nucleare Pisa Section, 56127 Pisa, Italy*
[*] *Correspondence: harari@cab.cnea.gov.ar*

Abstract

QUBIC (Q&U Bolometric Interferometer for Cosmology) is an experiment designed to measure the polarization of the cosmic microwave background (CMB), the relic radiation from the Big-Bang. Detailed measurements of tiny temperature anisotropies in the CMB shaped our understanding of the early Universe. Accurate measurements of its polarization may reveal even earlier features, in particular the presence of gravitational waves with primordial origin. Such measurements can probe inflationary cosmological models, which postulate that quantum effects during an accelerated expansion at the earliest stages after the Big-Bang produced gravitational waves along with the density fluctuations that later seeded galaxy formation. QUBIC will join other international efforts currently pursuing this goal using a novel approach, which combines the sensitivity of bolometric detectors with the control of systematic effects provided by interferometry. After its current calibration phase is completed a technological demonstrator already constructed in European laboratories will be deployed in Alto Chorrillos, a site in the Puna near San Antonio de los Cobres, Salta, Argentina. The complete first module of the instrument is planned to be installed during 2020. We review the scientific goals of the project, the instrument design and its expected performance.

Keywords:
bolometric interferometry, cosmic microwave background, cosmology, gravitational waves, polarization, transition-edge sensors

Introduction

The oldest light in the Universe is the Cosmic Microwave Background (CMB) radiation, discovered by Penzias and Wilson in 1965 [1]. It has a thermal distribution with a temperature of 2.725 K. It brings us information about the conditions in the Universe almost 14 billion years ago, when no planets, stars or galaxies had yet formed. This was the time, 380,000 years after the Big-Bang, when the Universe had expanded enough so that the CMB temperature dropped down to the point that electrons and protons could combine into neutral atoms, from which photons scatter much less efficiently than from free electrons. The CMB photons bring us a picture of the Universe at such early times.

Tiny variations in the temperature of the CMB that arrives from different directions in the sky have been measured with increased precision since 1992 [2]. They are interpreted as the manifestation of small primordial inhomogeneities in the matter density that acted as seeds for the formation of galaxies and other large scale structures in the Universe. Their measurement allows a high-precision determination of the parameters of the current cosmological model [3].

The CMB was predicted to be linearly polarized [4]. The polarization was imprinted by anisotropic Thomson scattering during the last few interactions of CMB photons with free electrons, a process somewhat similar to how light is polarized after reflection off a surface. This small effect was experimentally verified for the first time in 2002 by the Degree Angular Scale Interferometer (DASI), located at the South Pole [5]. The process that imprinted the polarization was mostly driven by density inhomogeneities, responsible also for most of the CMB anisotropy. Gravitational waves can also leave their imprint in the CMB polarization [6, 7, 8]. A method was devised to disentangle what fraction of the polarization originates from gravitational waves [9, 10] . It is based upon a decomposition of the polarization properties into E-modes, invariant under reflections, and B-modes, that change sign under a reflection. Scalar (density) fluctuations at first order generate E-modes only, while tensor (gravitational waves) fluctuations can produce both. The E-modes are much larger than the expected B-modes, and have been measured with increasing accuracy since 2002, providing further confirmation of the Big-Bang paradigm and increasing the precision on the determination of cosmological parameters. On the contrary, B-modes imprinted by gravitational waves have not been observed yet.

B-modes in the CMB polarization have been observed at relatively small angular scales, of the order of a few arc minutes [11, 12]. These B-modes were predicted to exist as a consequence of weak gravitational lensing, the distortion of photon trajectories away from the straight line in an inhomogeneous gravitational field. Gravitational lensing rotates primordial E-modes into B-modes [13]. Measurement of these "secondary" B-modes is a great accomplishment, since an accurate mapping of the lensing effect provides insight into the distribution of dark matter on large scales, and may even allow an indirect measurement of the mass of the neutrinos.

Primordial B-modes, with an amplitude that is expected to peak at an angular scale of the order of one degree, are searched for with great expectation, since they would be indirect evidence for the existence of gravitational waves with cosmological wavelengths, that can not be detected directly with current instruments such as the Laser Interferometer Gravitational-Wave Observatory (LIGO) [14]. Primordial gravitational waves would be produced during an inflationary phase in the expansion of the early Universe. Inflation is currently the dominant paradigm to understand why the energy-density in the Universe is so close to the critical value corresponding to spatial-flatness, and why otherwise causally-disconnected regions when the CMB photons decoupled have almost the same temperature today [15, 16, 17]. It also provides a mechanism to generate tiny perturbations in the matter density that much latter seed galaxy formation. This same mechanism generates primordial gravitational waves, but inflationary models do not make a definite prediction for their amplitude, and consequently for the amplitude of the signal in B-modes. Observation of the footprint of gravitational waves in the B-modes of the CMB poses a great experimental challenge, partly due to their likely minuscule amplitude and also because their signature can be contaminated with polarized foregrounds of galactic origin.

Several experimental efforts are currently pursuing the search for primordial B-modes. Some are located at the South Pole [18, 19], that offers the driest site in the world and hence the best atmospheric conditions for the task. Others are in the Atacama desert in Chile [20, 21, 22, 23], the second driest site on Earth. We review in this article the QUBIC project [24, 25, 26, 27, 28], that will soon join the search for primordial B-modes from the Puna in Salta, Argentina. QUBIC is a novel kind of instrument, that combines the sensitivity of bolometric detectors based on Transition-Edge Sensors [29] with the control of systematics granted by interferometric operation.

The outline of this article is as follows. In section 1 we review the scientific goals behind the quest for primordial B-modes. In section 2 we describe the design of the QUBIC instrument, with special emphasis on its most distinctive feature: its self-calibration properties based on interferometric operation. We review the characteristics of the site chosen for its installation in Alto Chorrillos, Salta. We summarize work on the detection and analysis chain and the expected performance of the instrument. We conclude in section 3 with a summary of the current status of the project, its schedule and future plans.

1. Footprints of primordial gravitational waves

Gravitational waves were predicted to exist by Einstein in 1915, and a century elapsed until a first direct detection was possible, when LIGO measured the emission from the coalescence of binary black holes [14]. In the meantime, indirect evidence of their existence was available since 1974, when Hulse and Taylor verified that the rate of change in the period of a binary millisecond pulsar matched the expectation from the energy it should radiate away in gravitational waves[30]. The ongoing quest for primordial B-modes is analogous in the sense that while their measurement would not imply a direct detection, it would provide an unmistakable signature that gravitational waves with cosmological wavelengths existed well before any astrophysical object was formed.

1.1. E and B-modes

Temperature anisotropies are usually characterized through an expansion over the celestial sphere in spherical harmonics

$$T(\theta,\phi) = \sum_{\ell m} a^T_{\ell m} Y_{\ell m}(\theta,\phi)\ . \tag{1}$$

From measurements of temperature anisotropies we have gained a great knowledge about the Universe, such as its content in ordinary (baryonic) and dark matter, dark energy, its relatively negligible spatial curvature, the almost (but not quite) scale-invariant nature of the primordial matter inhomogeneities and their seemingly Gaussian distribution. We also learned that if primordial gravitational waves exist they contribute little to the observed anisotropies.

While this picture is quite compelling, there is still more to learn from measurements of the CMB polarization, particularly due to its sensitivity to the dynamics during the last few scatterings of the CMB photons. For instance, the observed anti-correlation of temperature and polarization confirms the coherence of fluctuations at scales larger than the horizon at the time when electrons and protons combined into neutral atoms [31]. This observation makes inflationary models of the early universe the most plausible explanation for the origin of density fluctuations, rather than for instance models based on topological defects, which do not produce fluctuations over scales larger than the horizon. Furthermore, the polarization properties of the CMB are particularly sensitive to the cosmological ionization and reionization history.

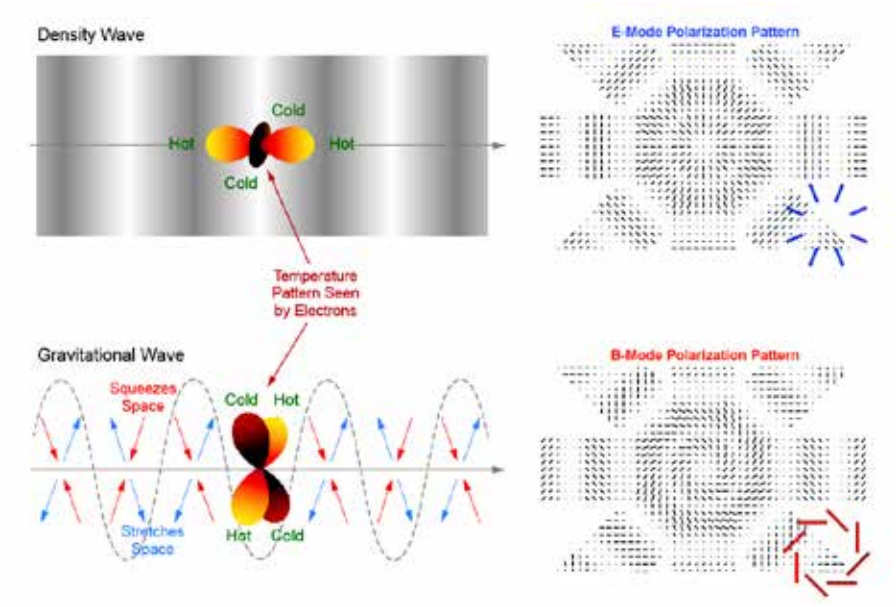

Figure 1. Illustration of polarization patterns induced by density waves compared to those by gravitational waves. Reproduced from [32].

Linear polarization is typically described in terms of Stokes parameters Q and U, that can be expanded in spherical harmonics with spin 2 [33]:

$$(Q \pm iU) = \sum_{\ell m} a^{(\pm 2)}_{\ell m} Y^{(\pm 2)}_{\ell m}\ . \tag{2}$$

Alternatively E and B-modes are defined through the linear combinations [9, 10]

$$\begin{aligned} a^E_{\ell m} &= -(a^{(+2)}_{\ell m} + a^{(-2)}_{\ell m})/2 \\ a^B_{\ell m} &= -(a^{(+2)}_{\ell m} - a^{(-2)}_{\ell m})/2i\ . \end{aligned} \tag{3}$$

E-modes are parity invariant, while *B*-modes change sign under a parity transformation. Characterization of CMB polarization properties in terms of *E* and *B*-modes is an invaluable source of information on different physical processes at work in the early Universe. *B*-modes can be used as a probe to infer if primordial gravitational waves drove partially the process that imprinted the polarization, in addition to density fluctuations. The origin of this possibility is illustrated in figure 1. Linear polarization can be imprinted in the CMB through Thomson scattering by electrons if the radiation has a quadrupolar anisotropy. The imprinted pattern of linear polarization differs depending on the type of motion of the electrons that scatter the radiation. Density waves produce a linear gradient in the gravitational potential that drives the motion of electrons, rotationally symmetric around the wave direction. Gravitational waves instead distort the gravitational potential differently in orthogonal directions perpendicular to their direction of propagation. The figure illustrates these different patterns in the rest frame of an electron. Shown also is the final polarization pattern after superposition of three crossing plane waves. Density waves do not imprint *B*-modes, while gravitational waves do.

Another contribution to *B*-modes comes from gravitational lensing that can convert a fraction of the CMB *E*-modes into *B*-modes[13]. The fluctuations in the gravitational potential of large scale structures distort the photon trajectories while preserving the orientation of the polarization, and thus alter the symmetry of the polarization pattern. The lensing contribution to *B*-modes can be disentangled and subtracted from a primordial signal through its different dependence on the angular scale as compared to that induced by gravitational waves, at least if the latter is not exceedingly smaller. It is also possible to generate *B*-modes by Faraday rotation of *E*-modes in primordial magnetic fields [34], but their frequency dependence would allow to clearly identify them if they actually existed. Density fluctuations can also produce *B*-modes through non-linear effects that generate secondary vector and tensor modes [35], but with a significantly reduced amplitude.

The major concern for contamination of a signal of primordial *B*-modes in addition to instrumental systematic effects are astrophysical foregrounds, particularly polarization by dust grains aligned by the galactic magnetic field and also synchrotron emission by relativistic electrons. They can in principle be accounted for through their angular power spectra and frequency dependence, distinct from that of the CMB. Measurements of CMB polarization at several frequencies are crucial for disentangling astrophysical foregrounds.

1.2. Quantum effects during inflation

An inflationary period in the early Universe [15, 16, 17] may have been the source for the tiny perturbations in the matter density that much latter seeded galaxy formation. Inflation can both generate quantum fluctuations and also drive them to cosmological scales. All fields have quantum fluctuations in their vacuum state. Quantum fluctuations at small scales in the field ϕ that drives the inflationary expansion are stretched to cosmological wavelengths and transferred to the matter density as inhomogeneities at later stages, when the expansion is radiation or matter-dominated. The wavelength of the fluctuations is expanded by a factor larger than 10^{30} during inflation, which explains their cosmological size in spite of their quantum origin. Their amplitude is almost the same when their wavelength is comparable to the cosmological horizon. The fluctuations in the field ϕ driving inflation and those in gravitational waves h have the same quantum origin and have comparable amplitude, determined by the value H of the Hubble constant (the rate of expansion) during the inflationary phase:

$$\langle h^2 \rangle = \frac{GH^2}{2\pi} \;\text{ with }\; H^2 = \frac{8\pi G}{3} V(\phi) \implies \langle h^2 \rangle = \frac{V(\phi)}{M^4_{\rm Planck}} \,, \tag{4}$$

where G is Newton's constant, and $M_{\rm Planck} \approx 10^{19}$ GeV is Planck's mass. The relative intensity between the tensor and scalar fluctuations predicted by inflation is typically described in terms of the dimensionless quantity r:

$$r = \frac{\langle h^2 \rangle}{\langle (\delta\rho/\rho)^2 \rangle} \;. \tag{5}$$

Here $\delta\rho/\rho$ are the relative density fluctuations, which are very well characterized by measurements of temperature anisotropies, and are of the order of 10^{-5}. This is why a measurement of r (the tensor-to-scalar ratio) is so relevant. It would reveal the presence of primordial gravitational waves, and determine the energy scale (the potential V) at which inflation took place:

$$V^{1/4} \approx \left(\frac{r}{0.01}\right)^{1/4} (10^{16}\text{GeV}) \,. \tag{6}$$

A value of r close to 0.01 would imply an energy scale close to that favoured theoretically for grand unified theories of fundamental interactions. Note, however, that there is no definite prediction for the value of r in inflationary models.

The inhomogeneities in the matter distribution generated by the quantum fluctuations of the field ϕ depend also on the details of the potential $V(\phi)$ driving inflation

$$\langle (\delta\rho/\rho)^2 \rangle = \frac{GH^2}{32\pi\varepsilon} \;\text{ with }\; \varepsilon = -\frac{\dot{H}}{H^2} \approx \frac{M^2_{\rm Planck}}{2} \left(\frac{V'}{V}\right)^2 \,, \tag{7}$$

where $\dot{H}$ is the time-derivative of the expansion rate, and V' is the derivative of the potential of the inflaton field, which determines the dependence of the density fluctuations with scale. Measurement of r would then also provide additional insight into the shape of the potential driving inflation, not only its absolute scale [36].

1.3. Bounds on primordial gravitational waves

In 2014 the BICEP2 experiment, located just next to where DASI measured E-modes for the first time in 2002, made the first detection of B-modes in the sky at degree angular scales [37], compatible with a value $r = 0.2$. It did so with an instrument operating at 150 GHz and scanning a region of the sky in which the galactic contamination was expected to be negligible. Subsequent measurements and analysis, in particular correlating data from BICEP2 and Keck Array at 150 GHz with that from the Planck satellite at 353 GHz, revealed [38] that the excess of B-modes observed at large angular scales was dominated by polarized emission by galactic dust. Figure 2 displays in the left panel the 95% confidence

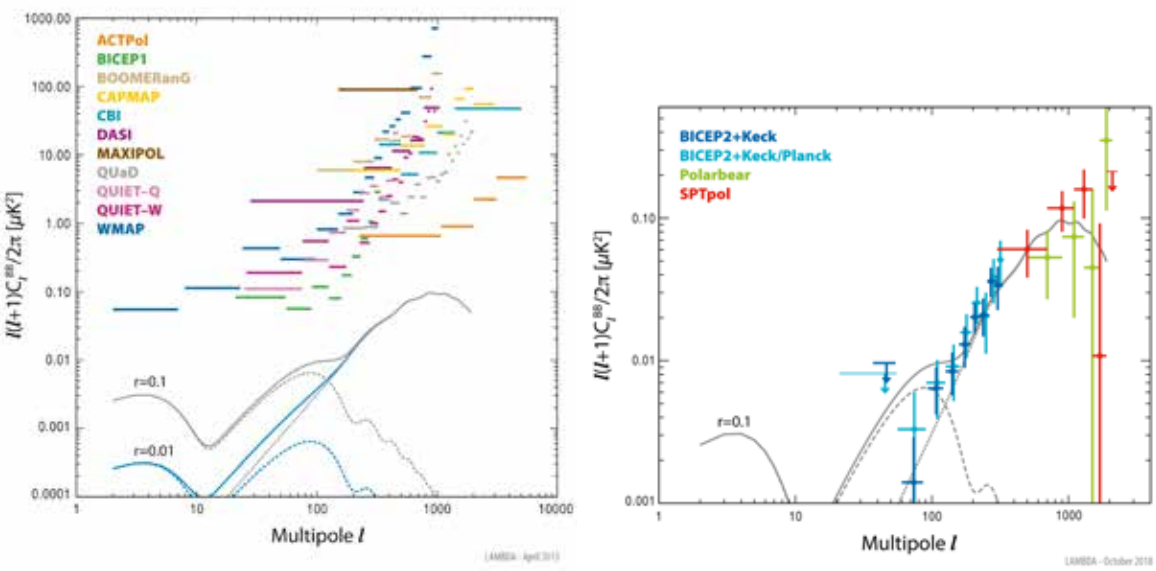

Figure 2. Left: 95% CL upper limits for the angular power spectrum in B-modes from different CMB experiments with no significant detections. Shown separately are the theoretical predictions for the contribution from lensing of E-modes (gray dotted line) and from primordial gravitational waves for $r = 0.1$ (gray dashed) and $r = 0.01$ (blue dashed lines). The solid lines correspond to the total power expected for $r = 0.1$ (gray) and $r = 0.01$ (blue). Right: observed B-modes from CMB experiments with significant detections. The lensing of E-modes into B-modes is detected with high significance, and at 95% confidence level $r < 0.06$. Figures reproduced from NASA-LAMBDA, https://lambda.gsfc.nasa.gov/.

level upper limits for B-mode power from different CMB experiments with no significant detections (as compiled in the NASA-LAMBDA site https://lambda.gsfc.nasa.gov/). Data from ACTPol, BICEP1, BOOMERanG, CAPMAP, CBI, DASI, MAXIPOL, QUaD, QUIET-Q, QUIET-W, and WMAP are included. Plotted is the rotationally invariant angular power spectrum $C_\ell^{BB} = \frac{1}{2\ell+1}\sum_m a_{\ell m}^{B*} a_{\ell m}^{B}$ for the B-modes. The corresponding angular scale in terms of the multipole moment is about $1^\circ(180/\ell)$. As reference theoretical predictions in a ΛCDM cosmology with values of the tensor-to-scalar ratio $r = 0.1$ (gray) and $r = 0.01$ (blue) are shown. The dashed lines are the tensor contributions and the solid lines are the total power after addition of the expected signal from weak gravitational lensing of E-modes (gray dotted line). Note that the signal in B-modes from primordial gravitational waves peaks at degree angular scales ($\ell \approx 80$) while that of lensing of E-modes peaks at significantly smaller angular scales ($\ell \approx 1000$). A reionization bump is also predicted for the tensor modes at larger angular scales ($\ell < 10$). The right panel of figure 2 displays the B-mode power measured by experiments with significant detections. Results from BICEP2, Planck, POLARBEAR, and SPTpol are included. The BICEP2 + Keck data points show the CMB contribution after separation into CMB, dust, and synchrotron components. The BICEP2 + Keck/Planck data points show results with dust foreground subtraction based on measured cross-power between Planck and BICEP2 + Keck. The other points show results without any foreground subtraction.

The signal expected from rotation of E-modes into B-modes by weak gravitational lensing is detected with high significance, and at 95% confidence level the tensor-to-scalar ratio is currently bound to be $r < 0.06$ [39], which already disfavours the simplest inflationary models of the early Universe.

The quest for detection of primordial B-modes in the CMB continues to be a major experimental challenge. Accurate foreground contamination and removal of lensing effects for values as low as $r = 0.001$ are challenging, but potentially feasible [40].

In what follows we describe the approach taken by QUBIC to confront the challenge of measuring primordial B-modes.

2. Measuring primordial B-modes with QUBIC

2.1. The QUBIC instrument

QUBIC is an additive interferometer formed by different components, as schematized in figure 3. The detection system is

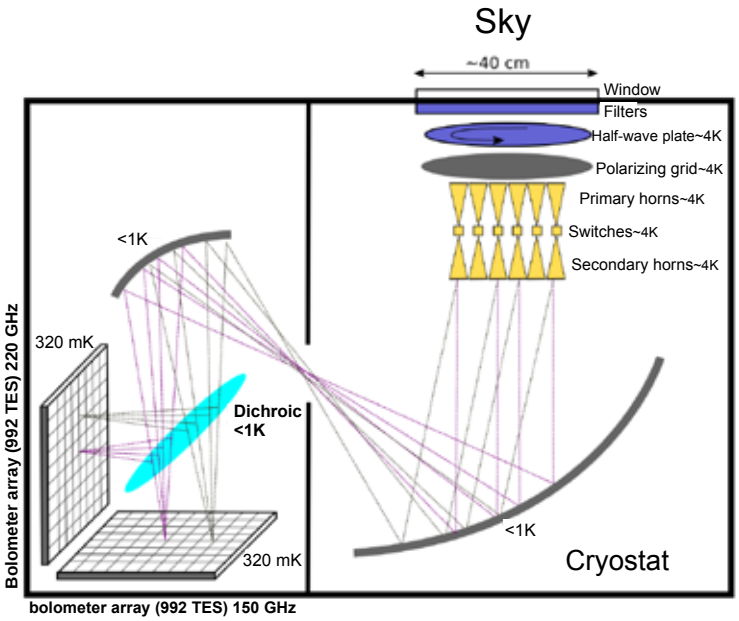

Figure 3. Schematics of the QUBIC instrument. Figure reproduced from [24].

contained inside a cryostat that is cooled down to 4K using pulse-tubes. The microwave signals to be measured enter the cryostat through a 45 cm diameter window made of ultra-high molecular weight polyethylene [41] that provides excellent transmission and mechanical stiffness. After the window, filters ensure a low thermal load inside the cryostat. Following this are a rotating Half-Wave-Plate (HWP) that modulates the polarization, and then a polarizing grid that selects one of the two linear polarization components.

Right below the polarizing grid an array of 400 corrugated horns receives the incoming radiation and defines the baselines for the interferometric operation of the instrument. These primary horns are followed by secondary back-horns that re-emit the signal towards an optical combiner constituted of a dual-mirror system. This combiner allows the radiation coming from different directions to sum coherently in the various locations of the detector focal planes, thus producing the interference fringes pattern. A key part of QUBIC is an array of switches placed between the two feed-horn arrays, which can be used to exclude particular baselines when the instrument operates in self-calibrating mode, as described in section 2.4.1.

Between the mirrors and the focal planes a dichroic filter splits the signal into its 150 GHz and 220 GHz sub-bands, imaged onto orthogonal focal planes, each equipped with 1024 Transition-Edge-Sensors (TES) cooled down to 320 mK. Of the set of 1024 TES, 992 are exposed to the sky radiation, while the rest are used to characterize systematic effects. The sensors are read using a cryogenic readout system based on superconducting quantum interference devices (SQUIDs) and Si-Ge application-specific integrated circuits (ASIC) operating at 4K with an unprecedented multiplexing factor equal to 128 [42, 43].

The TES technology is well developed and extensively used in several millimetric and sub-millimetric astronomical experiments. They have been chosen as detectors for the QUBIC first module. Other types of detectors such as Kinetic Inductance Detectors (KIDs) [44] will be considered for future QUBIC modules as they may offer an easier fabrication and readout, and larger scalability.

As mentioned before, the whole instrument will be integrated in a cryostat that needs to be operated without the use of cryogenic liquids in order to be usable in any remote observation site. The 4K stage is therefore ensured thanks to a pulse-tube refrigerator, which must remain with unchanged cooling efficiency when the instrument is tilted in elevation in the range between $\pm 30^\circ$ and 70° required to scan the region of the sky chosen for observation. The secondary and primary mirrors, dichroic filter and focal planes will be cooled down to 1K with a dedicated ^{4}He adsorption fridge and integrated in a special mechanical enclosure, the “1 K box”. The purpose of the 1K box in addition to thermal shielding is to assure the mechanical holding of these different parts. It was built stiff enough to guarantee the alignment of the optical components while the instrument scans the sky. The cryogenic stage for the detectors at 320 mK will be ensured through a ^{3}He/^{4}He absorption fridge. The outer dimensions of the cryostat (1.4 m in diameter and 1.6 m in height) allow for sufficient thermal insulation between the cryogenic instrument and the room-temperature shell. The total weight of the instrument is 800 kg,

and the weight of the overall internal structure that holds the horn array, the mirrors, the dichroic filter and the detectors has been limited to less than 150 kg in order to prevent too long a cooling time down to 1K.

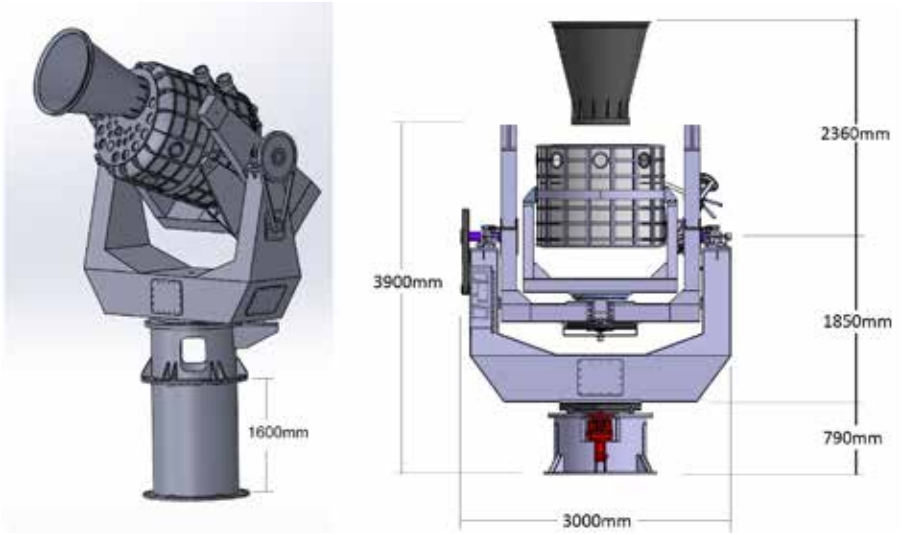

Figure 4. QUBIC assembly: cryostat with forebaffle on its mount (left); detail and dimensions (right).

QUBIC will host two arrays of bolometric detectors, operating respectively at 150 GHz and 220 GHz, that will observe interference fringes formed by the back-to-back horns on the focal planes of the optical combiner. The image formed is the result of the interference from the sum of the fields emitted by each of the 400 apertures.

Interferometry offers an improved control of instrumental systematics with respect to direct imaging, because interference fringes from different baselines can be calibrated individually. This feature is made possible in QUBIC thanks to the electromagnetic shutters inserted between the primary and secondary horns. Each shutter consists of a blade operated by a solenoid magnet that can slide into a smooth circular waveguide, and acts as a RF switch.

In the self-calibration mode, pairs of horns are successively shut when observing an artificial partially polarized source. QUBIC will use for external self-calibration a source able to radiate a typical power of few mW through a feedhorn with a well-known beam, and a low level of cross-polarisation, typically less than -30 dB. The source is a microwave synthesizer operated around 10 GHz followed by a multiplication chain which brings the frequency in the millimeter wave range to generate quasi-monochromatic signals in both QUBIC frequency bands. This external calibration source will be located in the far-field of the interferometer, at about 40 m from the instrument and it will be mounted on top of a tower near the instrument shelter inside an insulation box suitable to maintain the device within a specified temperature range. In addition, two carbon fiber sources located inside the cryostat, just next to to the array of back-to-back horns and switches, will also be used for calibration purposes [45].

The instrument will be installed on a mount, following a design as in Figure 4. It will be able to rotate 360° in azimuth, from 30° to 70° in elevation, and ±15° around the optical axis, with a pointing accuracy better than 20 arcsec. A forebaffle with 1 m length and 14° aperture will be used to reduce radiation from unwanted sources by more than 20 dB in directions between 20° and 40° away from the optical axis, and more than 40 dB beyond. A ground shield will also be included to minimize the brightness contrast between the sky and the ground.

Figure 5. Pictures of various QUBIC components. From left to right: integration of the instrument inside the cryostat, 1 K box, array of 64 back-to-back horns with individual switches, and focal plane on top of the cryogenic detection chain.

The QUBIC instrument is currently in a phase of laboratory calibration of its so-called “Technological Demonstrator” (TD). The TD uses the cryostat and 1K box built for the first module, but has a reduced focal plane and horn array and a smaller optical combiner compared to the full instrument. The TD has one-quarter of the TES focal plane (i.e. 256 pixels)

operating at 150 GHz and 64 back-to-back horns with their respective switches. The TD has already been integrated at the APC laboratories in Paris (see Figure 5) and is in the process of calibration, with very satisfactory preliminary results, as will be described in section 3. After calibration the TD will be sent to Argentina for installation on site while the construction of the complete first module continues. The TD was not designed to produce scientific results but will serve to demonstrate the feasibility of bolometric interferometry both in the laboratory as well as in the field.

A more detailed description of the QUBIC instrument can be found in its Technical Design Report in [27]. The QUBIC instrument is being built by an international collaboration with participating laboratories in France, Italy, UK, Ireland, USA and Argentina.

2.2. The Alto Chorrillos site

2.2.1. The site

The QUBIC instrument will be deployed in Alto Chorrillos, Salta, Argentina (24° 11'11.7" S, 66° 28'40.8" W) at 4,870 meters above the sea level, in what is known as the Puna de Atacama region. This location is 180 km away from the Chajnantor site in Chile where other millimeter-wave experiments and observatories are located (ALMA, APEX, Advanced ACTPol, POLARBEAR and CLASS) and offers similar atmospheric properties [46, 27]. It is next to the location of the Large Latin American Millimeter Array (LLAMA), a bi-lateral cooperation project between Argentina and Brasil that is installing a 12 m radiotelescope operating at millimeter and submillimeter wavelenghts (for more details see the article by G. Romero in this same volume). This location has been characterized during several years within the framework of the site selection process for the Cherenkov Telescope Array project, and for the LLAMA project, which has atmospheric requirements similar to those of QUBIC. We here summarize these and further studies that have been performed on the site properties, and the status of the infrastructure being developed.

The city nearest to the site is San Antonio de los Cobres, at an altitude of about 3,700 meters above sea level and 200 km from Salta city, the province capital. Originally a mining town, it now has about 7000 inhabitants, and in the last decade the town has witnessed the efforts of several international collaborations that have characterized the atmosphere of the area, searching for sites suitable for the installation of astrophysical experiments. The national route 40 crosses the region in the S-N direction. The most important nearby city is Salta, but it is also possible to access the area from San Salvador de Jujuy. The valley of San Antonio de los Cobres, which gives its name to the river that runs through it, unfolds parallel to the Andes. This valley culminates to the north in the depression of the Salinas Grandes, 80 km away from San Antonio. The site where QUBIC will be installed is named "Alto Chorrillos". It is located about 16 km in a straight line from the city

Figure 6. Qubic Site (top) and elevation profile (bottom). The positions of QUBIC and San Antonio de los Cobres are detailed as well as the distance between the sites. The elevation profile is such that it is possible to establish a direct link for communications.

of San Antonio de los Cobres, at 4870 meters above the sea level (see Figure 6) and in the same area where the LLAMA antenna will be installed. Alto Chorrillos is located within a reserve of 400 hectares allocated by the Government of the Province of Salta to Argentina's National Research Council (CONICET) for the installation of LLAMA. A flat area of about 125 m x 150 m will be used for the installation of QUBIC. A detailed map of this area is shown in the left panel of

figure 7. It displays the site chosen for the installation of the first module, as well as those reserved for future modules. The right panel in the figure displays a simulation of an aerial view of the site including the shelter with the first module and the tower for the calibration source.

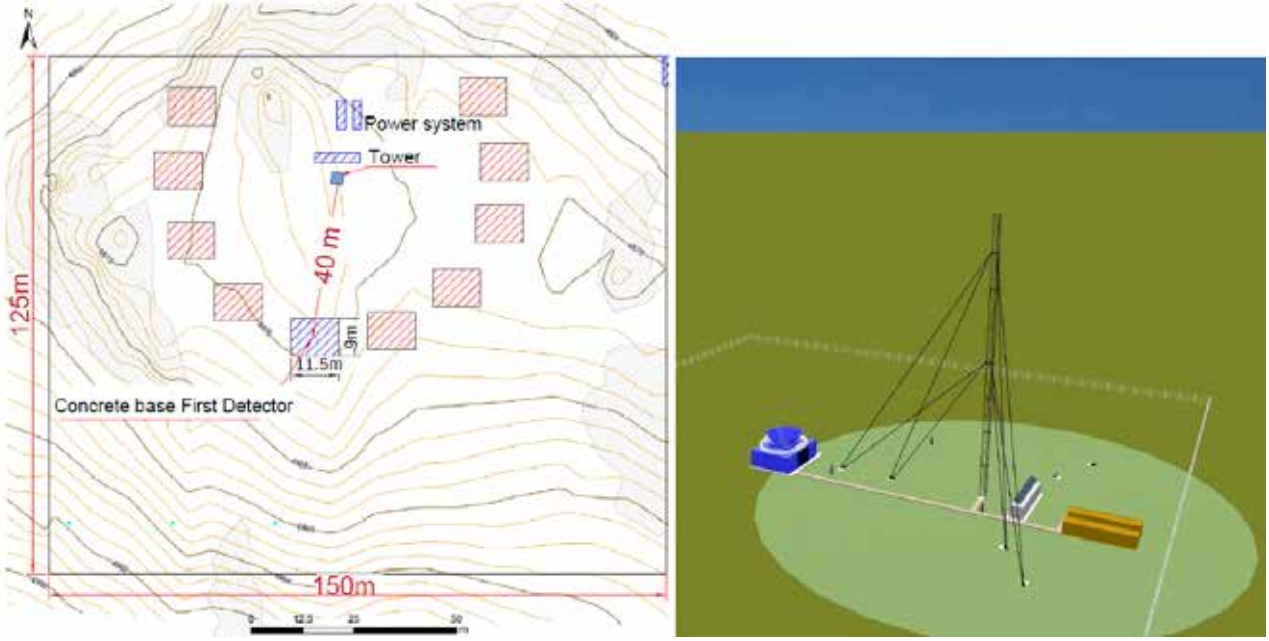

Figure 7. Left: detailed map of the area allocated to QUBIC. Slashed in blue the locations for the first installations, in red those reserved for future modules. Right: simulation of an aerial view for the first installations at the site, including the shelter with the first module and the tower for the calibration source.

The predominant climate in the area chosen for installation of the experiment is semi-arid continental, with significant fluctuations in temperature between day and night. The minimum temperature recorded was -16°C with a maximum of 35°C. Summer is a rainy season, but the rain is scarce (the annual average is 70-120 mm). The snowfalls are also scarce and they only whiten the tops of the mountains.

Emission from atmospheric water vapour in the site is the main source of photon noise measured by background-limited detectors such as those in QUBIC. During the last decade, the Argentine Institute of Radio Astronomy (IAR), which leads the LLAMA project in Argentina, has continuously carried out several campaigns to obtain weather measurements in Alto Chorrillos in order to establish the general climatic characteristics of the site and in particular to measure its atmospheric opacity. These measurements were performed using a tipping radiometer operating at 210 GHz, instrument lent by the National Autonomous University of Mexico. The results obtained from these observations and the permanent monitoring of opacity, show that the site is within the specifications required by LLAMA at the frequency of 210 GHz [46]. The measurements are summarized in the left panel of figure 8. These and further measurements of opacity at 210

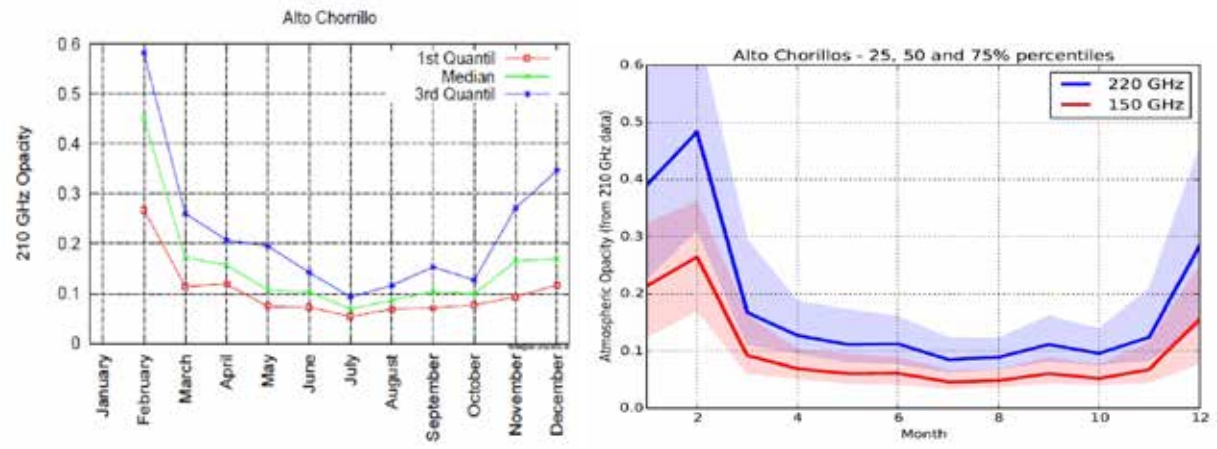

Figure 8. Left: atmospheric opacity at 210 GHz as measured in Alto Chorrillos for each month (reproduced from [46]). Right: extrapolations to 150 GHz and 220 GHz using an atmospheric model for Chajnantor (reproduced from [27]).

GHz (the published ones did not include January) were extrapolated to the frequencies at which QUBIC operates using an atmospheric emission spectrum model. Due to the proximity and similar geographical and geological characteristics, the Atmospheric Transmission at Microwaves (ATM) code [47] optimized for the atmospheric conditions in Chajnantor was used [27]. This is the site in Chile for the ALMA radio-telescopes, as well as for several other millimeter and submillimeter telescopes. The results of the extrapolation are shown in the right panel of figure 8. As we can see the atmospheric opacity is as good as $\tau < 0.20$ for all months, except for January and February (part of what is known as the "Bolivian winter"). The values of atmospheric opacities are comparable to the results for Chajnantor.

2.2.2. Weather measurements on site

In addition to the measurements of atmospheric opacity described above, meteorological data was collected in the context of the LLAMA project using a standard station installed in May 2010, provided by researchers from the Institute of Astronomy, Geophysics and Atmospheric Sciences of Brazil, in order to monitor the atmospheric temperature, humidity, pressure, and wind speed and direction. All the meteorological variables collected for LLAMA are within the ranges for smooth operation of QUBIC: temperature between $-15°$C and $+15°$C 90% of the time, wind speed with a maximum over 1 minute less that 20 m/s, clear skies 90% of the time and atmospheric opacity $\tau < 0.10$ (median) at 150 GHz and $\tau < 0.15$ (median) at 220 GHz.

Moreover, a new weather station was installed by the QUBIC collaboration in 2018, in order to record current data specifically at the QUBIC site. The ground data acquisition was performed using a DAVIS Vantage Pro II weather station (https://www.davisinstruments.com/solution/vantage-pro2/), located 3 meters above ground level and connected to a single board computer (SBC) and a data logger. The data were stored at the device in a convenient ad-hoc format, usually plain text. A simple database was designed to store all data in a consistent way, also providing a quick way to choose and process the data. The data were acquired every minute, all year round, and averaged every 10 minutes before the analysis. Figure 9 presents the results from the ground-based weather station in Alto Chorrillos. The average temperature and its dispersion

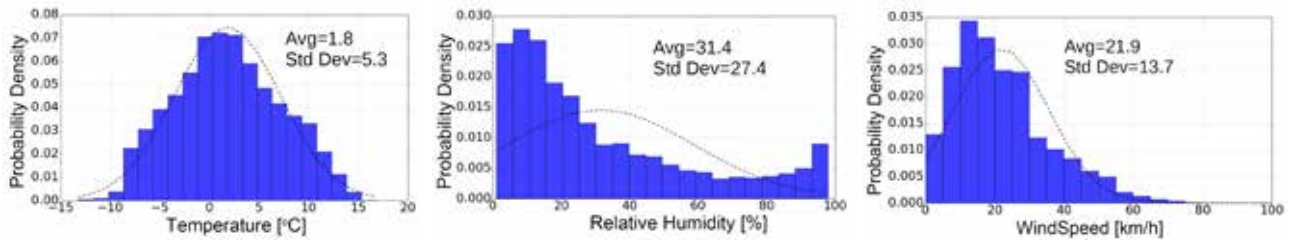

Figure 9. Histograms for the probability density of ambient temperature (left), humidity (center) and wind speed (right) at the Alto Chorrillos site. A normal distribution with the average and dispersion as in data is also plotted (dashed lines) for reference.

are $(1.8 \pm 5.3)°$C. The daily probability density for relative humidity is 31.4% in average with a standard deviation of about $\pm 27.5\%$. The analysis was performed for 24 hs. of data. The wind speed average is 21.9 km/h (6.1 m/s), with a standard deviation of ± 13.7 km/h. The wind gusts are, in general, a big restriction for astronomical facilities. In the case of the site chosen for QUBIC, the wind presents maximum speeds of 100 km/h (28 m/s). This is fundamental data to estimate the resistance needed by the shelter and the dome for the instrument.

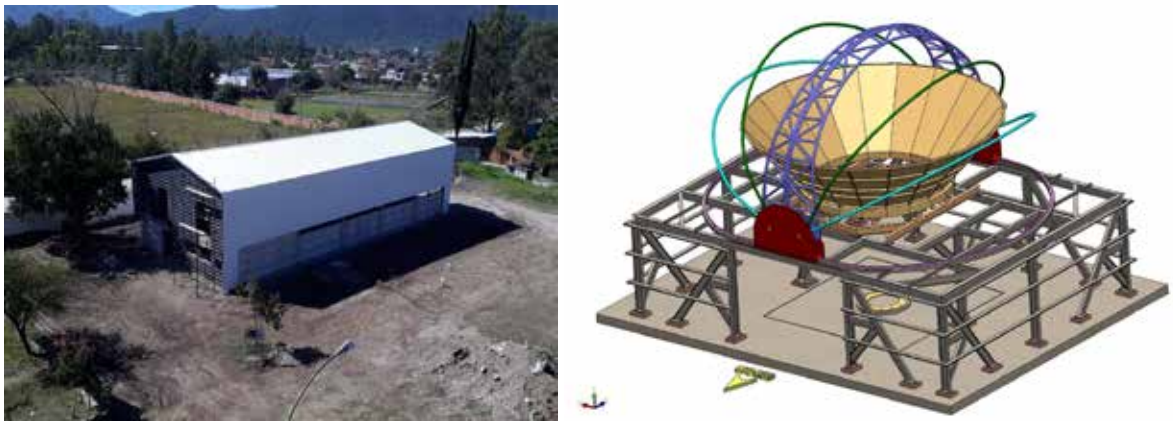

Figure 10. Ongoing construction of the Integration Laboratory in Salta City as of May 2019 (left) and design of the structure for shelter, dome and ground-shield for QUBIC (right).

2.2.3. Site development and infrastructure

Several developments related to the site are ongoing, mainly devoted to preparations to test the instrument upon arrival to Argentina and to secure its installation in Alto Chorrillos. The access road to the LLAMA site and from there to the QUBIC site has already been built, and constructions towards the installation of the first module are under way.

Figure 10 shows in its left panel the Integration Laboratory under construction in Salta city, the place where the instrument will be integrated and tested prior to installation in its final site, and the final design for the shelter and the dome for the instrument in its right panel. An open-foldable dome with high-tension textile membranes was chosen for the cover in order to reduce weight. The weather conditions, mainly the wind speed, were accounted for in the simulations of resistance of the complete building. The construction of the shelter is planned to be completed before the end of 2019.

2.3. Detection and analysis chain

2.3.1. Signal model and synthesized beam

The image that QUBIC will observe in each of the two focal planes is the result of an interferometric pattern that arises from the superposition of the signals of each of the secondary antennas in the horn array. Due to the time modulation introduced by the rotating half-wave plate (HWP), the signal measured by each of the bolometric detectors p in the focal plane with frequency ν and at time t can be described by:

$$R(p,\nu,t) = K[S_I(p,\nu) + \cos(4\phi_{HWP}(t))S_Q(p,\nu) + \sin(4\phi_{HWP}(t))S_U(p,\nu)] \tag{8}$$

where $\phi_{HWP}(t)$ is the angle of the HWP at time t, and K is an overall calibration constant that takes into account the efficiency of the optical chain. The three terms $S_{I,Q,U}$ in Equation 8 represent the sky signal in intensity and polarization convolved with the so-called synthesized beam (see Eq. 10).

As more and more horns are open in the observing array, the number of baselines increases (a baseline is the vector separating two horns). The constructive and destructive superposition of the re-emitted signals produces an effective beam which is highly non-trivial. In fact, the synthesized beam of QUBIC has a complicated shape, with a central peak and replications. The beam can be approximated by a central gaussian with secondary gaussian peaks, separated by an angular distance of about 8.5° with a width equal to the full-width at half-maximum (FWHM) at the observing frequency. Both the separation distance between peaks and their width depend on the frequency of the received signal. In the left panel of figure 11, a schematic plot of the synthesized beam for two monochromatic frequencies is shown, where it is clear the dependence on the observing frequency of the separation between primary and secondary peaks. The amplitudes of the primary and secondary peaks are modulated by a gaussian which is equal to the primary beam of the input horn. For a finite bandwidth, the beam is computed as the superposition of all the monochromatic beams included in the band, and due to the dependence on the frequency, the secondary peaks appear asymmetric and elongated. In the right panel of Figure 11 we show the synthesized beam of the central pixel, considering a 30% bandwidth.

2.3.2. Point source imaging

Taking into account all of the detectors in the focal plane, we can study the image obtained for a far-away point source located along the line of sight. The images in figure 12 shows the resulting synthesized beam on the focal plane. When QUBIC observes a far point-source located along the line-of-sight, with all 400 antennas open, the image formed in the focal planes is an interference pattern with the shape of the synthesized beam. It consists of peaks and lobes, and it is regarded as the beam that will convolve the sky-signal at observation time.

More specifically, if X is the signal from the sky (either in intensity, I, or polarization, Q, U), then the measured signal on the pixel p is $S_X(p) = \int X(\mathbf{n}) B^p_{synth}(\mathbf{n}) d\mathbf{n}$. This means that QUBIC data can be analyzed similarly to the data obtained from a normal imager, provided that we build a window function of the synthesized pattern for each pixel. The synthesized beam $B^p_{synth}(\mathbf{n})$ is obtained through the interference of the beams of different horns, and can be described, in the absence of optical aberrations, by

$$B^p_{synth}(\mathbf{n},\mathbf{r},\lambda) = \left| \sum_i B_{prim}(\mathbf{n}) B_{sec}(\mathbf{r}) \exp\left(i2\pi \frac{\mathbf{x}_i}{\lambda} \left(\frac{\mathbf{r}}{D_f} - \mathbf{n} \right) \right) \right|^2 \tag{9}$$

where $B^p_{prim}(\mathbf{n})$ is the primary beam (the input beam for horns pointing to the sky at direction $\mathbf{n}$); $B_{sec}(\mathbf{r})$ is the secondary beam acting at the $\mathbf{r}$ point in the focal plane (i.e. in the pixel p), $\mathbf{x}_i$ is the position of the horn i; D_f is the focal distance. For a square horn array the sum in the last equation can be computed analytically to give

$$B^p_{synth}(\mathbf{n},\mathbf{r},\lambda) = B_{prim}(\mathbf{n}) B_{sec}(\mathbf{r}) \frac{\sin^2\left[n_h \pi \frac{\Delta x}{\lambda} \left(\frac{r_x}{D_f} - n_x \right) \right] \sin^2\left[n_h \pi \frac{\Delta x}{\lambda} \left(\frac{r_y}{D_f} - n_y \right) \right]}{\sin^2\left[\pi \frac{\Delta x}{\lambda} \left(\frac{r_x}{D_f} - n_x \right) \right] \sin^2\left[\pi \frac{\Delta x}{\lambda} \left(\frac{r_y}{D_f} - n_y \right) \right]} \tag{10}$$

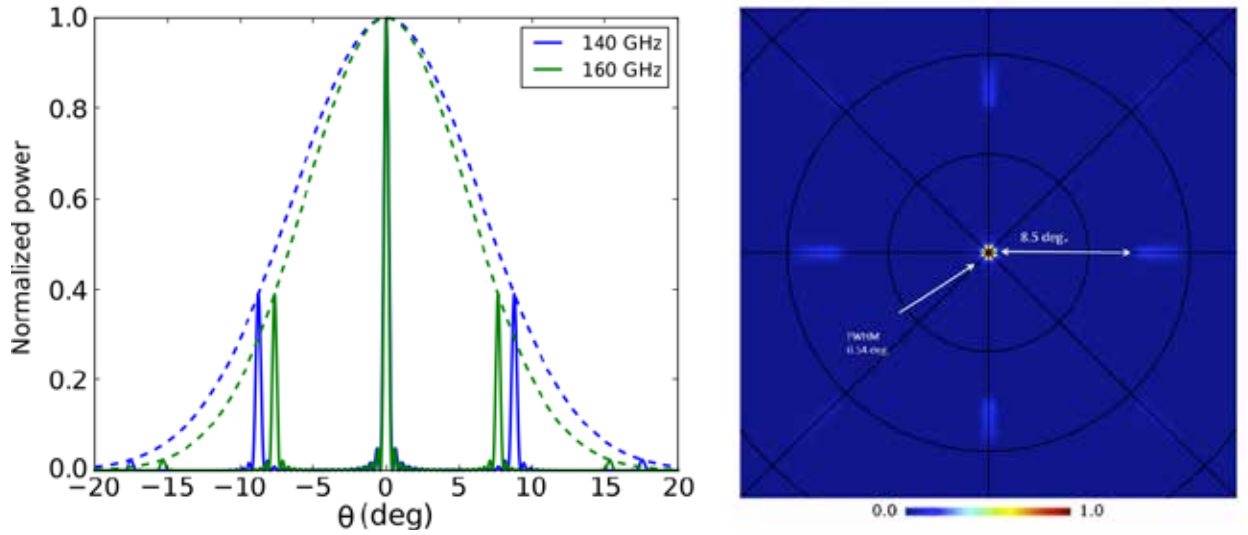

Figure 11. Left panel: Synthesized beam for the monochromatic case, for two nearby frequencies. The separation between the primary and secondary peaks of the beam depends on the frequency of the signal. Right panel: Simulation of the synthesized beam of the center pixel of the 150 GHz array, taking into account the finite (30%) bandwidth of the detectors. The addition of all of the secondary peaks of the monochromatic beams included in the band results on secondary peaks which are asymmetric and elongated. Figure adapted from [24] and [28].

where n_h is the number of horns on one side of the square horn array and Δx is the distance between them [24].

2.3.3. Map-making

QUBIC will observe a partial area of the sky, similar to the region observed by the BICEP2 Collaboration (another observational effort to measure the primordial B-modes [37]). It is a region with relatively low galactic foregrounds, although they cannot be neglected. This is the main reason why the instrument has two frequency bands, and the relevance of the spectro-imaging properties of QUBIC, which will be described in subsection 2.4.2. The contamination from foregrounds can be alleviated when the sky is observed in several frequencies.

When the signal is not a point-source but an extended region in the sky, as the QUBIC area will be, every detector in the focal plane will receive the signal from different directions in the sky, due to the non-trivial shape of the synthesized beam.

Exactly in the same way as for a usual imager, we can scan the sky with our synthesized beam with any scanning strategy, and any individual measurement results in the convolution of the sky through our synthesized beam. From the Time-Ordered Data (TOD) of each individual bolometer, we can reconstruct a map of the sky, taking into account the special shape of the synthesized beam.

2.4. Calibration and expected performance

2.4.1. Self-calibration

The design of QUBIC as a bolometric interferometer allows the exploitation of redundant interferometric patterns to control and reduce the systematics of the experiment. By using different combinations of open horns in the array, we can obtain a number of redundant baselines that can be used to self-calibrate the instrument. This technique is derived from radio-interferometry self-calibration [48].

To understand the basic concept of self-calibration, it is important to note that the interference pattern produced by two open horns will be exactly the same as one obtained with a different pair of open horns but defining exactly the same baseline (separation and orientation of the pair of open horns). For an ideal instrument, with no systematic effects, the interferometric pattern depends only on the baseline. Hence, we can use the observations obtained with equivalent baselines to account for the systematics of the instrument, by analysing the differences observed with different but equivalent baselines.

The theoretical framework of the self-calibration procedure is described in detail in [49]. The instrumental systematics are modelled via the use of Jones-matrices, which are used in cascade to describe the action of an optical chain onto the incoming radiation electric field (attenuation, polarization mixing, dephasing). For an instrument with several components, there is a Jones-matrix for each of them. In this way, the effect of each part of the instrument can be parametrized with a given model.

Systematic errors can come in the form of horn location errors, pointing errors, asymmetries of beams, bolometer location errors, diagonal and non-diagonal terms of the Jones-matrices, and so forth. Due to the time modulation of the polarized signal given by the HWP (eq. 8), and the subsequent action of the interference array, for a real instrument, there is

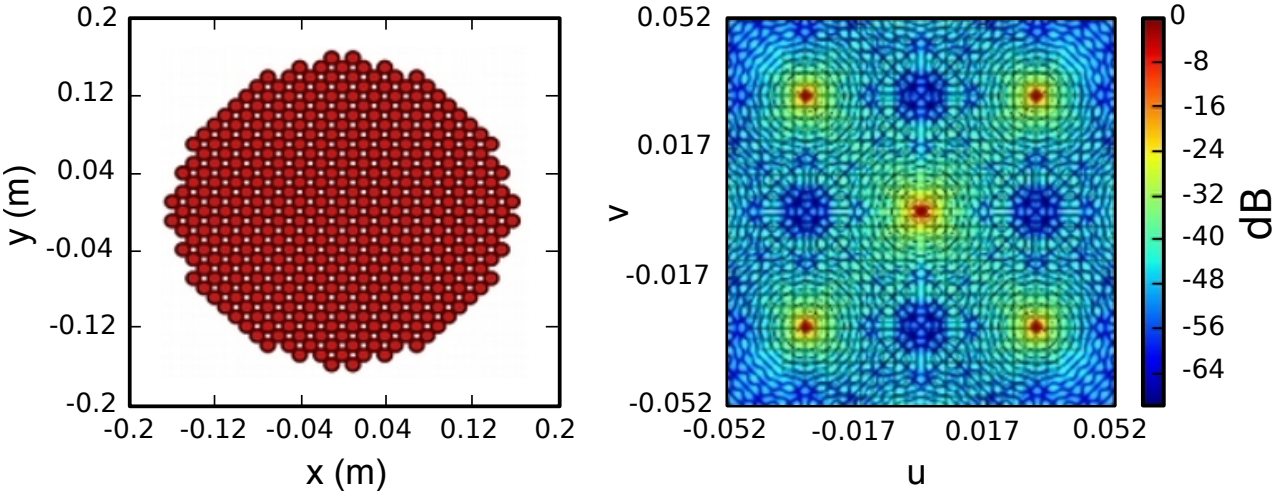

Figure 12. Left: QUBIC aperture plane showing all 400 antennas open to the sky. Right: the interference pattern formed on each of the focal planes when the instrument is observing a point-source located in the far field vertically along the instrument line-of-sight. The u and v coordinates are defined as: $u = \sin\theta\cos\phi$ and $v = \sin\theta\sin\phi$, where θ and ϕ are the angles on the celestial sphere defining the synthesized beam. Figure reproduced from [28].

the possibility of a leakage from Q to U and vice versa, due to uncertainties and errors in the process. Therefore, there will be a leakage between the E and B-modes, in particular from E to B (the original B-mode is expected to be much lower than the E-mode, hence the leakage from B to E might be neglected). We can further give a constraint to the induced value of the tensor-to-scalar ratio r. The leakage from E-modes to B-modes is significantly reduced by applying the self-calibration, even spending only 1 sec per baseline in the procedure. The leakage can be further reduced by spending more time on self-calibration. During the self-calibration phase, pairs of horns are successively shut while QUBIC observes an artificial partially-polarized source (a microwave synthesizer) in the far field. Then, the signal measured by each individual pair of horns is reconstructed and compared with each other. If the source is stable, then redundant baselines correspond to the same mode of the observed field, and therefore, a different signal between them can only be due to photon noise or instrumental systematic effects. Using a detailed parametric model of the instrument, we can fully recover the instrument parameters. The updated model of the instrument can then be used to reconstruct the synthesized beam and improve the map-making, thus reducing the leakage from E to B-modes.

In Figure 13 we show the improvement in the power spectrum estimation with self-calibration, depending on the time spent in the calibration mode. The more time spent in self-calibration mode, the lower the E to B leakage due to instrumental imperfections. In black solid lines, the prediction of the B-mode polarization power spectrum is displayed, for different values of the tensor-to-scalar ratio r.

2.4.2. Spectral imaging

The particular shape of the synthesized beam of the QUBIC experiment enables a peculiar and most convenient use of the instrument: that of a spectro-imager. Indeed, the dependence of the angular distance between primary and secondary peaks of the beam on the frequency of the observed signal allows the separation of the signal into different subfrequencies inside each channnel, providing information at more frequency bands than originally designed for. In this way, we can count on more frequency channels to disentangle the CMB polarization signal from those of polarized galactic foregrounds.

3. Current status and forecasts

The QUBIC instrument is currently undergoing its phase of laboratory calibration of its technological demonstrator version. A single focal plane with 256 TES detectors operating at 150 GHz and an array of 64 back-to-back horns along with a smaller optical combiner have been integrated into the final 1K box and cryostat. The horns array include the individual switches that enable the auto-calibration procedure. The cryogenic system has been succesfully cycled and tested to reach the expected performance.

An image of the synthesized beam at various frequencies has been successfully measured in several bolometers in the focal plane of the technological demonstrator, using the laboratory calibration source. As an example, in Fig. 14 we show a comparison between the predicted synthesized beam at 150 GHz and the one measured in one of the TES. The left panel displays the measurement, and the right panel shows the expected shape without aberrations (geometrical optics). The signal is normalized to the maximum value in each of the maps. There is some degree of saturation in the simulated image, to mimic what is observed in the measurement. Albeit only qualitative, the agreement shown here constitutes good evidence of the successful performance of the instrument design. A quantitative characterization of the response of all

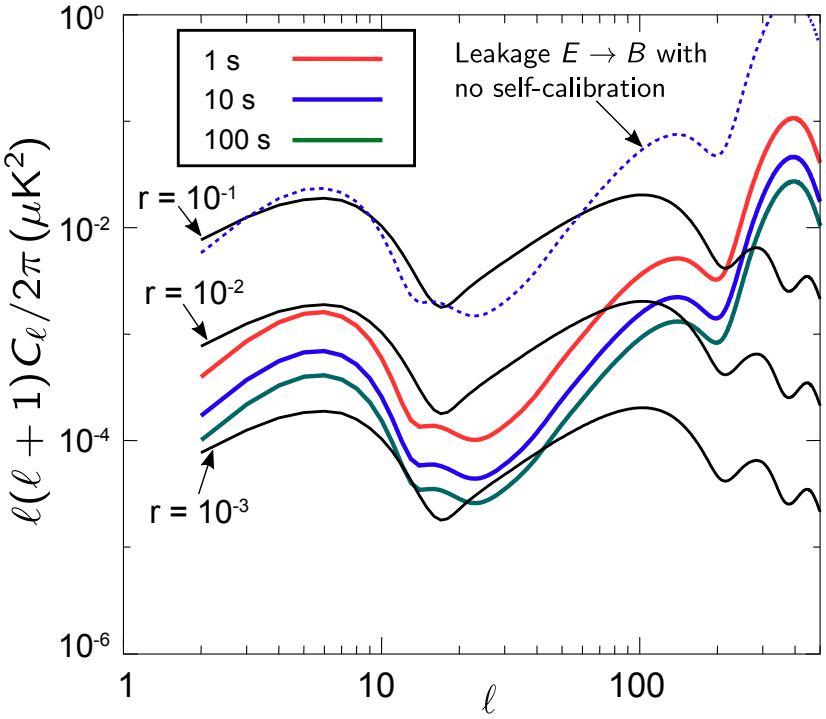

Figure 13. Improvement in the recovery of the *B*-mode power spectrum as a function of the time spent in the self-calibration mode. The three curves drawn with black solid lines represent theoretical B-mode power spectra calculated for three different values of the tensor-to-scalar ratio *r*. Figure reproduced from [28], adapted from [49].

detectors will be reported elsewhere, after the calibration of the technological demonstrator is completed. More details on the simulation of the optical beam combiner and horns array can be found in [50].

Furthermore, the angular resolution of the spectro-imager has been computed, and follows what is expected for the different subfrequency bands, namely, that the FWHM is reduced with increasing frequency.

After calibration is completed the TD will be shipped to Argentina for a first-light test on site in Alto Chorrillos. Meanwhile construction of the two complete focal panels at 150 GHz and 220 GHz, the full horns array and the final optical combiner will proceed. It is expected that the first module of the QUBIC instrument will be ready by 2020.

With two years of operation of its first module and an efficiency of 30% QUBIC is expected to be sensitive to values of the tensor-to-scalar ratio parameter *r* as low as 0.01. In Table 1 we summarise the expected sensitivity of QUBIC and other major ground-based experiments in the same frequency range, either running or expected to be deployed in the near future. It is important to notice that not only the reachable sensitivity should be taken into account, but also the systematic effects control and the possibility to remove foregrounds. In this sense, QUBIC has a unique status due to its particular architecture as a bolometric interferometer.

Project	Frequencies (GHz)	ℓ range	Ref.	$\sigma(r)$ goal (no fg.)	$\sigma(r)$ goal (with fg.)
QUBIC	150,220	30–200		6.0×10^{-3}	1.0×10^{-2}
Bicep3/Keck	95, 150, 220	50–250	[18]	2.5×10^{-3}	1.3×10^{-2}
CLASS ⋆	38, 93, 148, 217	2–100	[20]	1.4×10^{-3}	3.0×10^{-3}
SPT-3G †	95, 148, 223	50–3000	[19]	1.7×10^{-3}	5.0×10^{-3}
AdvACT ‡	90, 150, 230	60–3000	[21]	1.3×10^{-3}	4.0×10^{-3}
Simons Array	90, 150, 220	30–3000	[22]	1.6×10^{-3}	5.0×10^{-3}
Simons Observatory (SAT) ⋆⋆	27, 39, 93, 145, 225, 280	30–300	[23]	1.3×10^{-3}	3.9×10^{-3}

⋆ CLASS: Cosmology Large Angular Scale Surveyor; † SPT-3G: South Pole Telescope—3rd generation; ‡ AdvACT: Advanced Atacama Cosmology Telescope; ⋆⋆ SAT: Small Aperture Telescopes.

Table 1. Sensitivity of the main *B*-mode ground experiments operating in a frequency range similar to QUBIC. The label "fg" or "no fg" corresponds to the assumption on the foregrounds. Table extracted and expanded from [27, 28]. The entries for $\sigma(r)$ correspond to the estimates made in [40] for different experiments with the algorithms developed there (Appendix B1, no-delensing option). We acknowledge use of the public code CMB4CAST (https://portal.nersc.gov/project/mp107) for the computation of the last entry with the same method as in [40].

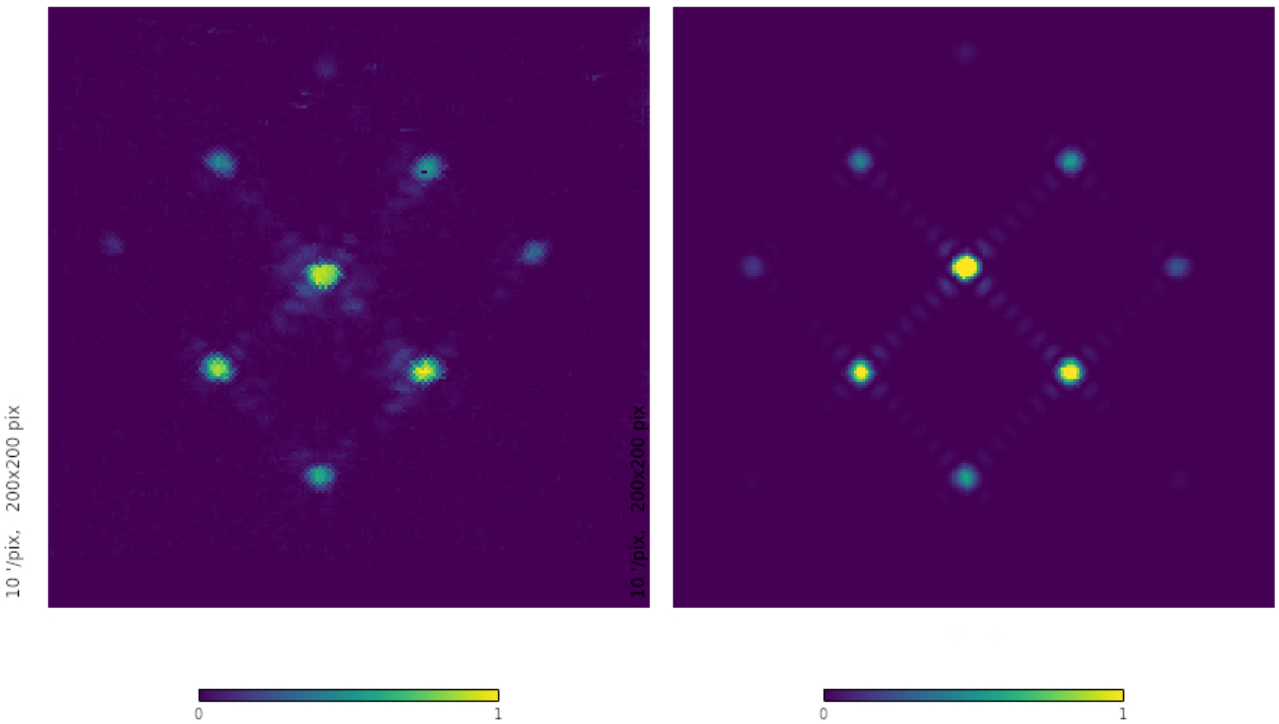

Figure 14. Comparison between the synthesised beam measured with one of the TES in the technological demonstrator (left panel) and the predicted beam without aberration effects (right panel).

In the future, more modules at additional frequencies could be added, aiming at improving the foreground removal, and increasing the sensitivity to the primordial *B*-mode polarization of the CMB.

Conclusions

The CMB provides a way to indirectly probe for the presence of primordial gravitational waves with cosmological wavelengths, with the size of the observable universe. Gravitational waves would have imprinted upon the CMB a specific pattern of *B*-mode polarization at the time the relic photons decoupled from matter almost 14 billion years ago. The quest for the detection of primordial *B*-modes in the CMB is a major experimental challenge, which is being pursued by several experiments, and up to now resulted in an upper bound on the tensor-to-scalar ratio $r < 0.06$ at 95% confidence level. The detection of primordial *B*-modes and the determination of the parameter r would be a major milestone in modern cosmology. It would test inflationary cosmological models, that predict that quantum effects at the earliest stages of the Big-Bang produced gravitational waves along with the density fluctuations that later seeded galaxy formation, but do not make definite predictions for their relative intensity.

QUBIC will soon join the existing efforts to search for primordial *B*-modes. It will do it from the Puna in Salta, Argentina, with a novel kind of instrument. With its unique architecture as a bolometric interferometer, it will benefit from the excellent sensitivity of the TES detectors, as well as from the high levels in the control of systematic effects provided by the self-calibration procedure based on the comparison of redundant baselines. Interferometric operation will also allow for spectral-imaging, which will improve the subtraction of astrophysical foregrounds with multi-frequency measurements.

After calibration is completed, QUBIC "Technological Demonstrator" will be shipped to Argentina for installation in Alto Chorrillos, while construction of the complete first module proceeds. In two years of operation of the complete instrument values of the tensor-to-scalar ratio r of order 0.01 will be probed with a method alternative to those of other current efforts. The successful performance of QUBIC will open a new road in the search of the elusive primordial *B*-modes of CMB polarization, footprints of gravitational waves from an inflationary period during the earliest moments in the history of the Universe.

Acknowledgments

QUBIC is funded by the following agencies. France: ANR (Agence Nationale de la Recherche) 2012 and 2014, DIM-ACAV (Domaine d'Interet Majeur—Astronomie et Conditions d'Apparition de la Vie), CNRS/IN2P3 (Centre national de la recherche scientifique/Institut national de physique nucléaire et de physique des particules), CNRS/INSU (Centre national de la recherche scientifique/Institut national de sciences de l'univers). Maria Salatino acknowledges the financial support of the UnivEarthS Labex program at Sorbonne Paris Cité (ANR-10-LABX-0023 and ANR-11-IDEX-0005-02.

Italy: CNR/PNRA (Consiglio Nazionale delle Ricerche/Programma Nazionale Ricerche in Antartide) until 2016, INFN (Istituto Nazionale di Fisica Nucleare) since 2017. Argentina: Secretaría de Gobierno de Ciencia, Tecnología e Innovación Productiva, Comisión Nacional de Energía Atómica, Consejo Nacional de Investigaciones Científicas y Técnicas. UK: the University of Manchester team acknowledges the support of STFC (Science and Technology Facilities Council) grant ST/L000768/1. Ireland: James Murphy and David Burke acknowledge postgraduate scholarships from the Irish Research Council. Duc Hoang Thuong acknowledges the Vietnamese government for funding his scholarship at APC. Andrew May acknowledges the support of an STFC PhD Studentship.

References

[1] A. A. Penzias and R. W. Wilson. A Measurement of Excess Antenna Temperature at 4080 Mc/s. *ApJ*, 142:419–421, July 1965.

[2] G. F. Smoot, C. L. Bennett, A. Kogut, E. L. Wright et al. Structure in the COBE differential microwave radiometer first-year maps. *ApJL*, 396:L1–L5, September 1992.

[3] Planck Collaboration: N. Aghanim, Y. Akrami, M. Ashdown, J. Aumont et al. Planck 2018 results. VI. Cosmological parameters. *arXiv eprints 1807.06209*, July 2018.

[4] M. J. Rees. Polarization and Spectrum of the Primeval Radiation in an Anisotropic Universe. *ApJL*, 153:L1, July 1968.

[5] J. M. Kovac, E. M. Leitch, C. Pryke, J. E. Carlstrom, N. W. Halverson, and W. L. Holzapfel. Detection of polarization in the cosmic microwave background using DASI. *Nature*, 420:772–787, December 2002.

[6] A. G. Polnarev. Polarization and Anisotropy Induced in the Microwave Background by Cosmological Gravitational Waves. *Soviet Astronomy*, 29:607–613, December 1985.

[7] R. Crittenden, R. L. Davis, and P. J. Steinhardt. Polarization of the Microwave Background Due to Primordial Gravitational Waves. *ApJL*, 417:L13, November 1993.

[8] D. D. Harari and M. Zaldarriaga. Polarization of the microwave background in inflationary cosmology. *Physics Letters B*, 319:96–103, December 1993.

[9] U. Seljak and M. Zaldarriaga. Signature of Gravity Waves in the Polarization of the Microwave Background. *Physical Review Letters*, 78:2054–2057, March 1997.

[10] M. Kamionkowski, A. Kosowsky, and A. Stebbins. A Probe of Primordial Gravity Waves and Vorticity. *Physical Review Letters*, 78:2058–2061, March 1997.

[11] D. Hanson, S. Hoover, A. Crites et al. Detection of B-Mode Polarization in the Cosmic Microwave Background with Data from the South Pole Telescope. *Physical Review Letters*, 111(14):141301, October 2013.

[12] The Polarbear Collaboration. A Measurement of the Cosmic Microwave Background B-mode Polarization Power Spectrum at Sub-degree Scales with POLARBEAR. *ApJ*, 794:171, October 2014.

[13] M. Zaldarriaga and U. Seljak. Gravitational lensing effect on cosmic microwave background polarization. *Physical Review D*, 58(2):023003, July 1998.

[14] B.P. Abbott et al. (LIGO Scientific Collaboration and Virgo Collaboration. Observation of gravitational waves from a binary black hole merger. *Phys. Rev. Lett.*, 116:061102, Feb 2016.

[15] A. H. Guth. Inflationary universe: A possible solution to the horizon and flatness problems. *Physical Review D*, 23:347–356, January 1981.

[16] A. D. Linde. A new inflationary universe scenario: A possible solution of the horizon, flatness, homogeneity, isotropy and primordial monopole problems. *Physics Letters B*, 108:389–393, February 1982.

[17] A. Albrecht and P. J. Steinhardt. Cosmology for grand unified theories with radiatively induced symmetry breaking. *Physical Review Letters*, 48:1220–1223, April 1982.

[18] H. Hui, P. A. R. Ade, Z. Ahmed, K. D. Alexander, M. Amiri, D. Barkats, S. J. Benton, C. A. Bischoff, J. J. Bock et al. BICEP3 focal plane design and detector performance. In *Millimeter, Submillimeter, and Far-Infrared Detectors and Instrumentation for Astronomy VIII*, volume 9914 of *Society of Photo-Optical Instrumentation Engineers (SPIE) Conference Series*, page 99140T, Jul 2016.

[19] B. A. Benson, P. A. R. Ade, Z. Ahmed, S. W. Allen, K. Arnold, J. E. Austermann, A. N. Bender, L. E. Bleem et al. SPT-3G: a next-generation cosmic microwave background polarization experiment on the South Pole telescope. In *Millimeter, Submillimeter, and Far-Infrared Detectors and Instrumentation for Astronomy VII*, volume 9153 of *Society of Photo-Optical Instrumentation Engineers (SPIE) Conference Series*, page 91531P, Jul 2014.

[20] K. Harrington, T. Marriage, A. Ali, J. W. Appel, C. L. Bennett, F. Boone, M. Brewer, M. Chan et al. The Cosmology Large Angular Scale Surveyor. In *Millimeter, Submillimeter, and Far-Infrared Detectors and Instrumentation for Astronomy VIII*, volume 9914 of *Society of Photo-Optical Instrumentation Engineers (SPIE) Conference Series*, page 99141K, Jul 2016.

[21] S. W. Henderson et al. Advanced ACTPol Cryogenic Detector Arrays and Readout. *J. Low. Temp. Phys.*, 184(3-4):772–779, 2016.

[22] K. Arnold, N. Stebor, P. A. R. Ade, Y. Akiba, A. E. Anthony et al. The Simons Array: expanding POLARBEAR to three multi-chroic telescopes. In *Millimeter, Submillimeter, and Far-Infrared Detectors and Instrumentation for Astronomy VII*, volume 9153 of *Proc. SPIE*, page 91531F, August 2014.

[23] P. Ade, J. Aguirre, Z. Ahmed, S. Aiola, A. Ali et al. The Simons Observatory: science goals and forecasts. *Journal of Cosmology and Astro-Particle Physics*, 2019(2):056, Feb 2019.

[24] QUBIC Collaboration: E. Battistelli, A. Baú, D. Bennett, L. Bergé, J. P. Bernard, P. de Bernardis, G. Bordier, A. Bounab et al. QUBIC: The QU bolometric interferometer for cosmology. *Astroparticle Physics*, 34:705–716, April 2011.

[25] M. Piat, E. Battistelli, A. Baù et al. QUBIC: the Q&U Bolometric Interferometer for Cosmology. *J. Low. Temp. Phys.*, 167(5-6):872–878, 2012.

[26] A. Tartari, J. Aumont, S. Banfi, P. Battaglia, E. S. Battistelli, A. Baù, B. Bélier, D. Bennett, L. Bergé, J. P. Bernard et al. QUBIC: A Fizeau Interferometer Targeting Primordial B-Modes. *J. Low. Temp. Phys.*, 184(3-4):739–745, 2016.

[27] J. Aumont, S. Banfi, P. Battaglia, E. S. Battistelli, A. Baù, B. Bélier, D. Bennett, L. Bergé et al. QUBIC Technical Design Report. *arXiv:1609.04372*, Sep 2016.

[28] A. Mennella, P. Ade, G. Amico, D. Auguste, J. Aumont, S. Banfi, G. Barbaràn, P. Battaglia, E. Battistelli, A. Baù et al. QUBIC: Exploring the Primordial Universe with the Q&U Bolometric Interferometer. *Universe*, 5:42, January 2019.

[29] K.D. Irwin and G.C. Hilton. *Transition-Edge Sensors*, pages 63–150. in *Cryogenic Particle Detection*, C. Enss (editor), Springer, Berlin, Heidelberg, 2005.

[30] R. A. Hulse and J. H. Taylor. Discovery of a pulsar in a binary system. *Astrophysics Journal Letters*, 195:L51–L53, January 1975.

[31] D. N. Spergel and M. Zaldarriaga. Cosmic Microwave Background Polarization as a Direct Test of Inflation. *Physical Review Letters*, 79:2180–2183, September 1997.

[32] The BICEP/Keck Collaboration: P. A. R. Ade, Z. Ahmed, R. W. Aikin, K. D. Alexander, D. Barkats, S. J. Benton, C. A. Bischoff, J. J. Bock et al. Measurements of Degree-Scale B-mode Polarization with the BICEP/Keck Experiments at South Pole. *arXiv:1807.02199*, Jul 2018.

[33] M. Zaldarriaga and U. Seljak. All-sky analysis of polarization in the microwave background. *Physical Review D*, 55:1830–1840, February 1997.

[34] C. Scóccola, D. Harari, and S. Mollerach. B polarization of the CMB from Faraday rotation. *Physical Review D*, 70(6):063003, September 2004.

[35] S. Mollerach, D. Harari, and S. Matarrese. CMB polarization from secondary vector and tensor modes. *Physical Review D*, 69(6):063002, March 2004.

[36] David H. Lyth. What Would We Learn by Detecting a Gravitational Wave Signal in the Cosmic Microwave Background Anisotropy? *Physical Review Letters*, 78(10):1861–1863, Mar 1997.

[37] Bicep2 Collaboration. Detection of B-Mode Polarization at Degree Angular Scales by BICEP2. *Physical Review Letters*, 112(24):241101, June 2014.

[38] BICEP2/Keck Collaboration and Planck Collaboration: P. A. R. Ade, N. Aghanim, Z. Ahmed, R. W. Aikin, K. D. Alexander, M. Arnaud, J. Aumont, C. Baccigalupi et al. Joint Analysis of BICEP2/Keck Array and Planck Data. *Physical Review Letters*, 114(10):101301, March 2015.

[39] BICEP2 Collaboration and Keck Array Collaboration: P. A. R. Ade, Z. Ahmed, R. W. Aikin, K. D. Alexander et al. Constraints on Primordial Gravitational Waves Using Planck, WMAP, and New BICEP2/Keck Observations through the 2015 Season. *Physical Review Letters*, 121(22):221301, November 2018.

[40] J. Errard, S. M. Feeney, H. V. Peiris, and A. H. Jaffe. Robust forecasts on fundamental physics from the foreground-obscured, gravitationally-lensed CMB polarization. *JCAP*, 3:052, March 2016.

[41] G. D'Alessandro, A. Paiella, A. Coppolecchia, M.G. Castellano, I. Colantoni, P. de Bernardis, L. Lamagna, and S. Masi. Ultra high molecular weight polyethylene: Optical features at millimeter wavelengths. *Infrared Physics & Technology*, 90:59 – 65, 2018.

[42] D. Prêle, F. Voisin, M. Piat, T. Decourcelle, C. Perbost, C. Chapron, D. Rambaud, S. Maestre, W. Marty, and L. Montier. A 128 Multiplexing Factor Time-Domain SQUID Multiplexer. *J. Low. Temp. Phys.*, 184(1-2):363–368, 2016.

[43] M. Salatino et al. Performance of NbSi transition-edge sensors readout with a 128 MUX factor for the QUBIC experiment. *Proc. SPIE Int. Soc. Opt. Eng.*, 10708:1070845, 2018.

[44] P. K. Day, H. G. LeDuc, B. A. Mazin, A. Vayonakis, and J. Zmuidzinas. A broadband superconducting detector suitable for use in large arrays. *Nature*, 425:817–821, October 2003.

[45] F. Pajot et al. Planck Pre-Launch Status: HFI Ground Calibration. *Astron. Astrophys.*, 520:A10, 2010.

[46] F. A. Bareiles, R. Morras, F. P. Hauscarriaga, J. C. Olalde, L. Guarrera, and E. M. Arnal. Alto Chorrillos: otra alternativa para instalar una antena para ondas milimétricas y submilimétricas en Argentina . *BAAA*, 53:199–202, September 2010.

[47] J. R. Pardo, J. Cernicharo, and E. Serabyn. Atmospheric transmission at microwaves (ATM): an improved model for millimeter/submillimeter applications. *IEEE Transactions on Antennas and Propagation*, 49:1683–1694, December 2001.

[48] A. Liu, M. Tegmark, S. Morrison, A. Lutomirski, and M. Zaldarriaga. Precision calibration of radio interferometers using redundant baselines. *MNRAS*, 408:1029–1050, October 2010.

[49] M.-A. Bigot-Sazy, R. Charlassier, J.-C. Hamilton, J. Kaplan, and G. Zahariade. Self-calibration: an efficient method to control systematic effects in bolometric interferometry. *A&A*, 550:A59, February 2013.

[50] C. O'Sullivan, D. Burke, D. Gayer, J. D. Murphy, S. Scully et al. Simulations and performance of the QUBIC optical beam combiner. In *Millimeter, Submillimeter, and Far-Infrared Detectors and Instrumentation for Astronomy IX*, volume 10708 of *Society of Photo-Optical Instrumentation Engineers (SPIE) Conference Series*, page 107082I, July 2018.

Bio

QUBIC is an international collaboration involving universities and laboratories in France, Italy, UK, Ireland, USA and Argentina. It is building an experiment aimed to reveal the existence of primordial gravitational waves through their effects upon the polarization of the cosmic microwave background, the relic radiation from the Big-Bang. The instrument will be installed in Alto Chorrillos, near San Antonio de los Cobres, Salta, Argentina.

Science Reviews
from the end of the world

Vol. 1, No. 4, September 2020 // pp. 66-73 /

The ANDES Deep Underground Laboratory

Xavier Bertou

CNEA/CONICET, Centro Atómico Bariloche, Argentina

Abstract

Deep Underground Laboratories (DUL) provide a unique environment to address some key questions in basic and applied science. A penetrating radiation due to cosmic rays is present at ground level at a rate of a few hundred particles per square meter per second. Moving deep underground with more than 1000m of overburden allows a reduction of this flux by 5 to 8 orders of magnitude. Frontier experiments in search for dark matter or neutrino properties can be designed and operated in DUL thanks to this background reduction. The ANDES DUL is foreseen to be built at the same time as the Agua Negra tunnel planned between the Argentine province of San Juan and the Chilean region of Coquimbo. It is designed to be a world class deep and large laboratory, operated by an international consortium.

Keywords:
Deep Underground Laboratories (DUL), dark matter, ANDES DUL, Agua Negra tunnel

Introduction

Everywhere on Earth a background flux of ionizing secondary particles from cosmic ray interactions in the upper atmosphere is present. While the precise flux depends on the altitude and geomagnetic latitude (higher at highest altitudes and closer to the magnetic poles), it is roughly of the order of a few hundred particles per square meter per second, half of which being electrons, positrons and gammas, the other half being mostly muons (neutrons, protons and more exotic particles are found in smaller amounts). They have been of utmost importance in the first stages of the construction of particle physics as we know it nowadays, and are still one of the main topic of interest in Astroparticle Physics, with the Pierre Auger Observatory as the flagship experiment for their observation. However, for many measurements this background flux of ionizing particles is more of a hindrance, and experiments try to reduce it by using active or passive shielding. For a small reduction, using lead and polyethylene (to absorb neutrons) can be quite efficient, and with some active muon veto, background flux reductions of up to 4 orders of magnitude can be achieved (see [1] for example). However, if more reduction is needed, the only viable option is to go deep underground to use a large rock overburden as natural shielding.

Since the 1960s experiments have been installed deep underground to study neutrino physics, starting with the precursor experiments in India and South Africa in 1965 discovering atmospheric neutrinos and the Homestake experiment in the US, measuring solar neutrinos. In the late 1970s/early 1980s it was decided to go forward with permanent underground installations and the first DUL were built (Baksan in Russia, Modane in France, Gran Sasso in Italy, Kamiokande in Japan). Built under more than 1000 m of rock overburden, they provide strong reduction in the cosmic background and opened the way to detailed neutrino physics studies, and the search of dark matter, among other topics. They have been key in the advance of neutrino physics, providing site for the experiments that resulted in the last Nobel prizes in the area (2002 and 2015). Current DUL are constantly being improved and new ones have been built recently (such as CJPL in China, 2010), while other are planned for the near future (SURF in the USA, SUPL in Australia, and hopefully INO in India).

DUL are mostly of two types, either built together with a road tunnel, or in an already existing mine. Building a laboratory in a tunnel implies almost surely having to build it at the same time as the tunnel, meaning there are little windows of opportunity to build those. They however benefit from an horizontal access to the laboratory helping significantly the installation of large pieces of equipment and experiments. Some mines or otherwise already built tunnel (such as the CJPL

one) also benefit from horizontal access. While they differ in many aspects (size, depth, access, radioactive environment, water presence...), there are many common issues to DUL and a global network of DUL is being worked upon to address them, with the most critical one being safety.

Finally, as of 2019 all DUL in operation are in the northern hemisphere. While it may not appear as an important laboratory parameter when studying neutrinos or other particles that can cross the Earth almost without interacting, there are reasons to look for sites in the southern hemisphere, as eventual effects of propagation through the Earth could be relevant, and some sources of background are location dependent. A worldwide well distributed network of DUL can be of specific interest to study dark matter signal modulation or MSW effects on neutrino propagation. It furthermore pushes for more international collaboration and enlarges the underground science community. It is in this context and with the construction of a new tunnel between Argentina and Chile that the ANDES project was proposed.

1. Science in Deep Underground Laboratories

DUL were initially built to access weakly interacting particle properties, driven by particle physics and basic science. Neutrino physics and dark matter search are the two main research topics in these laboratories. However, the extremely low background of DUL opened the window to many other studies, from nuclear astrophysics to biology. A complete review of these topics is out of the scope of this article, but a brief overview is given below.

1.1. Neutrino physics

Neutrino physics is a very active topic in DUL and has been extremely successful in the last 20 years, leading to the discovery of neutrino oscillations, changing significantly the view the high energy physics community had on the neutrino and solving the long lasting issue of the solar neutrino flux. The measurement of the neutrino mixing angles has been performed from solar [2], atmospheric [3], and nuclear power plant [4] neutrinos, but there are still many unknowns. First, while the mass squared difference between the different neutrino types is well determined by the oscillation measurements, the absolute scale for masses and the mass hierarchy are still unknown (see for example the review [5]). Then, it is still unclear whether neutrinos and anti-neutrinos are 2 different particles or the same, as proposed by E. Majorana in 1937 [6]. Finally, a last parameter from the oscillation parameters is missing. This phase, δ_{CP} could be violating the CP symmetry in the leptonic sector, and could lead to an explanation on why we live in a matter dominated universe. Other topics such as existence of a fourth sterile neutrino (or three right handed neutrinos [7]), effects of propagation in matter [8, 9], are also of importance for the understanding of neutrino physics. Most of these topics are searched for nowadays either by pointing a beam of man-made neutrinos to an underground laboratory hosting a huge neutrino detector (see for example [10]), or by looking for an elusive phenomenon, the neutrinoless double-beta decay [11].

Then neutrino themselves can be used as probes to understand macroscopic objects given their capability to escape most dense environments. There are still many fusion reactions in our Sun to be explored through neutrinos [12], and the role of neutrinos in supernovae explosion is still not fully understood. The observation of a supernova exploding in our galaxy would bring a whole new set of data to understand the phenomena (up to now only a distant supernova has been observed in neutrino [13]). Neutrinos are also produced in natural radioactive decays in the Earth (from uranium, thorium and potassium) and these geoneutrinos have been recently observed [14]. Better understanding of them could bring significant information in the geoscience sector, starting from the thermal balance of the Earth.

1.2. Dark matter search

The current understanding of the structure of the Universe is described by the cosmological standard model called ΛCDM, where Λ stands for the cosmological constant, explaining the observed acceleration of the universe [15, 16], and CDM referring to Cold Dark Matter. Dark matter is a form of non baryonic matter that we don't directly observe but which existence we infer from numerous observations, from rotation curves of galaxies [17], cluster formation [18], gravitational lensing [19], observation of collisions of galaxies [20], the Cosmic Microwave Background [21], and more. All these observations are compatible with our understanding of gravity if in addition to the normal observed matter, an extra component, the dark matter, is added, at a ratio of 6 to 1 (i.e. 85% of the total matter content of the Universe is in form of dark matter). It should mostly be cold, ie not relativistic, in order to explain the observations.

For many years, the best candidate for dark matter was thought to be the WIMP, Weakly Interactive Massive Particle, as in order to get the correct amount of dark matter via thermal production in the early universe a 100 GeV particle with a cross-section at the electroweak level is needed, and supersymmetric models naturally propose such a candidate. This coincidence is widely referred as the "WIMP miracle" [22]. After decades of search, the absence of signal in large detectors optimized for WIMP detection (noble gas double phase TPC such as Xenon [23]) and at the LHC [24] motivated alternative explanations for dark matter. Recently, lighter dark matter particles from a dark sector are becoming a well motivated target for direct searches [25], for which the LHC is already producing relevant limits [24].

While a lot of efforts in dark matter searches are done outside of DUL (searches for axions [26], production at LHC, indirect astrophysical searches for annihilation signals [27]), the most promising research is done in DUL. For dark matter candidates above 10 GeV, double phase noble gas TPC are leading the effort using Xenon [23] or Argon [28]. At

lower mass, a lot of different detection techniques and target materials are used, from cryogenic crystals [29], silicon sensors [30, 31], and liquid or gaseous detectors [32]. In most of these detectors a characteristic interaction signal is searched on as low a background as possible (ideally zero-background detectors once all the rejection techniques are applied). While most detectors have reported no signal and set limits in the mass-cross section plane of parameters, one experiment has reported a modulation in their detector counting compatible with the observation of a WIMP wind due to the movement of the Sun within the Galaxy, modulated by the movement of the Earth around the Sun [33]. Most interpretations of this signal are in contradiction with other experimental limits, and new experiments are trying to confirm or reject this observed modulation [34]. One of the arguments against this modulation being caused by dark matter are potential seasonal atmospheric effects. This is an example of measurement where a complementary detector in the southern hemisphere could give a final statement (if the effect is atmospheric, as the seasons are inverted in the southern hemisphere the phase of the modulation should change by 6 months, while if it is a genuine extra-solar signal then the phase wouldn't change). Finally, one can try to distinguish dark matter from potential noise (including neutrino coherent interactions when looking for extremely low cross sections [35]) by trying to measure the direction of propagation of dark matter particles [36].

1.3. Multidisciplinary studies

The very low cosmic background of DUL is essential for neutrino physics and dark matter searches, but can also be used for many other measurements and experiments. Extremely low levels of radioactive decays can be measured in DUL, measurements that would be impossible at the surface as they would be dominated by noise from cosmic ray interactions. This research area is quickly growing and has still a lot of potential as many possible users are not aware of the existence of DUL with unique environmental capabilities, and DUL directors and staff can't imagine all the areas which could benefit from it and contact the relevant researchers.

As examples of a wide range of different studies, one can mention the impact of cosmic radiation on cells, where it has been determined that a minimum of exposition to radiation seems necessary to train cells into repairing damage [37], evolution of fish populations over long periods of time [38], environmental studies [39], impact of cosmic rays on microchips [40] or even wine evaluation against fraud [41]. Specific experiments can be also instrumented to measure nuclear processes at energies relevant for astrophysics [42], and have led to some reestimation of the age of globular clusters [43].

2. The Agua Negra Deep Experiment Site

Figure 1. Map of existing (yellow dots) and planned (red dots) DUL over the world [44].

Figure 1 shows the existing and planned DUL. As already stressed all the existing DUL are in the northern hemisphere. Two DUL are in planning for the southern hemisphere, the Stawell Underground Physics Laboratory (SUPL) in Australia, planned 1 km deep in the Stawell Goldmine, a small size laboratory aimed at hosting the Sodium Iodide with Active Background Rejection Experiment (SABRE) [45], and the Agua Negra Deep Experiment Site (ANDES), planned as a world class laboratory at the border between Argentina and Chile to be constructed along a new tunnel in the Andes, the Agua Negra tunnel.

2.1. The Agua Negra tunnel

The world economic evolution with the growing importance of the Asian market makes it crucial for Argentina and Brazil to access the pacific. The current main pass through the Andes is the Cristo Redentor tunnel, and is becoming insufficient for the growing commercial exchange. It furthermore suffers from closure during strong snowfalls in winter time. Many options have been looked forward to improve the situation, and the most advanced one as of 2019 is the Agua Negra tunnel.

The Agua Negra tunnel is planned where the current Agua Negra international crossing is located, 300 km north of the Cristo Redentor tunnel, connecting the San Juan Argentine province to the Coquimbo province in Chile. It is planned as a high altitude tunnel, at roughly 4000 m of altitude, but in a dry region where snowfalls are no major issue. It will consist of two 14 km long, 12 m diameter road tunnels, the southern one allowing to drive from Chile to Argentina, while the northern one will go from Argentina to Chile. Feasibility studies were started in 2005, and the presidents of Argentina and Chile signed a Bi-National Integration treaty, which included the San Juan - Coquimbo tunnel option, in October 2009. This treaty was then approved by both countries parliaments. In August 2010, a MERCOSUR meeting in San Juan marked the launch of the final part of the planning of the tunnel, with strong support from the Argentine, Chilean, and Brazilian presidents. The EBITAN (bi-national entity in charge of the political and technical aspects of the Agua Negra tunnel) was formed and approved by the congress of both countries. In 2012 a first international tender process was started, where companies were supposed to bid for the construction and provide a financing scheme. 3 years later, the Inter-American Develop Bank (IDB) approved the financing of the project and the tunnel entered a new phase. A fifth of the estimated 1.5 B$ cost of the tunnel has already been put forward by the IDB and the last phase of the tender process is expected to end in 2021. Construction would last 8 years, likely 2022-2029.

2.2. ANDES design and layout

The ANDES design and layout was developed starting in 2011 around the central idea of having a main hall about the height and width of a Gran Sasso hall, but only half its length, as this is the typical size needed for next generation large experiments searching for dark matter. A large pit able to host a next generation neutrino detector was also planned since the beginning. Then a few extra halls were thought to host technical services and other experiments.

In 2014 the design was assessed by a former director of SNOLAB and the resulting documents were submitted to the Lombardi company, in charge of the design of the Agua Negra tunnel. In 2015 a conceptual design was requested to the company [46]. The resulting design was discussed in an international workshop in 2017 and then presented to the EBITAN that approved its inclusion in the tunnel civil work plan. In 2018 the basic engineering design was requested to Lombardi (for a cost of about 0.5 M$, financed by the San Juan province), and was finalized in June 2019 [47]. With these documents (and the technical tender documents to include ANDES in the tunnel civil work, not yet finalized), it is expected to have ANDES at the same level of design as the tunnel by the end of 2020, ready for the construction to start in 2021. The construction of ANDES would start once the tunnel is excavated to the planned location of the laboratory, after 4 years of civil work. The laboratory itself would take 6 years of construction to completion. The total cost of the underground civil work for the laboratory is expected to be around 73 M$ [47].

The final design can be observed in figure 2, and its main features are described below.

2.2.1. Location and access

The laboratory is foreseen to be located at the km 4.5 of the tunnel (from the Chilean side), at the same level as the main ventilation hall where a specific ventilation tunnel coming from Chile ends. This location has been chosen in order to optimize the integration to the tunnel and the ventilation processes. A study of the muon background expected in areas between this location and another location at the frontier between both countries shows the muon flux is minimum in this area and changes by less than 10% in between these 2 locations. While the baseline design is to locate the laboratory at km 4.5, the final location may change if the geology is not adequate for the construction.

The laboratory will be accessed directly from the southernmost road tunnel, going from Chile to Argentina. In order to access it from Argentina one will have to go to Chile by the northernmost tunnel and then come back to the laboratory. It should be noted that the whole area will be bi-national so no migration duties will be necessary as long as one goes back to the corresponding country. Safety doors will allow entering the laboratory space, where a large parking space will be available, giving access to technical halls (for ventilation, cooling, water waste, technical services) and the main office hall. A safety exit allowing to access the second tunnel in case of a fire in the Chile-Argentina tunnel is also located in this access zone.

The laboratory section will not be accessible by vehicles except large tucks needing to discharge containers. In that case they will be able to maneuver and move backwards to the main access tunnel for the laboratory, where various cranes will unload the containers. An internal escape gallery allows a safety exit in case of fire in the laboratory.

2.2.2. Main, secondary hall and large pit

The main, secondary halls and the large pit are the three main areas foreseen for large experiments, in particular for direct dark matter search and neutrino physics.

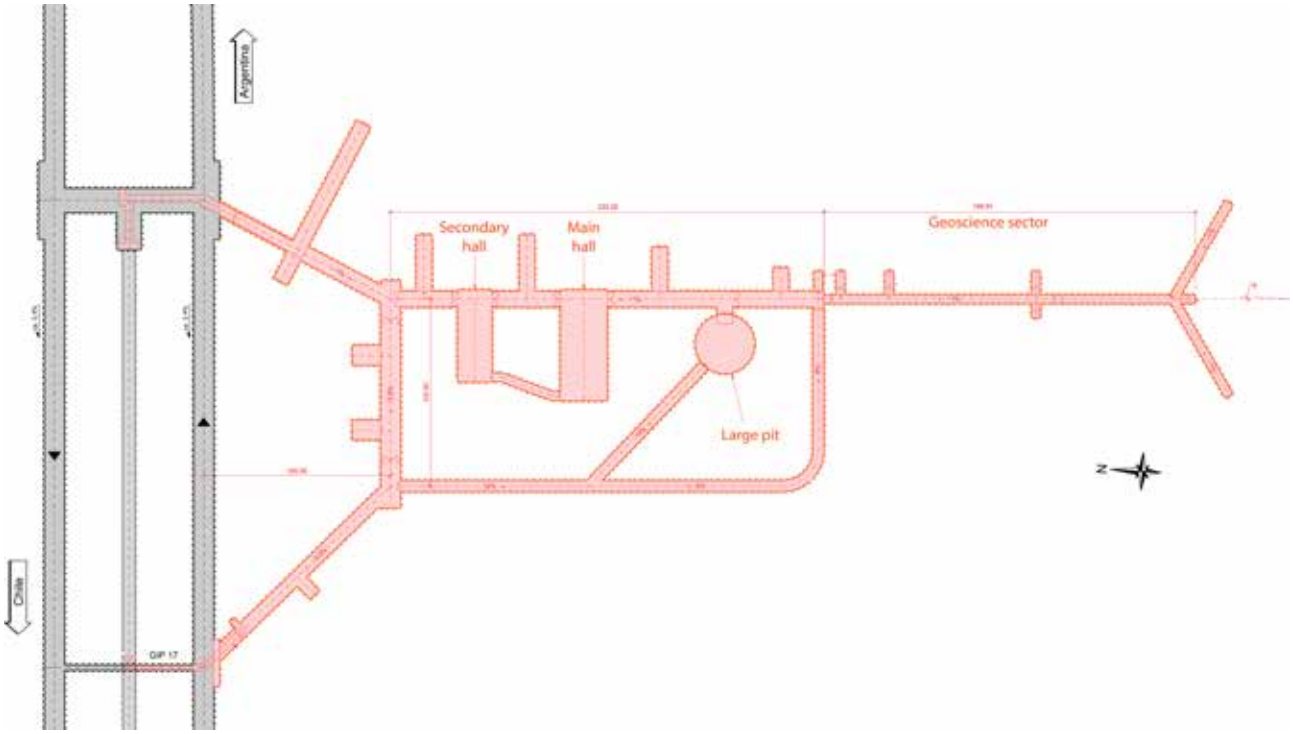

Figure 2. Final design for the ANDES deep underground laboratory, adapted from the basic engineering phase [47]. See text for details.

The main and secondary halls mainly differ in their dimensions. The main hall is 50 m × 21 m × 22 m while the secondary is 40 m × 16 m × 14 m. They both are overlooked by a 40 t crane that follows the cavern shape to optimize the available height. To reach optimally the full height in the main cave, the central part is below the access tunnel level by one meter. This is a design similar to the main hall of Canfranc (in a larger size). This also helps containing eventual material leak from experiments.

The secondary hall is mainly foreseen for modular structures that can host specific long term laboratories or short term experiments subject to regular changes. The main hall on the other hand is foreseen for two or three major long term experiments, especially for direct dark matter search or neutrinoless double beta decay.

The Large pit is the single large cavern of the laboratory. Its useful volume is 30 m of diameter and 30 m of altitude. It is foreseen for a single large experiment, in particular a large neutrino experiment [48]. The size was fixed in order to host a 3 kt scintillator neutrino experiment (10 times the size of Borexino [12]). The main access is from the top with a rotating crane allowing to access any place within the pit. A secondary access from the bottom is available for the installation of the experiment. The bottom access door can be sealed and the full pit is designed to be waterproof allowing it to be filled with purified water shielding without mixing with the water from the rock.

2.2.3. Geoscience sector

The geoscience sector was added to the ANDES design in 2017, and is based on the experience of the Black Forest Observatory [49]. It is located at the end of the main laboratory access tunnel and consists of a long tunnel with 2 final tunnels in a Y shape, designed for the installation of a tiltmeter. Different halls are foreseen for the installation of specific instruments, such as superconductive gravimeters, strainmeters, long period and short period seismometers.

The overburden is not of the highest importance for the geoscience sector. On the other hand, the stability of the sensors environment is of the utmost importance for a precise measurement, and this can be achieved with a significant overburden, as long as the geoscience sector is air tight. This implies the use of air-locks, with the whole geoscience sector being sealed except during the installation of new equipment or reparation phases.

In addition to the sealed sector, a specific geomaterial laboratory will be installed in the secondary hall, allowing on one hand a continuous analysis of the gasses and fluids at the rock face, and on the other hand studies of geomaterials from other sources. It will be strongly integrated to the low radiation measurement laboratory.

2.2.4. Multidisciplinary halls

Multiple extra halls will host a variety of experiments. While it is probably ambitious to plan for all the uses an underground laboratory can have for the next 100 years, at start the distribution of the halls is foreseen based on current activity in other underground laboratories. In particular, the first room, isolated from the other rooms, is foreseen to possibly host a particle accelerator to do nuclear astrophysics similar to the LUNA experiment in Gran Sasso [42]. As it can produce noise to other

experiments it is oriented in a way that points away from other caverns.

The second supplementary hall is foreseen for the clean laboratories. Two clean rooms will be installed, one accessible only from the other one through an air shower. The first one will act as a clean room available for activities in the underground laboratory, while the second one will host the low radiation laboratory, featuring high purity germanium detectors for very low radioactive material measurements.

The last specific area will be a biology dedicated laboratory, with different sectors for plants, cells, multipurpose experiments, and a specifically designed area for work on animals, to ensure no contamination to other areas of the laboratory.

2.3. ANDES operation and organization

Since its start ANDES was foreseen not only as a laboratory that would host international experiments, but as an international laboratory. It is currently coordinated by the ANDES Unit within the CLAF (Latinamerican Center for Physics, a type II UNESCO institute recognized by most latinamerican countries), with representatives of Argentina, Brazil, Chile and Mexico. Advanced contacts aim at widening the unit to include more partners, not necessarily from Latin America. In the short term Colombia, France and Germany could be added to the coordination, while other countries such as Italy could act as observers of the structure.

In the longer term a more structured organization is being designed, based on similar international science oriented institutions such as the CERN [50] and SESAME [51]. In particular the SESAME model (itself based on CERN) is being pursued given the similar expected organizational size of ANDES and SESAME. ANDES would therefore be run by a council formed by *member* and *observer* states, in charge of taking the scientific decisions needed to guarantee the excellence of the laboratory and funding the basic operation of the laboratory.

In addition to the underground laboratory and its operational organization, two support centers are foreseen, one in Argentina and one in Chile. Given the geography and relatively high altitude of the planned tunnel, cities are at some distance. The Chilean support laboratory is foreseen in La Serena, a large connected city with well developed local scientific infrastructure. It is however at 200 km from the tunnel. A closer center is therefore foreseen in Argentina and aimed at being more operational, running daily activities at the underground site. Each support center will be associated with national authorities (local universities, local research centers) and a strong focus will be put in order to host a visitor center in each country, as these will allow a direct contact between the population and a world class research center, something uncommon in the region.

Finally a strong effort will be done in order to link the local universities in Argentina and Chile to the laboratory, through the organization of undergraduate and graduate courses. A strong link to existing underground laboratories and foreign educational structures will be pursued, in particular with the Canfranc laboratory in Spain and the Gran Sasso Science Institute [52].

Acknowledgments

The author would like to stress the participation of Claudio Dib, Osvaldo Civitarese, Ronald Shellard, João Carlos Costa dos Anjos, Juan Carlos d'Olivo, Luis Manuel Villaseñor, Hernán Asorey, Mariano Gómez Berisso, Joaquín Venturino, Andreas Rietbrock and Alberto Etchegoyen in pushing forward for the establishment of the ANDES initiative. The project wouldn't have advanced without the strong support of the San Juan provincial government in Argentina and of the Coquimbo region in Chile. The support of other DUL management was also essential, in particular the SNOLAB, Modane and Gran Sasso. Finally, the author would like to thank the Geoconsult and Lombardi companies that have helped designing the laboratory.

References

[1] G. Heusser et al. GIOVE: a new detector setup for high sensitivity germanium spectroscopy at shallow depth. *European Physical Journal C*, 75:531, Nov 2015.

[2] Q. R. Ahmad et al. Measurement of the Rate of ν_e + d –>p + p + e^- Interactions Produced by ^{8}B Solar Neutrinos at the Sudbury Neutrino Observatory. *Physical Review Letters*, 87(7):071301, August 2001.

[3] Y. Fukuda et al. Evidence for Oscillation of Atmospheric Neutrinos. *Physical Review Letters*, 81:1562–1567, August 1998.

[4] F. P. An et al. Observation of Electron-Antineutrino Disappearance at Daya Bay. *Physical Review Letters*, 108(17):171803, April 2012.

[5] P. F. de Salas et al. Neutrino mass ordering from oscillations and beyond: 2018 status and future prospects. *Frontiers in Astronomy and Space Sciences*, 5:36, 2018.

[6] E. Majorana. Teoria simmetrica dell elettrone e del positrone. (Italian) [Symmetrical theory of the electron and the positron]. *Il Nuovo Cimento (8)*, 14(4):171–184, April 1937.

[7] M. Drewes. The Phenomenology of Right Handed Neutrinos. *International Journal of Modern Physics E*, 22:1330019–593, August 2013.

[8] S. P. Mikheyev and A. Y. Smirnov. Resonance enhancement of oscillations in matter and solar neutrino spectroscopy. *Yadernaya Fizika*, 42:1441–1448, 1985.

[9] L. Wolfenstein. Neutrino oscillations in matter. *Phys. Rev. D*, 17:2369–2374, May 1978.

[10] DUNE Collaboration. The DUNE Far Detector Interim Design Report Volume 1: Physics, Technology and Strategies. *arXiv e-prints*, pp. arXiv:1807.10334, Jul 2018.

[11] M. J. Dolinski et al. Neutrinoless Double-Beta Decay: Status and Prospects. *arXiv e-prints*, pp. arXiv:1902.04097, Feb 2019.

[12] BOREXINO Collaboration et al. The Borexino detector at the Laboratori Nazionali del Gran Sasso. *Nuclear Instruments and Methods in Physics Research A*, 600:568–593, March 2009.

[13] K. Hirata et al. Observation of a neutrino burst from the supernova sn1987a. *Phys. Rev. Lett.*, 58:1490–1493, Apr 1987.

[14] O. Smirnov. Geoneutrino : experimental status and perspectives. *Journal of Physics: Conference Series*, 1056:012055, jul 2018.

[15] S. Perlmutter et al. Measurements of Ω and Λ from 42 High-Redshift Supernovae. ApJ, 517:565–586, June 1999.

[16] A. G. Riess et al. Observational Evidence from Supernovae for an Accelerating Universe and a Cosmological Constant. AJ, 116:1009–1038, September 1998.

[17] V. C. Rubin et al. Rotational properties of 21 SC galaxies with a large range of luminosities and radii, from NGC 4605 /R = 4kpc/ to UGC 2885 /R = 122 kpc/. ApJ, 238:471–487, June 1980.

[18] A. V. Kravtsov and S. Borgani. Formation of Galaxy Clusters. ARA&A, 50:353–409, Sep 2012.

[19] R. Massey et al. The dark matter of gravitational lensing. *Reports on Progress in Physics*, 73(8):086901, Aug 2010.

[20] M. Markevitch et al. Direct Constraints on the Dark Matter Self-Interaction Cross Section from the Merging Galaxy Cluster 1E 0657-56. ApJ, 606:819–824, May 2004.

[21] Planck Collaboration et al. Planck 2015 results. XIII. Cosmological parameters. A&A, 594:A13, September 2016.

[22] G. Jungman et al. Supersymmetric dark matter. Phys. Rep., 267:195–373, March 1996.

[23] E. Aprile et al. Dark matter search results from a one ton-year exposure of xenon1t. *Phys. Rev. Lett.*, 121:111302, Sep 2018.

[24] The ATLAS collaboration et al. Constraints on mediator-based dark matter and scalar dark energy models using 13 tev pp collision data collected by the atlas detector. *Journal of High Energy Physics*, 2019(5):142, May 2019.

[25] R. Essig et al. Dark Sectors and New, Light, Weakly-Coupled Particles. *arXiv e-prints*, pp. arXiv:1311.0029, Oct 2013.

[26] Q. Yang. Axions and dark matter. *Modern Physics Letters A*, 32(15):1740003, May 2017.

[27] J. M. Gaskins. A review of indirect searches for particle dark matter. *Contemporary Physics*, 57(4):496–525, Oct 2016.

[28] C. E. Aalseth et al. The DarkSide Multiton Detector for the Direct Dark Matter Search. *Adv. High Energy Phys.*, 2015:541362, 2015.

[29] CRESST Collaboration et al. First results from the CRESST-III low-mass dark matter program. *arXiv e-prints*, pp. arXiv:1904.00498, Mar 2019.

[30] R. Agnese et al. First Dark Matter Constraints from a SuperCDMS Single-Charge Sensitive Detector. Phys. Rev. Lett., 121(5):051301, Aug 2018.

[31] A. Aguilar-Arevalo et al. First Direct-Detection Constraints on eV-Scale Hidden-Photon Dark Matter with DAMIC at SNOLAB. Phys. Rev. Lett., 118(14):141803, Apr 2017.

[32] C. Amole et al. Dark matter search results from the complete exposure of the PICO-60 C_3F_8 bubble chamber. Phys. Rev. D, 100(2):022001, Jul 2019.

[33] R. Bernabei et al. Improved model-dependent corollary analyses after the first six annual cycles of DAMA/LIBRA-phase2. *arXiv e-prints*, pp. arXiv:1907.06405, Jul 2019.

[34] G. Adhikari et al. Search for a Dark Matter-Induced Annual Modulation Signal in NaI(Tl) with the COSINE-100 Experiment. Phys. Rev. Lett., 123(3):031302, Jul 2019.

[35] C. Bœhm et al. How high is the neutrino floor? J. Cosmology Astropart. Phys., 2019(1):043, Jan 2019.

[36] CYGNO Collaboration. CYGNO: a CYGNUs Collaboration 1 m$\hat{3}$ Module with Optical Readout for Directional Dark Matter Search. *arXiv e-prints*, pp. arXiv:1901.04190, Jan 2019.

[37] N. Lampe et al. Background study of absorbed dose in biological experiments at the Modane Underground Laboratory. In *European Physical Journal Web of Conferences*, volume 124, pp. 00006, Sep 2016.

[38] D. Gutiérrez et al. Anoxic sediments off central peru record interannual to multidecadal changes of climate and upwelling ecosystem during the last two centuries. *Advances in Geosciences*, 6:119–125, 2006.

[39] J.-L. Reyss et al. Large, low background well-type detectors for measurements of environmental radioactivity. *Nuclear Instruments and Methods in Physics Research Section A: Accelerators, Spectrometers, Detectors and Associated Equipment*, 357(2):391 – 397, 1995.

[40] J. L. Autran et al. Real-time neutron and alpha soft-error rate testing of cmos 130nm sram: Altitude versus underground measurements. In *2008 IEEE International Conference on Integrated Circuit Design and Technology and Tutorial*, pp. 233–236, June 2008.

[41] M. S. Pravikoff et al. Neutrino, wine and fraudulent business practices. *CERN Proc.*, 1:287–294, 2019.

[42] H. Costantini et al. LUNA: a laboratory for underground nuclear astrophysics. *Reports on Progress in Physics*, 72(8):086301, jul 2009.

[43] C. Gustavino. The impact of LUNA results on astroparticle physics. In F. Giovannelli and G. Mannocchi, editors, *Frontier Objects in Astrophysics and Particle Physics*, pp. 77, Jan 2009.

[44] A. Ianni. TAUP Underground Laboratory plenary presentation, 2017.

[45] C. Tomei. Sabre: Dark matter annual modulation detection in the northern and southern hemispheres. *Nuclear Instruments and Methods in Physics Research Section A: Accelerators, Spectrometers, Detectors and Associated Equipment*, 845:418 – 420, 2017. Proceedings of the Vienna Conference on Instrumentation 2016.

[46] Lombardi. Nuevo Estudio Conceptual - ANDES, 2015.

[47] Lombardi. Ingeniería Básica de Anteproyecto - ANDES, 2019.

[48] P. A. N. Machado et al. Potential of a neutrino detector in the andes underground laboratory for geophysics and astrophysics of neutrinos. *Phys. Rev. D*, 86:125001, Dec 2012.

[49] D. Emter et al. The black forest observatory, schiltach. *Soil Dynamics and Earthquake Engineering*, 13(1):73 – 75, 1994.

[50] CERN. http://www.cern.ch/.

[51] SESAME. http://www.sesame.org.jo/.

[52] GSSI. http://www.gssi.it/.

Bio

Xavier Bertou

Xavier Bertou has a PhD in Astrophysics from the University of Paris VI. He has been a member of the Pierre Auger Collaboration for 25 years and is the impulsor and coordinator of the ANDES initiative through the ANDES-CLAF unit. He works in astroparticle physics (mostly neutrino physics and dark matter search lately) at the Particle and Radiation Detection Laboratory at the Bariloche Atomic Center in Argentina.

INSTRUCTIONS FOR AUTHORS

GUIDELINES

1. Length

Research reviews should not be less than 7000 words or more than 10,000 words (plus up to 15 figures and up to 50 references).

2. Structure

Whenever possible articles should adjust to the standard structure comprising:
(a) Graphical abstract,
(b) Abstract,
(c) Introduction describing the focus of the review,
(d) Article main body including assessment and discussion of available information (may be further subdivided),
(e) Conclusions,
(f) Bibliography.

3. Format

Authors must submit their articles in a Microsoft Word archive. Figures must be embedded in the article and also submitted in a separate .zip or .rar file.

4. References

References must be numbered in the text ([1] [2] [3]) and identified with the same numbers in the *References* section. Up to 50 references are allowed. The following are examples to take into account in each case.

BOOKS:
- *Single author*
Chung, R. *General Chemistry: Fundamental Knowledge,* 2nd ed.; McGuffin-Hill: Kansas City, 2003.
- *More than one author*
Chung, R.; Williamson, M. *General Chemistry: Fundamental Knowledge*, 2nd ed.; McGuffin-Hill: Kansas City, 2003.
- *Edited Book*
Kurti, F. Photodissociation and Reactive Scattering. In *The Rise of Chemical Physics*; White, AD, Ed.; Wilson: New Jersey, 2007; Vol. 128; p. 257.
- *Book in Series*
Goth, V. Polymer Chemistry. In *The Foundational Course in Organic Chemistry*; ACDC Symposium Series 1151; American Chemical Fraternity: Seattle, 2014; pp 123-149.
- *Article from a reference book*
Powder and Metallurgy. *Dictionary of Chemical Technology*, 3rd ed.; Wilson: New Jersey, 1971; Vol. 12, pp 68-82.

ARTICLES:
- *Article in a scientific journal*
Evans, A.; Stitch, M.; Smithers, ET; Nope, JJ Complex Aldol Reactions to the Total Synthesis of Phorboxazole B. *J. Am. Chem*. Soc. 2012, 122, 10033-10046.
- *Article in a popular/non-scientific magazine*
Tatum, CJ Super Organics. *Wireless* , June 2001, pp 76-93.
- *Article from an online journal*
Turkey-Lopez, E. Inexact Solutions of the Quantum Double Square-Well Potential. *Chem. Ed.* [Online] 2007, 11, pp. 838-847. http://chemeducator.org/bibs/0011006/11060380lb.htm (accessed Aug 5, 2019).

PUBLICATION ETHICS

The journal considers that the primary objective of all submissions must be a contribution of relevant and appropriate content, and that all review processes must be structured based on that general criterion. Therefore, there is an emphasis on the concern to maintain the highest quality and ethics standards in the reception, evaluation and publication of articles. These standards include the three participants of the process: author, reviewer and editor.

1. Author's responsibilities

- Submitted manuscripts should maintain rigorous scientific criteria for data validation and conclusions.
- All data (Figures, Tables, etc.) reproduced from previous published articles must give the appropriate recognition to the source. Plagiarism is cause enough to reject the submission.
- Authorship must include all individuals who have contributed in a substantial way to the composition, prior investigation, and execution of the paper. Minor contributions must be acknowledged, but these contributors should not be listed as authors. The main author or authors of the article will make sure that all participants of the paper have approved the final version of the document submitted.
- All authors must reveal in their final manuscript any financial or other type of conflict of interests that might interfere with the results and interpretations in their research. All funding received to carry out the project must be acknowledged.
- After the article is published, in the event an author notices a crucial fault or inaccuracy, he or she should immediately report that fault or inaccuracy, so that an Erratum can be issued as soon as possible.

2. Reviewer's responsibilities

Reviewing is a time-consuming process that is carried out *ad honorem* by *bona fide* scientists conversant with the subject of the reviewed paper. The quality and the ethical standards of the journal depend critically on the quality of the reviewing process, and the following guidelines are established:

- All documents sent to the journal for review will be considered confidential documents and will not be discussed with external third parties.
- When invited, a potential reviewer should decline if: (a) the subject of the article is not within his/her area of expertise; (b) there is any kind of conflict of interest; (c) if the review cannot be finished within the period established by the journal.
- Any criticism or objections to the paper should be done in a neutral tone and based on reasonable grounds, not limited to simple opinions or purely subjective expressions.

3. Editor's responsibilities

- The editors are responsible for selecting the papers that will be published in the journal. The Editorial Management must comply with the ethical standards of the journal, as well as with all legal guidelines, including the prohibition of plagiarism and any other form of copyright infringement.
- The editors will evaluate and make decisions on the articles sent to the journal regardless of the gender, sexual orientation, religious beliefs, ethnic origin, nationality or political ideology of the authors.
- Revealing information identifying reviewers is forbidden.
- The final version of all materials can be published only with the prior approval of their author.
- The editors will refrain from publishing manuscripts that imply a conflict of interests because of any possible connection with other institutions, companies and authors.
- Before deciding to send an article to a peer review, the editors are committed to thoroughly read all texts received and determine their appropriateness to the thematic universe of the journal.
- If a misbehavior or unethical action by an author or reviewer is identified, the editors must request the informer of such conduct or action to provide the evidence that may justify a possible investigation. All accusations will be handled seriously until reliable results are obtained regarding its truthfulness or falseness. If an investigation takes place, the editors are responsible for choosing the appropriate way in which it will be carried out. They can also request the advice and assistance from the Editorial Board, as well as from reviewers and authors.
- In the event a serious non-malicious mistake or a dishonest conduct by an author or a reviewer is proved, the editors shall act according to the nature and seriousness of the case. The actions the editors may take include, but are not limited to: notifying the author or reviewer of the existence of a serious mistake or misapplication of the ethical standards of the journal; writing a strong statement that reports and warns about a bad practice or unethical behavior; publishing that statement; unilaterally withdrawing the reported paper from the review or publication process; revoking the paper if it has already been published; communicating the journal's decision and the reasons behind it to the general public; and banning paper submissions by the people involved for a certain period of time.

PRIVACY STATEMENT

The names and email addresses entered in this journal site will be used exclusively for the stated purposes of this journal and will not be made available for any other purpose or to any other party.

NEXT ISSUE

Vol. 2, No. 5

TO BE PUBLISHED ON DECEMBER 15, 2020

We are preparing a special issue covering the ongoing R&D projects on COVID-19 in Argentina.

ISSN 2683-9288

Science Reviews
from the end of the world

Centro de Estudios sobre Ciencia, Desarrollo
y Educación Superior
538 Pueyrredón Av. - 2° C – Second building
Buenos Aires, Argentina - C1032ABS
(54 11) 4963-7878/8811
sciencereviews@centroredes.org.ar
www.scirevfew.net